Indian J Pure & Appl Phys, Vol 21 No. 9 pp. 493-554
SEPTEMBER 1983
CODEN:IJOPAU ISSN:0019-5596
21(9) 493-554 (1983)

INDIAN JOURNAL OF PURE & APPLIED PHYSICS

Published by
PUBLICATIONS & INFORMATION DIRECTORATE, CSIR
NEW DELHI
in association with
THE INDIAN NATIONAL SCIENCE ACADEMY, NEW DELHI

Indian Journal of Pure & Applied Physics

Published by the Publications & Information Directorate, CSIR, Hillside Road, New Delhi 110012
Editor-in-Chief : Y R Chadha

The Indian Journal of Pure & Applied Physics is issued monthly. The Directorate assumes no responsibility for the statements and opinions advanced by contributors. The editorial staff in its work of examining papers received for publication is assisted, in an honorary capacity, by a large number of distinguished scientists, working in various parts of India.

Communications regarding contributions for publication in the journal should be addressed to the Editor, Indian Journal of Pure & Applied Physics, Publications & Information Directorate, Hillside Road, New Delhi 110012.

Correspondence regarding subscriptions and advertisements should be addressed to the Sales & Distribution Officer, Publications & Information Directorate, New Delhi 110012.

Annual Subscription
Rs. 120.00 £20.00 $45.00

Single Copy
Rs. 12.00 £2.00 $4.50

50% Discount is admissible to research workers and students and 25% discount to non-research individuals, on annual subscription. Payments in respect of subscriptions and advertisements may be sent by cheque, bank draft. money order or postal order marked payable *only* to **Publications & Information Directorate, New Delhi 110012.** Claims for missing numbers of the journal will be allowed only if received within 3 months of the date of issue of the journal plus the time normally required for postal delivery of the journal and the claim.

Announcements

Grant of Financial Assistance to Scientists for Attending International Conferences Abroad

The Indian National Science Academy (INSA) invites applications from scientists interested to avail of financial support from the Academy for attending international conferences to be held abroad during 1984-85. Preference in selection of candidates will be given to those who have been invited to deliver plenary lecture/preside over a session or whose paper has been accepted for presentation and who will be provided subsistence allowance during their stay abroad by some agency. Support by INSA will be limited to a maximum of half international travel plus half maintenance allowance for the duration of the conference and registration for conferences organized by International Council of Scientific Unions. In the case of other conferences the financial support will be limited to a maximum of Rs. 4000/- only. To be eligible for the Young Scientists Travel Grant, the applicant should be 35 years or below on the date of commencement of the conference and the selected candidates will be supported fully or partially for their travel cost by INSA or jointly by INSA and Committee on Science and Technology in Developing Countries. Further details and application forms can be had from:

The Executive Secretary
Indian National Science Academy
Bahadur Shah Zafar Marg
New Delhi 110002

Workshop on X-ray Crystallographic Data Storage, Retrieval & Dissemination

The National Information Centre for Crystallography (NICRYS) has announced the organization of its first workshop on the above topic during 28-30 November 1983. The object of the workshop is to bring together both current as well as potential users of NICRYS data facility, for discussion and mutual exchange of views. The workshop will have the following programme:

Brief outline courses on the methods of use of the data facility followed by illustrative talks.

Reports of experiences of users and their views with regard to possible improvements.

Discussion of future activities of the centre and possible enlargement of the circle of potential users.

As the workshop is limited to 30 participants and a limited number of 'observers who may be potential users, those interested should immediately contact:

The Convener, NICRYS Workshop
Department of Crystallography and Biophysics
University of Madras,
Madras 600025

Indian Journal of Pure & Applied Physics

VOLUME 21 NUMBER 9 SEPTEMBER 1983

CONTENTS

Continued overleaf

CONTENTS

---

*The author to whom all correspondence is to be addressed is indicated by the (*) mark.

Indian Journal of Pure & Applied Physics
Vol 21, September 1983, pp. 493-497

Negative Resistance in Si P^+-N-N^+ Structures & Generation of Microwave Power

ASHOK K SAXENA†* & W S KHOKLE
Solid State Devices Division, Central Electronics Engineering Research Institute, Pilani 333031

Received 28 *August* 1982; *accepted* 11 *March* 1983

P^+-N-N^+ structures have been fabricated in Si by boron diffusion into the n-type epitaxial layers supported by N^+ substrates. The current-voltage characteristics of these diodes have been measured beyond the avalanche breakdown voltage. These characteristics have shown that these devices produce negative resistance. A source of microwave power in the X-band of frequencies has also been developed using these diodes in a tapered waveguide cavity. An average signal strength of ~12 dB has been obtained.

1 Introduction

Since the historic discovery of transistor, there have been many attempts to develop semiconductor devices to operate in the microwave frequency range as amplifiers, oscillators, high speed switches, binary memories, etc. The ability of diodes and transistors to respond faithfully to high frequency external voltage variations is limited primarily by the minority carrier lifetime. Later, Au diffusion was used in semiconductors to increase the recombination rate and to shorten the carrier lifertime by introducing deep energy levels in the forbidden energy gap. By this technique, the lifetime could not be reduced below the nanosecond level and so p-n structures failed to operate in the microwave range.

The observation of negative resistance region in the forward current-voltage characteristic of tunnel diode led to the possibilities of its applications in microwave devices with such desirable features as: (1) negative resistance at low dissipation levels, (2) the high frequency response, (3) low noise characteristics, and (4) relative invariance of its characteristics with temperature. Being a majority carrier device, the tunnel diode has obvious advantages over transistors and diodes due to short tunneling-time of carriers, but its performance is seriously restricted due to very low power handling capability and the difficulty of isolating the input from the output.

The generation of microwave frequencies using reverse biased p-n junction diodes aroused much interest in the dc characteristics of such diodes beyond the avalanche breakdown voltage. Avalanche diodes can be designed and operated in various modes. The first of these is called the IMPATT mode—an acronym for IMPact Avalanche and Transit Time. A typical structure is N^+-P-I-P^+ and is called the Read diode after its discoverer. It consists of two regions: (1) a narrow avalanche region in the P-type layer in which the carriers multiply due to impact ionization when the device is reverse biased; and (2) a drift region in the I (intrinsic)-layer in which the carriers drift with saturated velocities due to high electric field. The negative resistance in the Read diode occurs due to the phase shift between terminal current and voltage of the diode. This phase shift consists of two parts: (1) phase delay of 90° caused by the avalanche multiplication; and (2) an additional phase delay caused by the finite transit time of avalanche generated carriers drifting through the I-layer. It is thus obvious that the external current is more than 90° out of phase with the voltage, causing the resistance to be negative. For a detailed study, the reader is referred to an article by Schroeder and Haddad[1].

The Read diode is a convenient structure for a theoretical analysis and physical understanding but at the same time more difficult to fabricate in the laboratory. The most widely used IMPATT diode structure is of the type P^+-N-N^+ or its complementary N^+-P-P^+ type. This three layer structure is much easier to fabricate than the four layer structure of Read diode. At high current densities, the current-voltage characteristics of these three layer structures reverse biased into avalanche breakdown region are determined by the space charge of current carriers. The influence of this charge can lead either to negative or positive static resistance depending upon the various device parameters[2]. The second mode of operation of avalanche diodes is called the TRAPATT mode—an acronym for TRAPped Avalanche and Transit Time[3]. For this mode of operation, the operating current densities are higher than for IMPATT mode but the frequency is much lower than the transit time mode frequency. In addition to these p-n junction devices,

† Present address: Department of Electronics and Communication Engineering, University of Roorkee, Roorkee 247672

there are some special materials from groups 3-5 (GaAs, InP, etc.) which also show negative resistance but due to the intervalley electron transfer of electrons in the various conduction bands. For a detailed study of the utility of negative resistance in semiconductor, the reader is referred to the well known monograph by Roy[4].

In the present paper, we have described the fabrication of various diodes of P^+-N-N^+ type in Si and measured their current-voltage characteristics beyond the avalanche breakdown voltage. The dc negative resistance has been observed in these structures. A microwave cavity has been developed in the X-band using rectangular waveguide. These diodes have proved useful as good sources for microwave power when used in this cavity.

2 Device Structure and Fabrication

A typical diode structure and impurity profile are shown in Fig. 1 where N_a = acceptor concentration, N_d = donor concentration, N_1 = surface concentration in the P^+ layer, N_2 = donor concentration in the substrate, N_o = donor concentration in N-layer, x_o = thickness of the n-type epitaxial layer and $x_a = P^+$ diffusion depth.

The fabrication process starts with a Si wafer consisting of N-type epitaxial layer supported by a heavily doped N^+ substrate. To form the P^+-N junction, boron was diffused into the epitaxial N-layer and the required junction depth x_a and surface concentration N_1 were obtained by subsequent 'drive in' process. This gives a complementary error function type of impurity distribution in the P^+ layer as shown in Fig. 1(b). Four-point probe method of resistivity measurement[5] was used to measure the surface concentration and impurity profile in the P^+ layer.

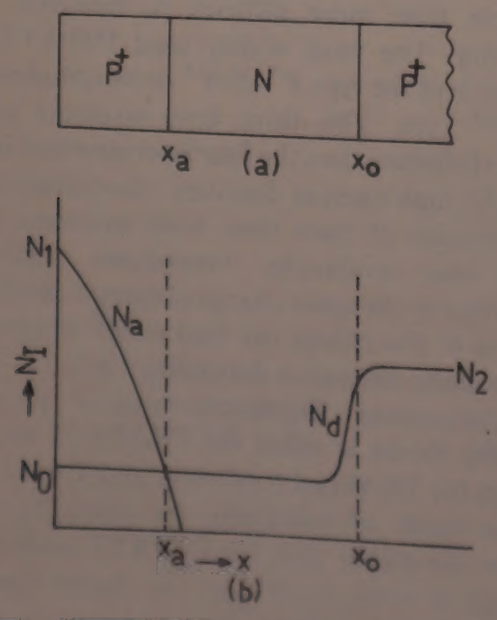

Fig. 1—(a) Device structure and (b) impurity profile

The junction depth and hence the width of the N-region after diffusion were determined by the method of junction staining[5].

After diffusion, the N^+ substrate was thinned down to remove any back diffusion and then high purity Al metal was used to make the ohmic contact to the substrate. The slice was then diced into individual diodes and each diode mounted on an Au plated Kovar pedestal with the N^+ substrate in contact with the pedestal. A thin Au wire was then bonded on the P^+ layer and then the standard Mesa structure was obtained to avoid the edge breakdown in the diodes. The diodes were closed with a Au plated Kovar cap, insulated from the pedestal by a ceramic ring housing the diode.

3 Measurements

To operate the diodes into avalanche region, high current densities are needed. If we want to go into IMPATT or TRAPATT mode of oscillations of the diode, the current densities may be much higher than this. Here we encounter one problem because if we apply pure dc bias to the diode, large currents will flow near the breakdown and the diode will be burnt due to excessive heating at the junction. To avoid this heating effect in diodes at high currents, the diode is operated under pulses of short duration superimposed on dc just below the breakdown voltage.

The experimental arrangement is shown in Fig. 2. Because of the short pulses, the current flows only for a short period of time and thus the excessive heating at the junction is avoided. The current through the diode I_d is measured as the voltage drop $(V_1 - V_2)$ across a 50 ohm resistance in series with the diode. The diode voltage V_d is just the voltage V_2 which was measured directly on a calibrated oscilloscope. The pulse width could be varied from 30 ns to 1000 ns and the maximum pulse amplitude was nearly 40 V. It was not possible to take observations below 200 ns because of a little ringing problem in the output pulse. All the measurements were taken at a peak repetition frequency of 1 kHz. The two capacitors in the circuit serve the purpose of isolating the dc signal from the ac.

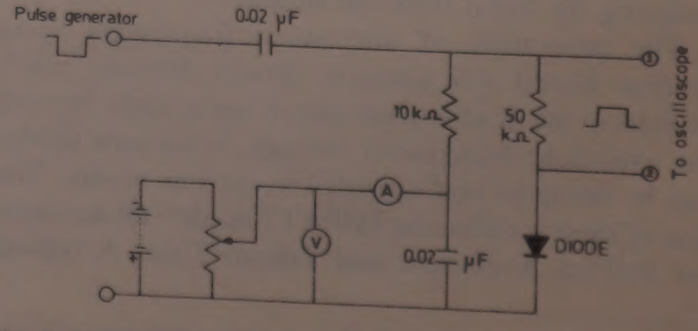

Fig. 2—Experimental arrangement for the measurement of current-voltage characteristics of the diode

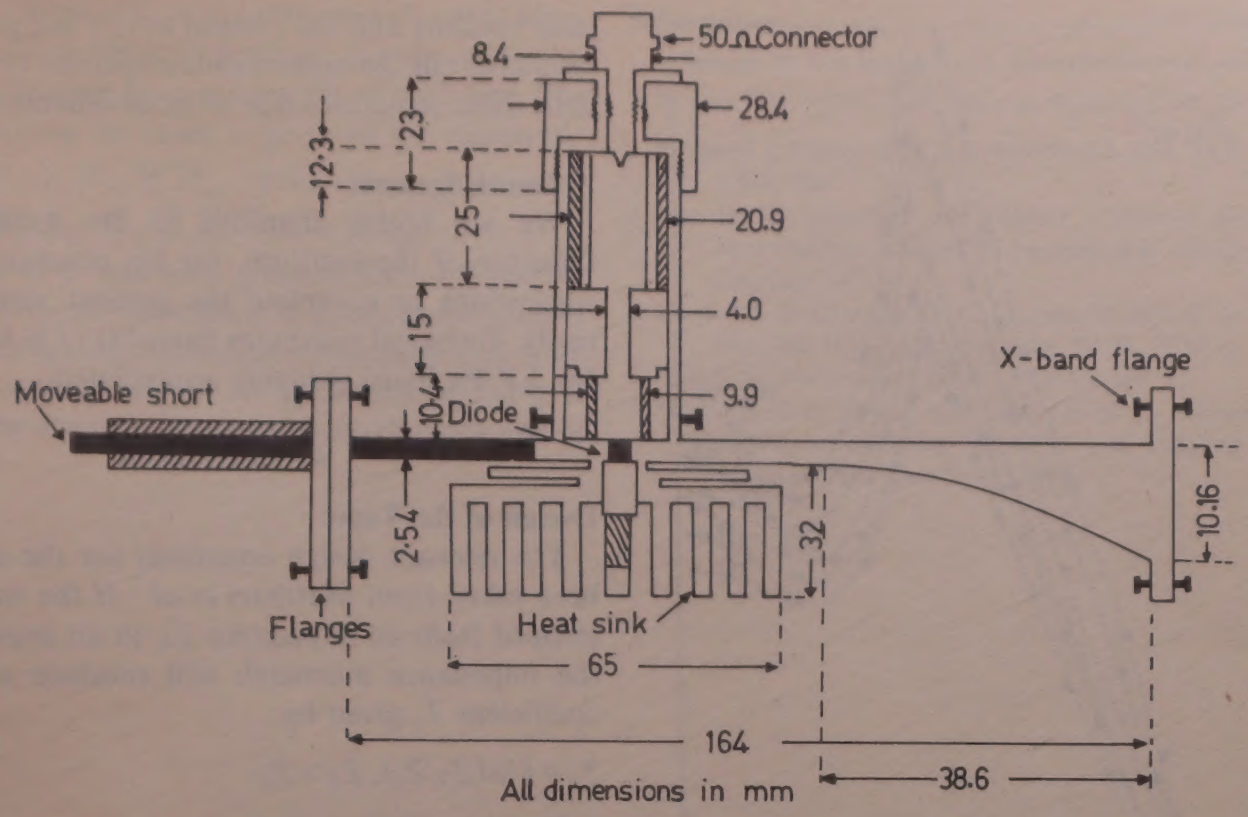

Fig. 3—Details of the microwave cavity

4 Microwave Cavity and Experimental Arrangement

A Dolph-Chebyshev type of microwave cavity has been designed in a rectangular waveguide for operation in the X-band of frequencies (8.2 to 12.4 GHz). This type of filter gives the shortest length of taper for a given improvement in reflection coefficient, in addition to good impedance matching between the diode and the microwave circuit[6]. Such a cavity has been designed (Appendix A) and the details are shown in Fig. 3. The waveguide portion consists of a taper with a moveable short at one end as shown. To effectively dissipate the joule heat, an integrated heat sink has been provided below the diode. The bias to the diode is applied through the 50 ohm coaxial connector and a coaxial cavity which isolates the dc and rf signals.

A photograph of the complete experimental arrangement for the oscillator is shown in Fig. 4. As shown, the output from the cavity is fed to a waveguide type screw tuner and then to an attenuator. Finally the output from the attenuator is given to a crystal detector which is connected to a VSWR meter. The bias to the diode is applied as explained in Fig. 2. When a slotted section was inserted in the circuit (not shown in the photograph), the signal strength was measured on a VSWR meter as a function of the detector position on the slot.

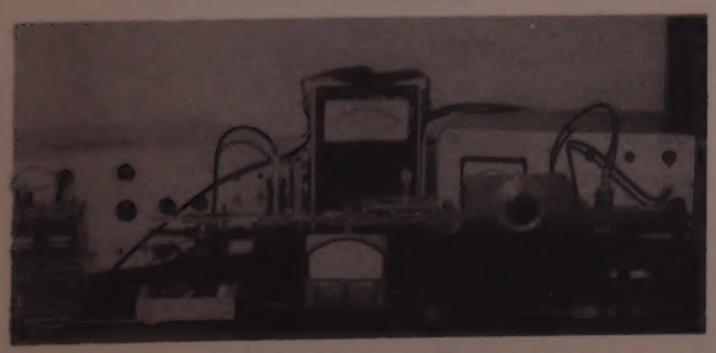

Fig. 4—Complete experimental set-up of the oscillator

5 Results and Discussion

The current (I_d)-voltage (V_d) characteristics of a diode are shown in Fig. 5 for various pulse widths w_p. As the diode voltage is increased by increasing the pulse height, the diode current increases, reaches a peak at a critical voltage and then decreases. Thus negative resistance is produced at the device terminals, which is also found to be dependent upon the pulse width. If the dc bias on the diode is increased, then the current through the diode also increases without changing the nature of the I_d-V_d curves. After a certain voltage, the current I_d again increases slowly with the voltage, giving a positive device resistance.

In Fig. 6, we have plotted the strength of the microwave signal obtained from the oscillator circuit of Fig. 4, as a function of the detector position on the slotted section. The oscillator gives about 12 dB average signal strength, which should be sufficient for many applications.

The same diodes could also be used for operation in the TRAPATT mode for which the operating current

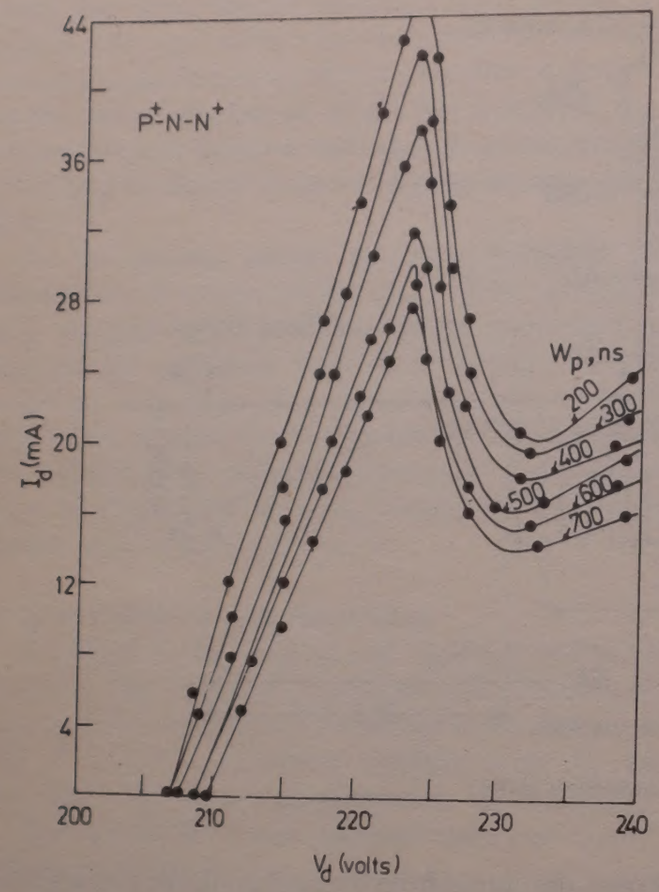

Fig. 5—Typical current-voltage characteristics of a diode

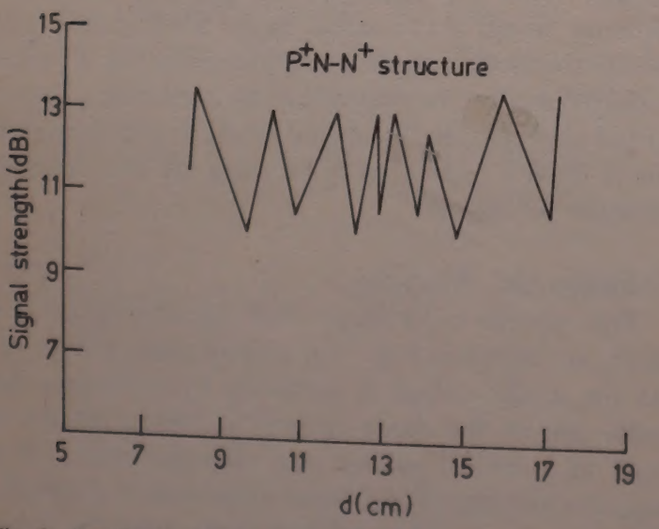

Fig. 6—Oscillator signal strength as a function of the detector position on the slotted section

levels are much higher than the IMPATT mode. The increased current level will also increase the heat dissipation within the *p-n* junction, most of which is dissipated within the semiconductor layers, thus resulting in high junction temperature. These excessive temperatures deteriorate the device performance and ultimately cause device failure. A technique which is generally applied to solve this problem is the flip chip bonding of the diode, i.e. for P^+-N-N^+ diodes, the P^+ surface is in contact with the pedestal instead of the N^+ surface. The diodes were also fabricated with this flip chip bonding and the coaxial cavity designed for this oscillator but the experiments could not be completed with these structures due to nonavailability of time.

Acknowledgement

We are highly thankful to Dr Amarjit Singh, Director of the institute, for his constant help and suggestions to complete the present work satisfactorily. Technical assistance from Mr G N Murthy and Mr J P Pachauri is highly appreciated.

APPENDIX A

Design of the Taper

The relevant design equations for the cavity have been taken from Matthaei *et al.*[7] If the waveguide is stepped from an impedance Z_0 to an impedance Z_T, the impedance mismatch will produce a reflection coefficient T_o given by

$$T_o = \tfrac{1}{2}\ln(Z_T/Z_o),\ Z_T > Z_0 \qquad \ldots (1)$$

For the Dolph-Chebyshev filter, the relation between the cut-off wavelength λ_{gc} and the reduction ratio P is

$$P = T/T_o = 1/\cosh(2\pi l/\lambda_{gc}) \qquad \ldots (2)$$

where l is the length of the taper. All wavelengths shorter than λ_{gc} will give a reduction of mismatch equal to or better than P.

Let a and b represent the width and height of the waveguide. If subscripts 1 and 2 refer to the narrow and wide ends of the taper respectively, then $a = 22.86$ mm, $b_1 = 2.54$ mm, $b_2 = 10.16$ mm. Let $P = 0.01$. Now

$$\frac{\lambda_{gc}}{\lambda} = \frac{\lambda_c}{\sqrt{\lambda c^2 - \lambda^2}} \qquad \ldots (3)$$

where $\lambda_c = 2a$ is the cut-off wavelength for the dominant TE_{10} mode of transmission, λ = free-space wavelength at mid frequency of the X-band. Thus λ_{gc} and hence l is calculated from Eq. (2) as 38.6 mm. The waveguide impedance is

$$Z = 754(b/a)(\lambda_{gc}/\lambda) \qquad \ldots (4)$$

Table 1—Calculated Values of x and b

x(mm)	b(mm)
0	10.16
4.82	9.56
9.65	8.40
14.47	6.73
19.30	5.07
24.12	3.83
28.95	3.07
33.77	2.69
38.60	2.54

Thus, we find that $Z_1 = 111$ ohm and $Z_2 = 444$ ohm. The minimum number of sections for the taper are found to be 8, each having a length of 4.82 mm. The impednace along the taper is given by the relations.

$$Z(+x/l) = (Z_2/Z_1)^{Q} \sqrt{Z_1 Z_2}, \quad \tfrac{1}{2} > x > 0$$
$$Z(-x/l) = (Z_2/Z_1)^{-Q} \sqrt{Z_1 Z_2} \quad 0 > x > -\tfrac{1}{2} \qquad \ldots (5)$$

The value of Q has been given in Ref. 7. Thus for various sections the impedance Z is calculated and, in turn, the waveguide dimension b is determined from Eq. (4). Calculated results are presented in Table 1, where x is the distance measured from the wide end of the taper.

References

1 Schroeder W E & Haddad G I, *Proc IEEE (USA)*, **61** (1973) 153.

2 Bowers H C, *IEEE Trans Electron Devices (USA)*, **15** (1968) 343.

3 Prager H J, Chang K K N & Weisbrod S, *Proc IEEE (USA)*, **55** (1967) 586.

4 Roy D K, *Tunneling and negative resistance phenomena in semiconductors*, edited by Pamplin B R, (Pergamon Press, London) 1977.

5 Kane P F & Larrabee G B, *Characterization of semiconductor materials* (Mc-Graw Hill, New York), 1970, p. 92 & 224.

6 Hall A H, *Microwave J (USA)*, **3** (1966) 109.

7 Matthaei G L, Young L & Jones E M T, *Microwave filters, impedance, matching networks and coupling structures* (McGraw Hill, New York) 1964.

Indian Journal of Pure & Applied Physics
Vol 21, September 1983, pp. 498-500

Effect of Electrode Resistance on Characteristics of Pb-Pb_xO_y-Pb Tunnel Junctions

A K GUPTA*, V S TOMAR & N D KATARIA
Low Temperature Section, National Physical Laboratory, New Delhi 110012

Received 5 *October* 1982

Lead-lead oxide-lead tunnel junctions have been made in a cross-type geometry and the temperature dependence of the junction resistance has been studied in detail from room temperature to liquid helium temperature. High resistance junctions ($\sim 1000\,\Omega$) show an increase in their resistance by about 20% as the temperature is lowered from room temperature (RT) to liquid helium temperature, while the low resistance junctions ($< 1\,\Omega$) show an anomalous behaviour. The I-V characteristics of such junctions indicated a negative slope at RT, which as the temperature is lowered increases, becomes infinite at a particular temperature and ultimately turns positive. It is shown that, even by adopting the four-probe technique for the measurement of conductivity, the electrode resistance makes a finite contribution and thus the effective resistance, instead of the true one, of the junction is actually measured.

1 Introduction

Tunnel junctions are very often made in a cross-type geometry by first depositing a metal film for base electrode, oxidizing its surface to form a suitable barrier and subsequently depositing another film perpendicular to the first one to serve as another electrode. The usual four-terminal technique as shown in Fig. 1 is used to measure the junction characteristics to eliminate resistances associated with contacts, measurement leads and the metal films serving as electrodes. It has been often observed[1] that the conductance of a metal-insulator-superconductor tunnel junction shifts discontinuously as the superconducting electrode turns normal. Osmun[2] has recently shown that this discontinuous shift is due to the finite resistance of the electrode in the normal (nonsuperconducting) state which is not eliminated in the usual four-terminal configuration. While studying the temperature dependence[3] of the I-V characteristics of Pb-Pb_xO_y-Pb Josephson tunnel junctions whose electrode resistances in the normal state are usually comparable to that of the junction resistance, we have found that it is almost impossible to measure the true resistance of the junction in the normal state due to the effect of the finite electrode resistance. Only when the electrode film becomes superconducting, the true resistance of the junction could be measured.

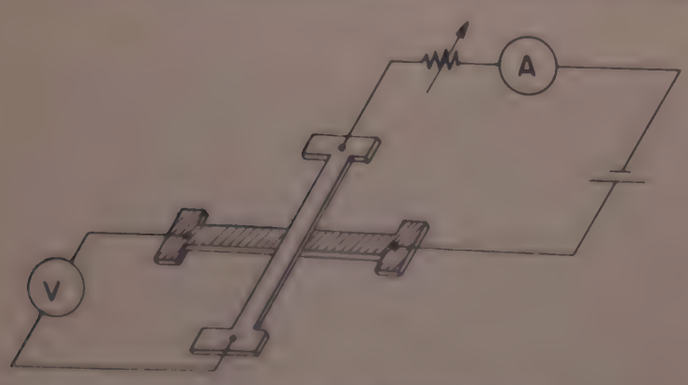

Fig 1 Schematic diagram of the four-terminal technique for measurement of characteristics of the tunnel junctions

2 Experimental Details

The Josephson junctions used in the present investigation were prepared on 1 in × 1 in microscope glass slides by thermal evaporation of 99.9999% pure lead in a vacuum of the order of 5×10^{-6} Torr. The details of fabrication technique are described elsewhere[4] and only the salient features are given here. The films were made by evaporating the lead through metal masks. The junction dimensions were 0.1×0.2 mm^2. After depositing the first film, dry oxygen was admitted into the vacuum chamber through a needle valve and the substrates were heated by infrared radiation to about 50°C by keeping an infrared lamp outside the glass belljar. The substrate temperature was monitored with the help of a copper-constantan thermocouple. The substrates were, in general, maintained at elevated temperature for about 1 hr and were subsequently allowed to cool for $\frac{1}{2}$ hr in an oxygen atmosphere to fabricate low-resistance junctions. However, by suitably changing these parameters, we were able to make the tunnel junctions with any desired resistance ranging from a few milli-ohms to several kilo-ohms. Electrical contacts to the thin film electrodes were made using indium. The junctions were mounted inside a magnetically shielded dewar and their characteristics were recorded using standard biasing and recording circuitry.

3 Results and Discussion

The junctions showed good tunnelling characteristics at the liquid helium temperature (LHT). Typical

I-V characteristics of a low-resistance junction at different temperatures are shown in Fig. 2. At 4.2 K, the lead is in the superconducting state, the *I-V* characteristic resembles that of an ideal Josephson tunnel junction. As the biasing current is increased, zero voltage supercurrent due to the dc Josephson effect is observed up to a critical current value (3.4 mA) above which switching to superconducting energy gap value takes place, and the usual quasi-particle tunnelling curve is followed. In the reverse path, the junction follows the quasi-particle curve. Fig. 3 shows the variation of the critical current with external magnetic field which is produced by passing current in a solenoid. A typical diffraction pattern type behaviour is obtained. The zero-voltage supercurrent is found to be absent in high-resistance junctions and only the quasi-particle tunnelling curve is observed. These results indicate that the junction barrier does not contain any metallic shorts and only tunnelling current is present[5].

When the resistances of both high- and low-resistance junctions were measured as a function of temperature, entirely different types of behaviour were observed. For high-resistance junctions ($\sim$1000 ohms), the measured value of its resistance (R_m) increased by about 20% in going from RT down to LHT. However, for low-resistance junctions, peculiar behaviour was observed. As shown in Fig. 2, negative slope in *I-V* curves was observed at RT which amounts to negative resistance. As the temperature was lowered, the value of R_m increases, passes through zero and then turns positive. It was also observed that, by just increasing the film thickness (which amounts to a decrease in the electrode resistance) and keeping all other parameters unchanged, the temperature at which R_m becomes zero shifted towards higher temperatures.

The above results clearly indicate that R_m is affected by the electrode resistances and it is not the true resistance of the junction. In the case of high-resistance

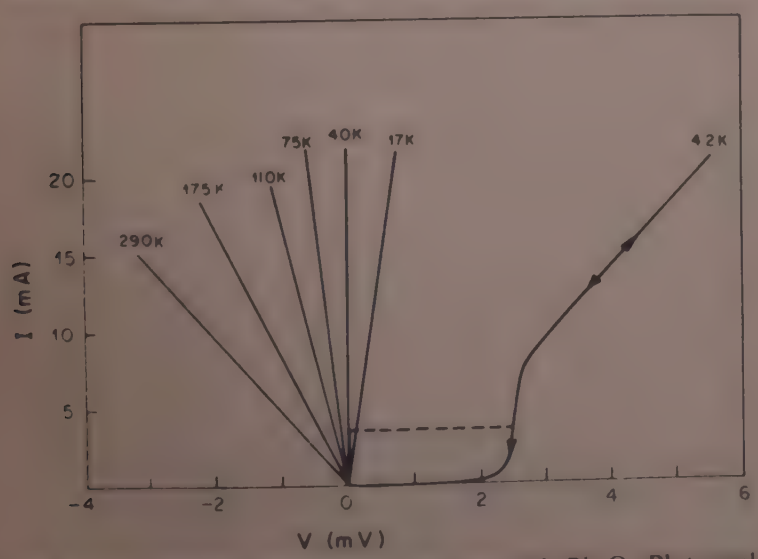

Fig. 2 *I-V* characteristics of a low-resistance Pb-Pb_xO_y-Pb tunnel junction at different temperatures

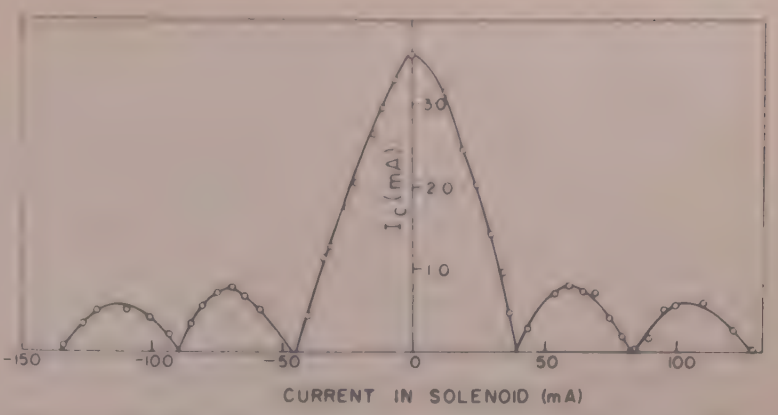

Fig. 3—Variation of the critical current with applied magnetic field which is produced by passing current in a solenoid

Table 1—Temperature Dependence of R_m, R_1 and R_2

(Values of R_m, R_1 and R_2 in ohms)

Temp. K	R_m	R_1	R_2
290	−0.210	3.66	18.33
175	−0.120	2.12	10.39
110	−0.060	1.50	7.41
75	−0.030	1.09	5.38
40	+0.003	0.63	3.11
17	+0.030	0.29	1.41
4.2	+0.45 ($R_m = R_t$)	0	0

junctions, the electrode resistance is negligible as compared to the junction resistance; thus R_m is not affected significantly. However, for the low-resistance junctions, as shown in Table 1 the RT value of the electrode resistances R_1(top) and R_2(bottom) is significantly greater than that of the junction resistance. The electrode resistance thus seriously affects R_m and makes it even negative. As the temperature is lowered, the resistance of the metal electrode decreases while the resistance of the tunnel junction (R_t) remains more or less constant. Thus its effect on R_m decreases with lowering of the temperature. This explains qualitatively the curves of Fig. 2. It may, however, be noted that even at 17 K, R_m is much different from R_t. Thus, as long as the electrodes are in the nonsuperconducting state, the measured value of the junction resistance is different from the actual resistance.

Recent measurements by Osmun[2] on tunnel junctions of MoRe-I-Metal system where the alloy film has high resistance in the normal state has also shown that the discontinuous shift in the conductance, when MoRe becomes normal, is due to electrode resistance. In this work[2], the effect of the finite resistance of only top electrode (alloy film) has been considered, the resistance of the bottom electrode (pure metal film) is considered to be negligible. In a four-terminal measurement in a cross-type junction the biasing current I is supplied from one edge of the oxide while

the voltage V_m is measured from the opposite edge. As the current flows along the face of the oxide it undergoes a potential drop due to the finite electrode resistance, resulting in a voltage profile along the oxide face. V_m is actually the minimum voltage across the oxide barrier. When the electrode is superconducting, the voltage is constant across the barrier surface and equal to V_m. As a result of this, the measured conductance G in the normal state is greater than the conductance in the superconducting state. Osmun[2] has derived an expression for the conductance for this case. If G_0 is the true conductance and $G(V_m)$ is the measured conductance, then

$$G(V_m)=G_0\sum_{n=0}^{\infty}\frac{(G_0R)^n}{(2n+1)!} \quad \ldots (1)$$

For $G_0R<1$, one may write

$$G=G_0+\frac{G_0^2R}{3!} \quad \ldots (2)$$

Thus the effect of the resistance of only one electrode is to increase the value of the conductance or to decrease the value of the resistance. It is consistent with our results except that it does not explain the observation of negative resistance at higher temperatures. However, it may be noted that, in our case, the resistances of both the electrodes are comparable to that of the tunnel junction and the resultant effect of the potential gradients at both the electrodes will have to be considered. It is, therefore, desirable to derive a generalized expression for the resistance on similar lines.

Acknowledgement

The authors are grateful to the Director, National Physical Laboratory, New Delhi for providing facilities and to Dr (Mrs) Madhu Prasad for help during early phase of the experimental work.

References

1 McMillan W L & Rowell J M, Tunnelling and strong coupling superconductivity, in *Superconductivity*, Vol 1, edited by R D Parks (Marcel Dekker, New York) 1969, 561.

2 Osmun J W, *Phys Rev B (USA)*, **21** (1980) 2829.

3 Prasad M, Gupta A K, Kataria N D & Tomar V S, *Study of lead-lead oxide-lead tunnel junctions down to liquid nitrogen temperatures*, paper presented at the Fourth National Symposium on Cryogenics, Bombay, 17-19 December 1979.

4 Prasad M, Gupta A K, Tomar V S & Kataria N D, *Indian J Cryogenics*, **6** (1981) 192.

5 Taylor B N, *J Appl Phys (USA)*, **39** (1968) 2490.

Indian Journal of Pure & Applied Physics
Vol 21, September 1983, pp. 501-505

Effects of Gamma Radiation and Rare Earth Additives on the Insulation of Sodium Silicate Glasses

A TAWANSI†, A F BASHA‡, M M ORSI* & S El-KONSOL††

Received 24 *June* 1981; *revised received* 16 *August* 1983

The dc resistivity of Na_2O-SiO_2-CaO glasses containing Ce^{3+}, Ce^{4+} and mixtures of $Ce^{3+}+Cu^{+}$ and $Ce^{4+}+Cu^{2+}$ ions was studied over the temperature range 303-623 K. The results were interpreted within the framework of the polaron hopping conduction mechanism of Mott and Davies. Experimental results indicated that Ce^{4+} forms stronger bonding than Ce^{3+} and that the lack of hopping sites in Ce^{4+}-glass is responsible for its higher resistivity value. Also some sort of electronic mutual interaction between Ce^{3+}, Cu^{+} and Cu^{2+} in the same glass matrix is considered to be of more impeding effect on the conduction process. The increased glass resistivity due to relatively low gamma radiation was ascribed to the impeding effect of the scattering of charge carriers and their decreasing mobility, while the increase due to tempering effect was ascribed to glass compaction. The relatively decreased resistivity at high gamma radiation dose was ascribed to the significant increase of the gamma-induced defects and charge carriers.

1 Introduction

Most of the rare earth (RE) metals (with the exception of Eu, Yb and one phase of Ce) are considered to have three valence electrons and this is the configuration assumed in all band studies done to-date. The atomic 5*d* and 6*s* states lie close to one another in energy and are widely separated from the 4*f* level. One expects the 5*d* and 6*s* electrons to form the conduction bands in metals and hence contribute to the conduction processes independently of the 4*f* electrons. The contribution to the conduction bandwidth from the 5*d* electrons is expected to be somewhat less than that of the 6*s* electrons since the spatial overlap of the 5*d* functions is somewhat less than that of the 6*s* functions. Note that this is expected to bear a strong similarity to the situation found in transition metals (TM).

Whereas the 5*d* and 6*s* electrons are far away from the nucleus, the 4*f* electrons are tightly bound to the atom and so they do not overlap the neighbouring atoms appreciably. As a result, the 4*f* electrons will form a very narrow energy band in the metal. The *d* electrons are similarly, but less strongly, confined and they form energy bands of narrow to moderate widths, because, being mostly localized, they can tunnel through the potential barrier. Their quasi-band nature accounts for the fact that the *d* band electrons exhibit both localized and itinerant properties[1].

The electronic band structure of metallic Ce in its two allotropic fcc forms (γ and α) has been extensively studied by Waber and Switendick[2]. Interest in this metal arises particularly from the α-γ phase transition (which is thought to be related to a change in occupation of the 4*f* level), and from the associated anomalous behaviour of the resistivity for the metal (by itself or as an impurity in other metals[3]). Burr and Ehara[4] measured the susceptibility at high temperatures (through the melting point) and found no evidence of a 4*f* to 5*d* electron transfer. Since no proposed configuration for cerium metal was generally accepted, five different atomic configurations $4f^{2-x}5d^{x}6s^{2}$ (with $x=0$, 0.5, 1.0, 1.5 and 2.0) were determined from relativistic HFS wavefunction[1]. Waber and Switendick[2] found a great sensitivity of the position of the 4*f* band to the assumed atomic configuration.

The importance of interband mixing (or hybridization) has come to some prominence as a consequence of the anomalous behaviour of cerium metal and its alloys[5]. This behaviour is thought to be associated[6] with the proximity of the cerium 4*f* level to the Fermi level, E_f. Alloys with cerium impurities are magnetic when the 4*f* level is below E_F and nonmagnetic when it is above E_F (Ref. 7). The closeness of E_{4f} to E_F makes interband effects large in the case of Ce.

The transitions of rare earth atoms have been extensively studied because these atoms, as additives in glass, have laser applications[8], while those of 3*d*-series have been the cause of pigmentation in glass since historical times. However, even today Ce remains the least well understood rare earth metal, in either polycrystalline or glassy matrices.

The present work concerns with the role of Ce (as a multivalence RE element) in the conduction mechanism of Na_2O-SiO_2-CaO-Ce_2O glasses. Also

† Physics Department, Mansoura University, Egypt
‡ Physics Department, Cairo University, Egypt
* Glass Research Division, National Research Centre, Dokki, Cairo, Egypt (Author for correspondence)
†† Reactor and Neutron Physics Department, Atomic Energy Establishment, Egypt

Table 1—Remarks on the Glass Samples with Various Amounts of CeO_2 and CuO (in g) per 100 g

Sample	CeO_2	CuO	Valency of		Melted at 1723 K under conditions
			Ce	Cu	
G-I	0.35	—	3+	—	Reducing*
G-II	0.35	—	4+	—	Normal
G-III	0.35	0.1	3+	1+	Reducing*
G-IV	0.35	0.1	4+	·2+	Normal

* 10 g of tartaric acid was added per 100 g of the glasses.

the effect of mixing Ce^{3+} with Cu^{3+} and/or Cu^{2+} on the conductivity of the same glass matrix is investigated.

2 Experimental Details

2.1 Sample Preparation

Glasses of the base composition: $72SiO_2.18Na_2O.10CaO$(wt %) were prepared using A R chemical grade materials. Sodium and calcium oxides were added as their respective carbonates. Washed white sand was used to introduce SiO_2. Copper and cerium oxides were added as: CuO and CeO_2. The batches of the glasses were melted at 1723 K in Pt-Rh crucibles in an electrically heated furnace under the conditions illustrated in Table 1. The melts were cast into discs and annealed at 773 K for 2 hr, after which the furnace was switched off to cool to room temperature. The specimens were then ground and well polished to obtain discs 2 mm thick for electrical measurements.

2.2 Irradiation Facilities and Electrical Measurements

The glass specimens were exposed to different γ-ray doses from a ^{60}Co gamma source (6300 Ci) with a dose rate of 6.316×10^4 rad/hr at room temperature. The dc electrical resistivities of (the irradiated) specimens were measured after 2 hr of irradiation. A simple indirect method was used to measure the resistivity and the details of the electrical circuit are presented elsewhere[9]. The applied field used was 500 V/cm, which lies in the ohmic range.

3 Results and Discussion

Fig. 1 shows the dependence of $\ln(\rho/T)$ with $1/T$ for the untempered and unirradiated glass samples studied. This dependence is characterized by two temperature regions. The lower temperature region at which the resistivity increases with temperature. And the higher temperature region at which $\ln(\rho T)$ is a linearly increasing function of $1/T$. The moisture and humidity content in the samples used may be taken as an attribution to the lower temperature region behaviour. The behaviour of the higher temperature region can be discussed in the following way. For a strongly disordered system (such as the glasses employed here), the main transport mechanism is the electronic hopping, i.e. the change in the occupation of localized states, that are in contact with a phonon heat bath[10]. Here a suitable formula for the resistivity, similar to that used by Austin and Mott[11] is

$$\ln(\rho/T)=\ln\left[\frac{RK}{e^2C(1-C)}\right]+2\gamma R+\frac{W}{KT} \quad \ldots (1)$$

where R is the mean distance between the ions, C and $(1-C)$ are the proportions of Ce^{3+} and Ce^{4+} respectively, ν is the rate of decay of the wavefunction, $(\psi \sim \exp(-\nu R))$ of an electron on Ce^{4+}, and

$$W=W_H+\frac{1}{2}W_D \quad \ldots (2)$$

In Eq. (2), W_H is the energy of polaron formation and W_D the Miller-Abrahams term. W_D is also called the disorder energy, which is the energy difference between initial and final sites due to variations in the local arrangements of the RE ions.

It is seen from Fig. 1 that glass G-II (containing Ce^{4+}) has a higher resistivity than that for glass G-I (containing Ce^{3+}). This can be interpreted if we consider that Ce^{4+} forms covalent bonds which are stronger than the Ce^{3+} ionic bonds. Thus it might be considered that the decrease in the hopping sites (and free charge carriers) in Ce^{4+} glass is responsible for its higher resistivity.

According to Bandyopadhyay and Isard[12] it was believed that hopping between neighbouring ions of different TM elements is evidently more favourable, energetically, than the hopping between ions of the

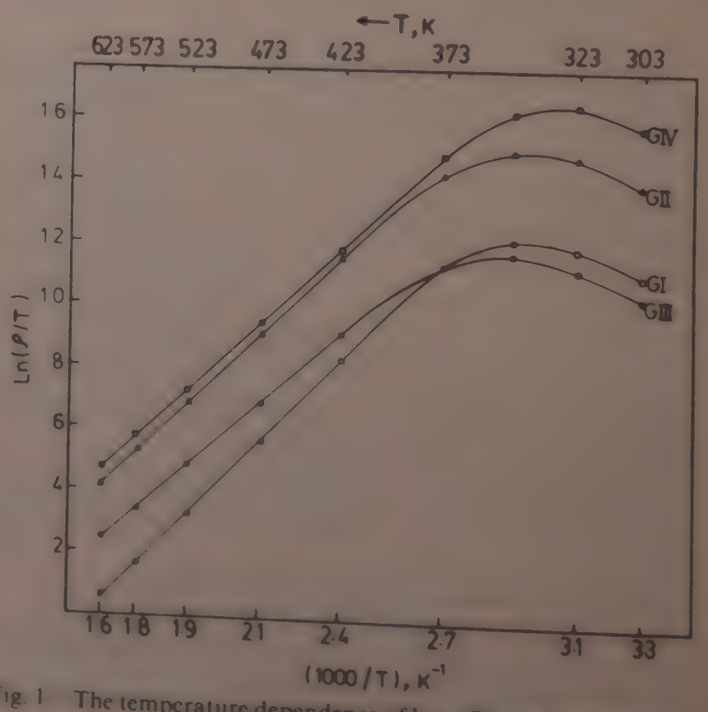

Fig. 1 The temperature dependence of $\ln(\rho T)$ for the untempered and unirradiated glasses

same element at greater average distance. However, the results shown in Fig. 1 point to a different conclusion; the resistivity of G-III and G-IV is higher than that for G-I. This might be interpreted as follows. Ce^{3+} has 4 highly localized 4*f*-electrons. On the other hand, Cu^{4+} and Cu^{2+} are of 3*d* itinerant electrons. According to Mott and Davis[13] the hopping process is enhanced in the highly localized states, i.e. RE-containing glass (sample G-I) must be of lower resistivity than of the RE-TM mixed one (samples G-III and G-IV). This agrees with our present results.

In a previous work[9], the present authors investigated the conduction mechanism of sodium silicate glasses containing Cu, Cu^{+} and/or Cu^{2+}. Comparing these results with the present ones, it is found that glass containing Ce^{3+}, Cu^{+} and Cu^{2+} (sample G-IV) is of higher resistivity than glass samples containing Cu^{+} and/or Cu^{2+}. This may be attributed to some sort of electronic mutual interaction between RE and TM elements. This interaction is thought to be of impeding effect on the conduction mechanism.

Fig. 2 shows the temperature dependence of $\ln(\rho/T)$ for glasses from G-I to G-IV tempered at 873 K for 5 hr. All tempered glasses are of higher resistivity than samples of the untempered ones. This result may be interpreted as that the untempered glass has an open structure of low density which permits larger fraction of charge carriers to participate in the hopping process. On the other hand, the tempered glass has the time to rearrange its structure to a compact one of higher density which inhibits the charge carrier motion. It is worth mentioning that gamma irradiation may also result in a glass compactness[14]. This could be considered as one of the causes for the observed increase of resistivity by γ-irradiation in the present work. The annealing effect, which has been observed in all glass samples, suggests that this effect is intrinsic to the bulk material and may be associated with bond rearrangement. This would support the assumption that the electrically active traps are associated with the bonding defects as suggested by Mott *et al.*[15] and Kastner *et al.*[16]

The reciprocal temperature dependence of $\ln(\rho/T)$ has been studied for all the glasses before and after irradiation with different doses of gamma radiation and similar results were obtained. Fig. 3 shows an example of this observed behaviour. From Fig. 3 and Table 2 it is clear that the value of the critical temperature T_c [defined here as the lower temperature limit of the $\ln(\rho/T)$ versus $(1/T)$ linear range] decreases with increasing radiation dose. This may suggest that the hopping process is enhanced at lower temperatures as the gamma radiation dose was increased as a result of the increase of the irradiation-induced defects.

From Fig. 3 it can be noticed that the resistivity of the glass increases on increasing the gamma radiation dose. Fig. 4 shows this same effect for all the glasses studied, at 393 K. From Fig. 4 it can be seen that glasses G-I and G-III are of similar behaviour; the values of $\ln \rho_{393}$ increase sharply up to a maximum value at about 0.19 Mrad. The resistivity of glasses G-II and G-IV decreases to a minimum at about 0.11 Mrad and increases to a maximum value at

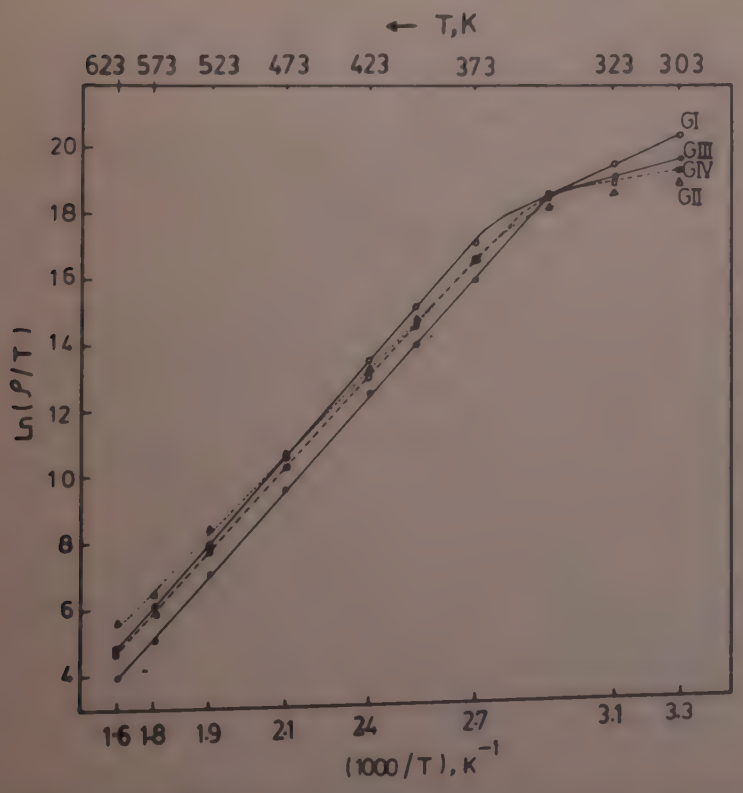

Fig. 2—The temperature dependence of $\ln(\rho/T)$ for glasses tempered at 873 K for 5 hr

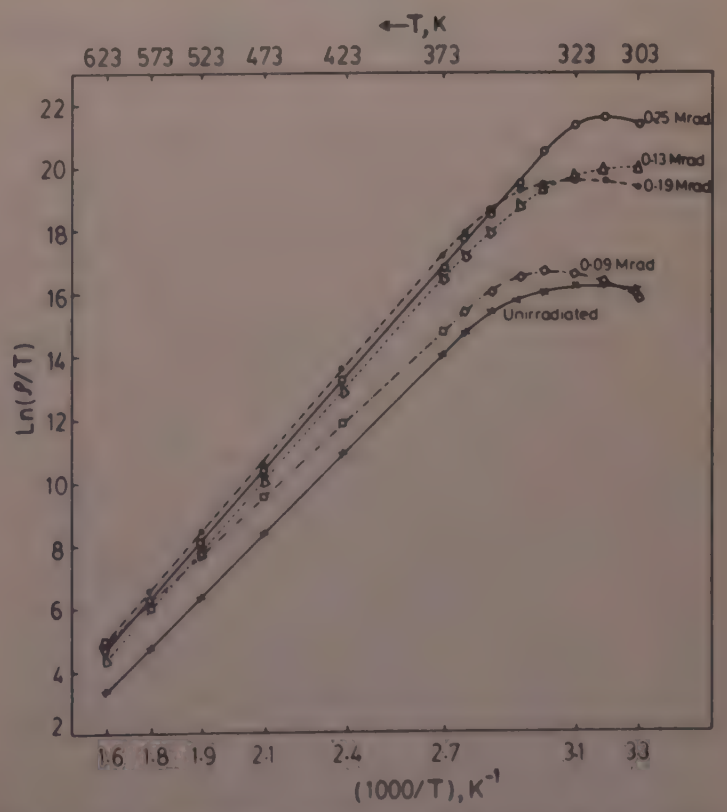

Fig. 3—The temperature dependence of $\ln(\rho/T)$ for glass G-IV before and after irradiation with different doses of gamma radiation

Table 2—Values of T_c (in K) and W (in eV) for All the Glass Samples Before and After Irradiation

Sample No.	Unirradiated*		Irradiated with a gamma dose (in Mrad) of							
			0.09		0.13		0.19		0.25	
	T_c	W	T_c	W	T_c	W	T_c	W	T_c	W
G-I	378 (384)	0.86 (0.87)	371	0.90	367	0.96	360	0.94	352	0.93
G-II	360 (364)	0.75 (0.66)	359	0.81	355	0.82	353	0.87	328	0.97
G-III	344 (387)	0.86 (0.55)	363	0.85	348	0.89	346	0.88	340	0.95
G-IV	356 (359)	0.82 (0.65)	355	0.76	348	0.94	344	0.94	328	0.94

* The values in the parenthesis are for untempered ones.

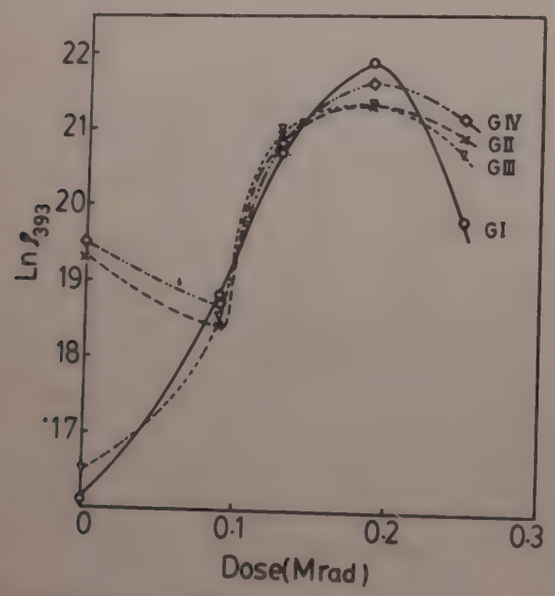

Fig. 4—The effect of gamma radiation on the resistivity (ρ) at 393 K for all the glass samples studied

about 0.19 Mrad. As a general observation (Fig. 4), at doses lower than 0.19 Mrad, the resistivity increases while for higher doses it shows a tendency to decreases.

It is well known[13] that most glasses possess submicroscopic crystalline structure in the form of helices or chains of silica. The substructure is basically random averaged over the volume of the glass, but over distances up to about 10 Å there is some correlation between adjacent SiO_4 tetrahedra. It is the substructure which forms the same electron trap as in bulk silica glass. Accordingly, the increase in resistivity of gamma irradiated samples up to 0.19 Mrad can be attributed to the impeding effect of the scattering of charge carriers and the decrease in their mobility. In addition, gamma irradiation has been reported to cause compaction to the glass structure[14]. Such compaction can be correlated with that occurring in glasses subjected to pressures and was recognized as resulting in a folding up of the SiO_4 tetrahedra rather than actual bond shortening[17]. Such folding process, in addition to the rupture of bonds by gamma irradiation,[18] is expected to increase the disorder of the glassy matrix. Consequently, this will result in an increase of W_D; the dwelling time also increases, giving a higher value of ν. The dwelling time is defined[10] as the mean time a carrier stays at a certain site including the possibility of leaving the site and returning.

Thus, according to Eq. (1), the electrical resistivity should increase. The second and third terms of Eq. (1) can be proved to be the main factors for the increased resistivity of the γ-irradiated glasses up to 0.19 Mrad. The value of the concentration of Ce^{3+} ions (c) is expected to decrease according to the well known reaction[18]

$$Ce^{3+} + h\nu \rightarrow Ce^{4+} + e$$

If the relative concentration of the reduced state is always greater than that of the oxidized state of cerium, then the multiplication of (c) by ($1-c$) will give products of larger values as the gamma radiation dose increases. This is because the amount of Ce^{4+} ions, i.e. ($1-c$), will increase progressively. As a result, the value $Rk/c(1-c)$ *should decrease. Experimentally* $ln(\rho/T)$ was found to increase (Fig. 4) up to 0.19 Mrad; this indicates that the first term of Eq. (1) has small or no effect on increasing the resistivity in this range. It is reasonable that increasing the electron trappers (Ce^{4+}) will increase the impeding and scattering effects which will lead to the increase of the resistivity.

At doses higher than 0.19 Mrad the number of the released charge carriers and defects caused by gamma irradiation increases significantly. Moreover, there is a possibility for the reaction[18].

$$Ce^{4+} + e \rightarrow Ce^{3+} + h\nu$$

to proceed in the highly-dosed samples. These may enhance the conduction and give a possible

explanation for the decrease of resistivity of the highly irradiated glasses after reaching a maximum value (Fig. 4).

References

1 Elliott R J, *Magnetic properties of rare earth metals*, (Plenum Press, London) 1972.

2 Waber J T & Switendick A C, in *Proc Fifth Rare Earth Conference*, Iowa, USA 1965, Book 11, p 75.

3 Rocher Y A, *Adv Phys* (*GB*), **11** (1965) 233.

4 Burr C R & Ehara S, *Phys Rev* (*USA*), **149** (1966) 551.

5 Sugawara T, *J Phys Soc Jpn* (*Japan*), **20** (1965) 2252.

6 Cogblin B & Blandin A, *Adv Phys* (*GB*), **17** (1965) 261.

7 Cogblin B, Maples N B & Toulouse G, *Int J Magn* (*GB*), **1** (1971) 333.

8 Robertson J, *Philos Mag B* (*GB*), **41**(2) (1980) 177-190.

9 Tawansi A, Basha A F, Morsi M M & El-Konsol S, *Acta Phys Acad Sci Hung* (*Hungary*), **53** (1983) in press.

10 Movaghar B, Pohlmann B & Schirmacher W, *Philos Mag B*(*GB*), **41**(1) (1980) 49-63.

11 Austin I G & Mott N F, *Adv Phys* (*GB*), **18** (1969) 41.

12 Bandyopadhyay A K & Isard J O, *J Phys D* (*GB*), **10** (1977).

13 Mott N F & Davis E A, *Electronic processes in non-crystalline materials* (Clarendon Press, Oxford) 1971.

14 Shelby J E, *J Appl Phys* (*USA*), **51** (1980) 2561.

15 Mott N F, Davis E A & Street R A, *Philos Mag* (*GB*), **32** (1975) 961.

16 Kastner M, Adler D & Fritzche H, *Phys Rev Lett* (*USA*), **37** (1976) 1054.

17 Bridgman P W & Simon J, *J Appl Phys* (*USA*), **24** (1953) 405.

18 Lell E, Kreidl N J & Hensler J R, in *Progress in ceramic science*, Vol 4, edited by J Burke (Pergamon Press, London) 1966.

Indian Journal of Pure & Applied Physics
Vol 21, September 1983, pp. 506-509

Molecular Association in Some *n*-Butanol Systems

SURJIT SINGH BHATTI*
Department of Physics, Guru Nanak Dev University, Amritsar 143005
and
DEVINDER PAL SINGH
Shivalik College, Naya Nangal 140126

Received 22 *November* 1982; *revised received* 8 *February* 1983

Results of ultrasonic velocity measurements in binary systems containing *n*-butanol as the common component have been used to evaluate several parameters. The other components are cyclohexane, acetone, cyclohexanone, cyclohexanol and chloroform. The trend of variation of these parameters at constant temperature but increasing butanol mole-fraction is indicative of the nature of molecular association in the mixtures.

1 Introduction

Ultrasonic velocity and absorption measurements have been used by many workers in the study of molecular interactions in liquids[1], polymers[2] and electrolytic solutions[3]. In this paper, we have evaluated a number of acoustic parameters for five binary mixtures containing cyclohexane, acetone, cyclohexanone, cyclohexanol and chloroform with *n*-butanol as a common component. The calculations are based on velocity (u) values obtained experimentally by Prakash and Srivastava[4] at 308.15 K as a function of increasing mole-fraction of *n*-butanol, x(Bu). The significance of these parameters and their mathematical expressions are given in literature[5,6].

The molar sound velocity ($R=Vu^{1/3}$) is known to be independent of temperature, pressure and concentration variations for unassociated liquids and for non-interacting molecules. Here these variations are shown in Fig. 1. The free-length (L_f) or the average distance travelled by sound waves between two molecules is another parameter studied here. The ratio $(L_f'/L_f)^3$ of the experimental value (L_f') and the ideal value (L_f) determines the relative association (RA) given in Table 1. The free-volume $V_f=(V-b)$, where V is the molar volume and b is the van der Waal constant, the coefficient of viscosity $\eta(=Mu/KV_f^{2/3})$ and the relaxation time $\tau=\eta\beta_S$) are given in Table 2. The adiabatic compressibility is obtained from the relation: $\beta_S=(u^2\rho)^{-1}$.

Excess parameters[6], given by the difference between experimental (exp) and ideal mixture (im) values, and percentage deviations give a measure of non-ideality of the system as a consequence of associative or other types of interactions. These are shown in Table 2. In Fig. 2 is shown the trend of the excess compressibility (β_S^E) variation with increase in x(Bu). The studies of Fort and Moore[5] show that there is usually increase in excess volume and excess compressibility if strong interactions between the unlike molecules are asbent; otherwise these are negative.

2 Results and Discussion

Variation of molar sound velocity (R) with x(Bu) shows that R is not constant so that the AB-interactions in these mixtures are expected to be associative. This is borne out by the rising trends of the relative association (RA), with increase in x(Bu). The fact that RA in *n*-butanol + cyclohexanol is less than one shows that in the pure cyclohexanol molecules, the molecular association is weaker compared to that in *n*-butanol. A similar statement could be made in respect of cyclohexanone. In *n*-butanol mixtures with cyclohexane, acetone and chloroform, however, RA variation is more pronounced.

The Fort and Moore[5] criterion also favours the above conclusion. The excess adiabatic compressibility

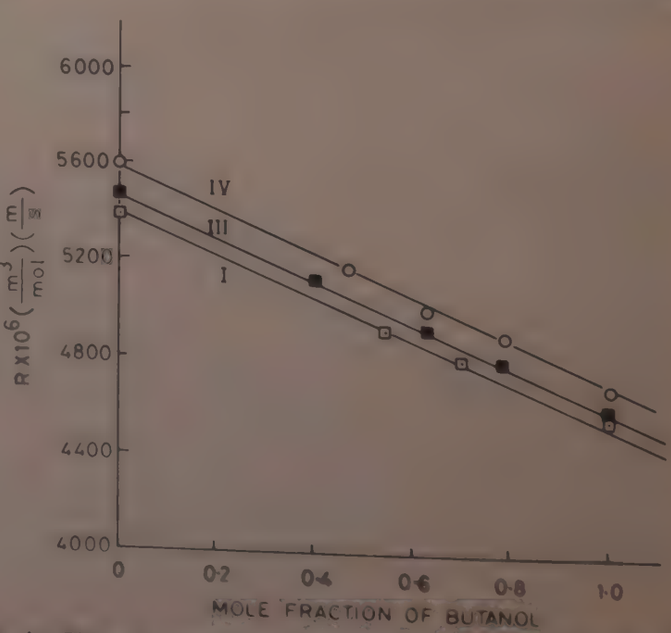

Fig. 1 Plots of molar sound velocity against mole fraction of butanol for mixtures with I, cyclohexane; III, cyclohexanone and IV, cyclohexanol

Table 1 — Free-length and Relative Association as Functions of Mole-fraction (x) of n-Butanol at 308.15 K

x	u m/s	ρ kg/m^3	$b \times 10^6$ m^3/mol	L_f pm	L_f' pm	RA	u^2(exp)/ u^2(im)
			I n-Butanol + cyclohexane				
0.000	1200	765.3	102.7	59.8	60.2	1.02	1.00
0.540	1166	779.8	94.0	58.0	60.3	1.18	0.94
0.700	1180	784.0	91.6	57.6	60.5	1.16	0.96
1.000	1204	798.2	86.4	54.9	58.9	1.23	1.00
			II n-Butanol + acetone				
0.000	1123	773.6	69.1	60.7	63.7	1.16	1.00
0.375	1133	790.9	74.9	56.1	62.6	1.38	0.93
0.546	1164	798.6	77.5	55.1	60.7	1.42	0.99
1.000	1204	798.1	86.4	54.9	58.9	1.23	1.00
			III n-Butanol + cyclohexanone				
0.000	1410	933.0	99.4	48.3	47.3	0.94	1.00
0.403	1344	884.6	94.1	50.3	50.7	1.02	1.03
0.628	1311	855.0	91.1	51.5	52.7	1.07	1.05
0.771	1294	834.9	89.3	52.5	53.9	1.08	1.07
			IV n-Butanol + cyclohexanol				
0.000	1440	937.9	101.1	49.1	56.3	0.84	1.00
0.463	1374	880.0	94.3	50.5	49.8	0.93	1.07
0.633	1329	852.8	92.1	53.0	52.1	0.94	1.06
0.776	1298	832.3	90.0	53.8	53.8	1.00	1.07
			V n-Butanol + chloroform				
0.000	947	1472.8	74.6	56.6	55.4	0.94	1.00
0.416	1003	1176.6	78.8	54.0	58.3	1.26	0.91
0.586	1039	1061.6	80.8	53.7	59.1	1.33	0.90
0.740	1093	960.2	82.8	52.0	59.2	1.31	0.92

shows negative values in the case of mixtures of n-butanol with cyclohexane, acetone and chloroform (Fig. 2) implying strong AB-type associative interactions. For mixtures with cyclohexanone and cyclohexanol, where this parameter assumes positive values (probably due to dispersion forces) such interactions should be weak. Negative excess compressibilities have been reported for *tert*-butanol + water systems by Patil and Raut[7].

The free-length observed experimentally in mixtures containing cyclohexane, acetone and chloroform shows a regular fall as the fraction of butanol is raised. This regular fall in L_f, according to Eyring and Kincaid[8], causes a rise in sound velocity in the mixture. This is also in accordance with the expected decrease in compressibility (proportional to free-length) following increase of ultrasonic velocity in these cases. Further, this trend is indicative of clustering together of the molecules (of the two types of liquids in each mixture) into some compact cage-like agglomerates due to associative effects of the polar group predominating over other types of interactions. Free-volume (V_f) decreases only in the mixture containing cyclohexane

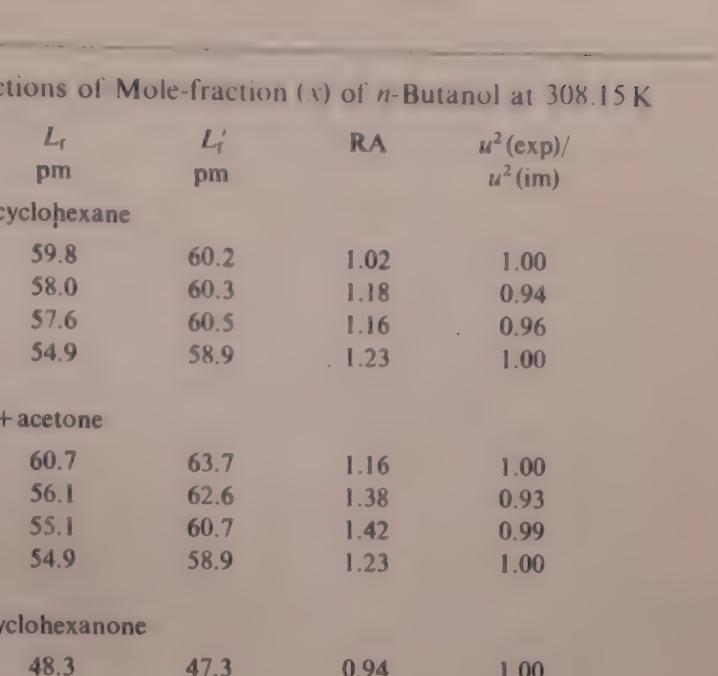

Fig. 2 Plots of excess adiabatic compressibility (β_S^E) against mole fraction of butanol for mixtures with I, cyclohexane; II, acetone; III, cyclohexanone; IV, cyclohexanol and V, chloroform

(dipole moment = 0) showing that here the clustering is not due to H-bonding or dipole-induced dipole interaction. It is primarily due to formation of spherical cage-like structures due to closer packing of

Table 2 — Relaxation Time and % Deviations as Functions of Mole-fraction (x) of n-Butanol at 308.15 K

x	$\beta_S \times 10^{11}$ m^2/N	$V_f \times 10^6$ m^3/mol	$\eta \times 10^4$ (N/m^2) s	$\tau \times 10^{15}$ s	$(\Delta V/V)$ %	$(\Delta u/u)$ %	$(\Delta R/R)$ %
			I n-Butanol + cyclohexane				
0.000	90.74	7.19	0.633	57.4	0.00	0.00	0.00
0.540	94.32	6.92	0.590	55.6	0.24	−3.10	−0.78
0.700	91.60	6.73	0.596	54.6	0.39	−1.93	−0.24
1.000	86.42	6.35	0.608	52.5	0.00	0.00	0.00
			II n-Butanol + acetone				
0.000	102.50	5.89	0.467	47.8	0.00	0.00	0.00
0.375	98.49	6.11	0.508	49.9	−0.87	−1.80	−1.58
0.546	92.42	6.09	0.544	50.3	−1.30	−0.28	−1.50
1.000	86.42	6.35	0.608	52.5	0.00	0.00	0.00
			III n-Butanol + cyclohexanone				
0.000	53.91	5.71	1.011	54.5	0.00	0.00	0.00
0.403	62.58	5.88	0.852	53.3	−0.22	1.27	0.11
0.628	68.05	5.97	0.773	52.6	−0.31	2.32	0.38
0.771	71.53	6.01	0.727	52.0	−0.33	3.31	0.72
			IV n-Butanol + cyclohexanol				
0.000	51.42	5.65	1.061	54.6	0.00	0.00	0.00
0.463	60.19	5.79	0.876	52.7	0.23	3.15	0.72
0.633	66.39	5.95	0.791	52.5	0.15	2.89	1.00
0.776	71.31	6.03	0.731	52.1	0.08	3.17	1.06
			V n-Butanol + chloroform				
0.000	75.71	5.51	0.836	63.3	0.00	0.00	0.00
0.416	84.48	5.95	0.712	60.1	−0.76	−5.08	−2.58
0.586	87.26	6.11	0.669	58.4	−0.75	−5.64	−2.74
0.740	87.18	6.20	0.646	56.3	−0.52	−4.04	−1.96

the molecules[9]. In the other two systems, the associative effects are either very weak or absent.

It may be pointed out here that the structuring envisaged here is not the same as that possible in clatharate hydration[10] of *tert*-butanol + water. This is due to the special structure of water. However, a similarity can exist. If structures similar to clatharate-hydrates were formed in these systems, there should be a very steep fall in the free-volume (V_f), which is not the case here. Also, the viscous relaxation times evaluated here are very low (10^{-15} s) and such transitions could occur only at very high frequencies (10^{15} Hz). These measurements of ultrasonic velocities are done usually at MHz frequencies.

The excess properties have a trend which supports the earlier inferences. The percentage deviations in molar sound velocity and the measured ultrasonic velocity in the mixtures containing cyclohexane, acetone and chloroform are negative. In the remaining two cases these deviations are positive. Negative deviations in most parameters, such as excess Grüneisen parameter[6] which depends upon ultrasonic velocity ($\Gamma = u^2 \gamma (C_p)$), are indicative of definite molecular association in the two species. The ratio $u^2(\text{exp})/u^2(\text{im})$ shows similar trends. Clearly, mixtures of n-butanol with cyclohexane, acetone and chloroform are characterized by intermolecular interactions which are associative in nature. In the case of n-butanol mixtures with cyclohexanone and cyclohexanol, these interactions are very weak.

In the case of the carbonyl groups of acetone and cyclohexanone, the oxygen atom has two lone pairs of electrons represented by two sp^2 hybridized orbitals. If one of these is collinear with the −OH...O axis, the interaction between the polar −OH group (of n-butanol) and the oxygen atom of the carbonyl group shoule be maximum. This is because the −OH bond induces a moment in the highly polarizable lone pair and would enhance the dipole moment of the AB-complex. The decreasing adiabatic compressibility of the acetone system points to increasing bond strength. This is possible only if the above argument is valid. In other words, the −OH group of n-butanol and one of the hybridized sp^2 orbitals of the oxygen atom are collinear in the carbonyl group of acetone. In cyclohexanone, however, the compressibility is increasing with the rise of butanol mole fraction, showing thereby a progressively weakening intermole-

cular interaction. This indicates that the $-OH$ group of butanol is unable to enhance the dipole moment of the cyclohexanone molecule. Perhaps their relative orientation is such that the resultant moment is decreased.

The addition of a diluent to the polar and associating molecules of butanol may cause a progressive breaking of H-bonds of the latter if the diluent is unable to form any complexes. This is not likely to be the case for *n*-butanol + cyclohexanone system as the RA does not decrease. However, the two species of atoms appear to interact very weakly. In comparison, the interaction between the *n*-butanol and acetone molecules appears to be much stronger for the reasons discussed above. The chloroform molecule has a CH-dipole and electronegative chlorine atoms. The dissociative effect of this molecule tends to increase the experimental free-length and adiabatic compressibility. The bonds between the two types of molecules (in *n*-butanol + chloroform) are, therefore, not very strong. In the case of *n*-butanol + cyclohexanol, the positive excess compressibility and the increasing values of free-volume point to rather weak interactions.

References

1 Bhatti S S, Virk J S & Singh D P, *Acustica (Germany)*, **50** (1982) 291.

2 Kor S K & Pandey S K, *J Chem Phys (USA)*, **64** (1976) 1333.

3 Bhatti S S & Lark B S, *Acustica (Germany)*, **48** (1981) 64.

4 Prakash S & Srivastava S B, *J Chem Thermodyn (GB)*, **7** (1975) 997.

5 Fort R J & Moore W R, *Trans Faraday Soc*, **61** (1965) 2102.

6 Pandey J D & Mishra R L, *Acustica (Germany)*, **36** (1976/1977) 342.

7 Patil K J & Raut D N, *Indian J Pure & Appl Phys*, **18** (1980) 499.

8 Erying H & Kincaid J F, *J Chem Phys (USA)*, **6** (1938) 620.

9 Hilderband J H & Scott R L, *Regular solutions* (Prentice Hall, New Jersey), 1962.

10 Tamura K, Maekawa M & Yasunaga T, *J Phys Chem (USA)*, **81**/**22** (1977) 2122.

Indian Journal of Pure & Applied Physics
Vol 21, September 1983, pp. 510-515

Equilibrium Properties of Semiclassical Fluid Mixture with Non-analytic Potentials

U N SINGH† & S K SINHA*
Department of Physics, L S College, Bihar University, Muzaffarpur 842001

Received 1 *September* 1982; *revised received* 11 *April* 1983

The problem of calculating the quantum corrections to the thermodynamic properties of a mixture of molecules using hard-core potentials is studied. The explicit expressions are given for the first order correction to (i) the free-energy and pressure of a binary mixture of hard-sphere and square-well molecules and (ii) to the 'excess' free-energy of a binary mixture of square-well molecules. Numerical results are reported. The quantum effect, which increases with increase of density and with decrease of temperature is minimum at $R=1.0$.

1 Introduction

This paper is concerned with the evaluation of thermodynamic properties of a semiclassical fluid mixture, whose molecules interact via hard-core plus attractive tail potential. We consider the case, when the constituent molecules have different diameters. For one-component fluid, this is usually calculated by the Wigner-Kirkwood (WK) method[1,2]; when the potential is analytic and by the 'modified' WK method[3,4], when the potential has a hard-core plus attractive-tail. This method can be extended to a mixture.

In recent years, both experimental[5] and theoretical[6] attempts have been made to understand the structural and thermodynamic properties of a binary mixture of hard spheres and square-well molecules. However, these are confined to a classical fluid mixture, in which both species of molecules have the same diameter. The semiclassical fluid mixture has been studied less thoroughly. The only work available for a mixture of hard-sphere and square-well molecules in the semi-classical limit is that of Singh and Sinha[7,8] who have considered the case when constituent molecules have same diameter. Very recently, Singh and Sinha[9,10] have studied the hard-sphere mixture whose constituent molecules have different diameters in the semiclassical limit.

In this paper, we study the thermodynamic properties of a mixture of hard-core molecules with different diameters in the semiclassical limit. It is assumed that the significant features of the structure of a quantum fluid are related to the repulsive part of the interaction and the attractive part plays a minor role[11].

In Sec. 2, we describe a general theory for calculating the thermodynamic properties of multicomponent mixtures whose molecules interact via a hard-core potential. The explicit expressions for the free-energy and equation of state are given there. We employ these expressions in Sec. 3 to obtain thermodynamic properties of a binary mixture (i) of hard-sphere and square-well molecules and (ii) of square-well molecular. The results are discussed in Sec. 4.

2 General Theory for Semiclassical Fluid Mixture

We consider an open system at volume V and temperature T, made up of species 1, 2,..., ν. There are N_1 molecules of species 1, N_2 of species 2, etc., such that the total number of molecules being $N=\sum_{i=1}^{\nu} N_i$. Further, we assume that the constituent molecules differ in size. In quantum statistical mechanics, the grand canonical partition function is given by

$$\Xi=\sum_{\{N_i\}}\left[\prod_{i=1}^{\nu}\frac{z_i^{N_i}}{N_i!}\right]\int\cdots\int W_N(1,2,\ldots,N)\prod_{l=1}^{N}d\bar{r}_l \qquad \ldots (2.1)$$

$$z_i=\lambda_i^{-3}\exp[\beta\mu_i] \qquad \ldots (2.2)$$

where μ_i is the chemical potential, $\lambda_i=(2\pi\hbar^2\beta/m_i)^{1/2}$ is the thermal wavelength and

$$W_N(1,2,\ldots,N)=\left[\prod_{i=1}^{\nu}\lambda_i^{3N_i}\right]\langle 1,2,\ldots,N|\exp[-\beta\hat{H}_N]|1,2,\ldots,N\rangle \qquad \ldots (2.3)$$

is the Slater sum of the system whose Hamiltonian is given by:

$$\hat{H}_N=-\frac{\hbar^2}{2}\sum_{i=1}^{\nu}\frac{1}{m_i}\sum_{l=1}^{N_i}\nabla_l^2+\sum_{i,j=1}^{\nu}\sum_{l<m}u_{ij}(l,m) \qquad \ldots (2.4)$$

where ∇_l^2 is the Laplacian operator of the particle l, $u_{ij}(l,m)$ is the pair potential between particle l of species i and particle m of species j.

If we divide the pair potential $u_{ij}(l,m)$ in the form:

† Permanent address: Department of Physics, R N College, Hajipur, Vaishali

$$u_{ij}(l,m) = u_{ij}^{hs}(l,m) + u_{ij}^{p}(l,m) \quad \ldots (2.5)$$

where $u_{ij}^{hs}(l,m)$ is the hard-sphere potential regarded as the reference potential and $u_{ij}^{p}(l,m)$ is treated as perturbation, then the Slater sum can be expanded about the hard-sphere Slater sum[4] and the grand partition function can be written as[7]:

$$\Xi = \sum_{\{N_i\}} \left[\prod_{i=1}^{v} \frac{z_i^{N_i}}{N_i!} \right] \int \cdots \int W_N^{hs}(1,2,\ldots,N) \times \prod_{l<m} [1 + f_{ij}^{c,p}(l,m)] \times \prod_{l<m<n} [1 + f_{ijk}^{III,p}(l,m,n)] \prod_{l=1}^{N} d\bar{r}_l \quad \ldots (2.6)$$

where

$$f_{ij}^{c,p}(l,m) = f_{ij}^{p}(l,m) + [1 + f_{ij}^{p}(l,m)] f_{ij}^{II,p}(l,m) \quad \ldots (2.7a)$$

$$f_{ij}^{II,p}(l,m) = \frac{\lambda_{ij}^2 \beta}{2\pi} \left[\frac{\partial^2 u_{ij}^{p}(l,m)}{\partial r_{lm}^2} - \frac{11}{12} \beta \left(\frac{\partial u_{ij}^{p}(l,m)}{\partial r_{lm}} \right)^2 \right] \quad \ldots (2.7b)$$

$$f_{ijk}^{III,p}(l,m,m) = -\frac{\lambda_{ij}^2 \beta^2}{24\pi} [\nabla_l u_{ij}^{p}(l,m) . \nabla_l u_{ik}^{p}(l,n) + \nabla_m u_{ij}^{p}(l,m) . \nabla_m u_{jk}^{p}(m,n) + \nabla_n u_{ik}^{p}(l,n) . \nabla_n u_{jk}^{p}(m,n)] \quad \ldots (2.7c)$$

$$f_{ij}^{p}(l,m) = \exp[-\beta u_{ij}(l,m)] - 1 \quad \ldots (2.7d)$$

and W_N^{hs} is the Slater sum of the hard-sphere fluid mixture.

The thermodynamic properties can be calculated if the partition function is known. Thus the free-energy of the system is given by:

$$\frac{\beta A}{N} = \frac{\beta A_{hs}}{N} + A_1^{p} + O(\beta^2) \quad \ldots (2.8)$$

where

$$A_1^{p} = \frac{1}{2} \beta \rho \sum_{i,j=1}^{v} x_i x_j \int g_{ij}^{hs}(r) u_{ij}^{p}(r) d\bar{r} \quad \ldots (2.9a)$$

A_{hs} and $g_{ij}^{hs}(r)$ are respectively the free-energy and the radial distribution function (RDF) of the quantum hard-sphere fluid mixture, $\rho = N/V$ is the number density and $x_i = N_i/N$ is the concentration of the species i.

The RDF $g_{ij}^{hs}(r)$ can be expanded about the classical hard-sphere RDF $g_{ij}^{chs}(r)$. The other terms in the series are the quantum corrections to the RDF. Thus the first order perturbation correction to the free-energy is the sum of the two terms; the first term is the main contribution due to the classical part and the second term arises due to the quantum effect. We consider the case when the quantum effect is small and attractive potential is weak. Then Eq. (2.9a) reduces to:

$$A_1^{p} = \frac{1}{2} \beta \rho \sum_{i,j=1}^{v} x_i x_j \int g_{ij}^{chs}(r) u_{ij}^{p}(r) d\bar{r} \quad \ldots (2.9)$$

The free-energy of the hard-sphere mixture in the semiclassical limit, valid to the first order quantum correction, is given by[9]

$$\frac{\beta A_{hs}}{N} = \frac{\beta A_{hs}^{c}}{N} + \frac{\pi}{\sqrt{2}} \rho \sum_{i,j=1}^{v} x_i x_j g_{ij}^{chs}(d_{ij}) d_{ij}^2 \lambda_{ij} \quad \ldots (2.10)$$

where A_{hs}^{c} is the free-energy of the classical hard-sphere fluid mixture, d_{ij} and λ_{ij} are, respectively, the diameter and thermal wavelength of the molecules of species i and j.

We use the van der Waals, one-fluid (vdWl) theory[12] of mixture to calculate the thermodynamic properties of the classical system. This theory approximates the properties of a mixture by those of a fictitious pure fluid with the parameters:

$$d_0^3 = \sum_{i,j} x_i x_j d_{ij}^3 \quad \ldots (2.11)$$

$$\varepsilon_0 = d_0^{-3} \sum_{i,j} x_i x_j \varepsilon_{ij} d_{ij}^3 \quad \ldots (2.12)$$

and[9]

$$\lambda_0 = d_0^{-2} \sum_{i,j} x_i x_j \lambda_{ij} d_{ij}^2 \quad \ldots (2.13)$$

where d_{ij} and ε_{ij} are unlike force parameters of the potential model.

In the vdWl theory of mixture, the free-energy and pressure of the classical hard-sphere fluid mixture are given as:

$$\frac{\beta A_{hs}^{c}}{N} = \frac{\beta A_0^{c}}{N} + \sum_i x_i \ln x_i + \text{Second order terms} \quad \ldots (2.14)$$

$$\frac{\beta P_{hs}^{c}}{\rho} = \frac{\beta P_0^{c}}{\rho} + \text{Second order terms} \quad \ldots (2.15)$$

where A_0^{c} and P_0^{c} are values for pure classical fluid containing N molecules in volume V at temperature T, the molecules interacting with a hard-sphere potential having diameter d_0. For a hard-sphere model, A_0^{c} and P_0^{c} are given by[13,14]:

$$\frac{\beta A_0^{c}}{N} = \eta_0 (4 - 3\eta_0)/(1 - \eta_0)^2 \quad \ldots (2.16)$$

$$\frac{\beta P_0^{c}}{\rho} = (1 + \eta_0 + \eta_0^2 - \eta_0^3)/(1 - \eta_0)^3 \quad \ldots (2.17)$$

where $\eta_0 = \pi \rho d_0^3/6$ ... (2.18)

To evaluate the integral appearing in Eq. (2.9a), we have used for the mixture RDF, the values obtained from the 0th order approximation in the conformal theory of Mo *et al.*[15] In this approximation, the mixture RDF g_{ij}^{chs} is equated to that of pure fluid at reduced density ρd_0^3, i.e.

$$g_{ij}^{chs}(r/d_{ij},\ \rho d_{ij}^3) \approx g_0^{chs}(r/d_{ij},\ \rho d_0^3) \quad \ldots (2.19)$$

$$\text{Thus} \quad A_1^p = \beta \sum_{i,j=1} x_i x_j \varepsilon_{ij} \left(\frac{d_{ij}}{d_0}\right)^3 I_{ij}^{(1)} \quad \ldots (2.20)$$

$$\text{where } I_{ij}^{(1)} = 2\pi(\rho d_0^3) \int_1^\infty g_0^{chs}(r^*, \rho d_0^3) \times u_{ij}^{p*}(r^*) r^{*2} \mathrm{d}r^* \quad \ldots (2.21)$$

$r^* = r/d_{ij}$, and $u_{ij}^{p*}(r^*) = u_{ij}^p(r/d_{ij})/\varepsilon_{ij}$

$I_{ij}^{(1)}$ is the pure fluid integral at reduced density $\rho_0^* = \rho d_0^3$. Its value depends upon the nature of the perturbation potential $u_{ij}^{p*}(r^*)$.

3 Binary Mixture

We consider a binary mixture consisting of one component of molecules of diameter d_{11} and other component of molecules of diameter d_{22}. For the unlike interaction, d_{12} and ε_{12} are given by[16]

$$d_{12} = \tfrac{1}{2}(d_{11} + d_{22}) \quad \ldots (3.1)$$

$$\varepsilon_{12} = \xi_{12}(\varepsilon_{11}\varepsilon_{12})^{1/2} \quad \ldots (3.2)$$

where ξ_{12} is an adjustable parameter. Further λ_{12} is given by[9]

$$\lambda_{12} = [(\lambda_{11}^2 + \lambda_{22}^2)/2]^{1/2} \quad \ldots (3.3)$$

The equation of state for a classical hard-sphere mixture is given by[17]

$$\frac{\beta P_{hs}^c}{\rho} = 1 + \frac{2\pi}{3}\rho \sum_{i,j} x_i x_j d_{ij}^3 g_{ij}^{chs}(d_{ij}) \quad \ldots (3.4)$$

With the help of Eqs. (2.17) and (3.4), Eq (2.10) can be expressed as:

$$\frac{\beta A_{hs}}{N} = \frac{\beta A_{hs}^c}{N} + (\lambda/d) A_1^{qc*} \quad \ldots (3.5)$$

$$\text{where } A_1^{qc*} = 3\sqrt{2} F \eta \frac{(1 - \frac{1}{2}\eta_0)}{(1-\eta_0)^3} \quad \ldots (3.6)$$

In deriving Eq. (3.5), we have used the following notations

$$d^3 = x_1 d_{11}^3 + x_2 d_{22}^3 \quad \ldots (3.7)$$

$$\lambda = d^{-2}(x_1 d_{11}^2 \lambda_{11} + x_2 d_{22}^2 \lambda_{22}) \quad \ldots (3.8)$$

$$F = d_0^3 \lambda_0 / d^2 \lambda \quad \ldots (3.9)$$

$$\text{and } \eta = \frac{\pi}{6}\rho^* = \frac{\pi}{6}\rho(x_1 d_{11}^3 + x_2 d_{22}^3) \quad \ldots (3.10)$$

Once free-energy is known, the equation of state for the quantum mechanical hard sphere mixture is given by:

$$\frac{\beta P_{hs}}{\rho} = \frac{\beta P_{hs}^c}{\rho} + (\lambda/d) P_1^{qc*} \quad \ldots (3.11)$$

$$\text{where } P_1^{qc*} = 3\sqrt{2} F \eta \frac{(1 + \eta_0 - \frac{1}{2}\eta_0^2)}{(1-\eta_0)^4} \quad \ldots (3.12)$$

We now apply the theory developed in Sec. 2 to binary mixtures consisting of (1) a component of hard-sphere molecules and another of square-well molecules, and of (2) both components of square-well molecules.

3.1 Binary Mixture of Hard-Sphere and Square-Well Molecules

We consider a binary mixture of hard-sphere (species 1) and square-well molecules (species 2) and assume that the interaction between unlike molecules is given by the hard-sphere interaction. Thus,

$$u_{ij}(r) = \infty, \ r < d_{ij}$$
$$= -\varepsilon_{ij}, \ d_{ij} < r < \gamma d_{ij}$$
$$= 0, \ r > \gamma d_{ij} \quad \ldots (3.13)$$

where $\varepsilon_{11} = \varepsilon_{12} = 0$, $\varepsilon_{22} \neq 0$ and $\gamma = 1.5$. This mixture is interesting both because of its simplicity and because of its extreme values for $\varepsilon_{11}/\varepsilon_{22}$ and $\varepsilon_{12}/\varepsilon_{22}$.

For this system, $I_{11}^{(1)} = I_{12}^{(1)} = 0$ and the first order perturbation contribution is due to $I_{22}^{(1)}$ term only. Thus

$$A_1^p = \beta \varepsilon_{22} A_1^{cp} \quad \ldots (3.14a)$$

$$A_1^{cp} = x_2^2 (d_{22}/d_0)^3 I^{(1)} \quad \ldots (3.14b)$$

$$\text{where } I_{22}^{(1)} = I^{(1)} = -2\pi\rho d_0^3 \int_1^\gamma g_0^{chs}(r^*, \rho d_0^3) r^{*2} dr^* \quad \ldots (3.15)$$

The integral $I^{(1)}$ can be evaluated from the relation[18]

$$I^{(n)} = C_n\{1 - \exp[-\alpha_n \rho_0^*/(\beta_n - \rho_0^*)] - (\alpha_n/\beta_n)\rho_0^*\} + D_n \rho_0^* + E_n \rho_0^{*2} \quad \ldots (3.16)$$

Table 1—Coefficients Used in Fit of $I^{(n)}$ for Square-Well Potential

Coefficient	Value for $n=1$	Value for $n=2$
α_n	1.50	2.75
β_n	$\sqrt{2}$	$\sqrt{2}$
C_n	−8.460822	−7.956887
D_n	−4.974192	−2.487096
E_n	−2.427212	9.919624

with $n=1$; where $\rho_0^*=\rho d_0^3$. The values for the parameters are given in Table 1. Thus, the free-energy of a binary mixture in the semiclassical limit, valid to the first order correction, is given by:

$$\frac{\beta A}{N}=\frac{\beta A_{hs}^c}{N}+\beta\varepsilon_{22}A_1^{cp*}+\left(\frac{\lambda}{d}\right)AA_1^{qc*} \quad \ldots (3.17)$$

and the equation of state is

$$\frac{\beta P}{\rho}=\frac{\beta P_{hs}^c}{\rho}+\beta\varepsilon_{22}P_1^{cp*}+(\lambda/d)P_1^{qc*} \quad \ldots (3.18)$$

where $$P_1^{cp*}=\rho\left(\frac{\partial A_1^{cp*}}{\partial\rho}\right) \quad \ldots (3.19)$$

3.2 Binary Mixture of Square-Well Molecules

We now consider a binary mixture of square-well (SW) molecules and assume that the interaction between the unlike molecules is also given by the square-well interaction.

The 'excess' free-energy for a SW mixture correct to the first order correction is given by:

$$\frac{\beta A_E}{N}=\frac{\beta[A_{hs}^c]_E}{N}+\sqrt{2\pi x_1x_2g_{12}^{chs}(d_{12})\rho d_{12}^3}\left(\frac{\lambda_{12}}{d_{12}}\right)$$
$$+2\beta\varepsilon_{12}x_1x_2\left(\frac{d_{12}}{d_0}\right)^3I^{(1)} \quad \ldots (3.20)$$

For additive hard-sphere, $g_{12}^{chs}(d_{12})$ is given by[19]:

$$g_{12}^{chs}(d_{12})=\frac{1}{1-\eta}+\frac{3x}{(1-\eta)^2}\mu \quad \ldots (3.21)$$

where $$x=\frac{\pi}{6}\rho(x_1d_{11}^2+x_2d_{22}^2) \quad \ldots (3.22)$$

$$\mu=\frac{d_{11}d_{22}}{d_{11}+d_{22}} \quad \ldots (3.23)$$

and η is defined by Eq. (3.10).

In terms of the reduced quantities,

$$T_{12}=\frac{kT}{\varepsilon_{12}}=\frac{1}{\beta\varepsilon_{12}} \quad \ldots (3.24)$$

$$\Lambda_{12}^*=\sqrt{2}\left[\frac{1}{(1+R)^2}(\varepsilon_{11}/\varepsilon_{12})^{1/2}\Lambda_{11}^{*2}\right.$$
$$\left.+\frac{R^2}{(1+R)^2}(\varepsilon_{22}/\varepsilon_{11})^{1/2}\Lambda_{22}^{*2}\right]^{1/2} \quad \ldots (3.25)$$

where $$\Lambda_{ii}^*=\frac{h}{d_{ii}(m_{ii}\varepsilon_{ii})^{1/2}}$$

and $R=d_{22}/d_{11}$.

Eq. (3.20) can be reduced to the form:

$$\frac{\beta A_E}{N}=\frac{\beta[A_{hs}^c]_E}{N}+\frac{\Lambda_{12}^*}{\sqrt{T_{12}^*}}A_E^{qc*}+\frac{A_E^{cp*}}{T_{12}^*} \quad \ldots (3.26)$$

where $$A_E^{cp*}=2x_1x_2\left(\frac{d_{12}}{d_0}\right)^3I^{(1)} \quad \ldots (3.27)$$

and $$A_E^{qc*}=\sqrt{\pi x_1x_2g_{12}^{chs}(d_{12})d_{12}^3} \quad \ldots (3.28)$$

4 Results and Discussion

4.1 Binary Mixture of Hard-Sphere and Square-Well Molecules

Eqs (3.17) and (3.18) have been used to calculate the free-energy (with respect to the ideal gas) and equation of state of the binary mixture of hard-sphere and square-well molecules in the semiclassical limit.

The classical values are correct to the first order of $\beta\varepsilon_{22}=T^{*-1}$. The results are reported for a range of ρ^* at

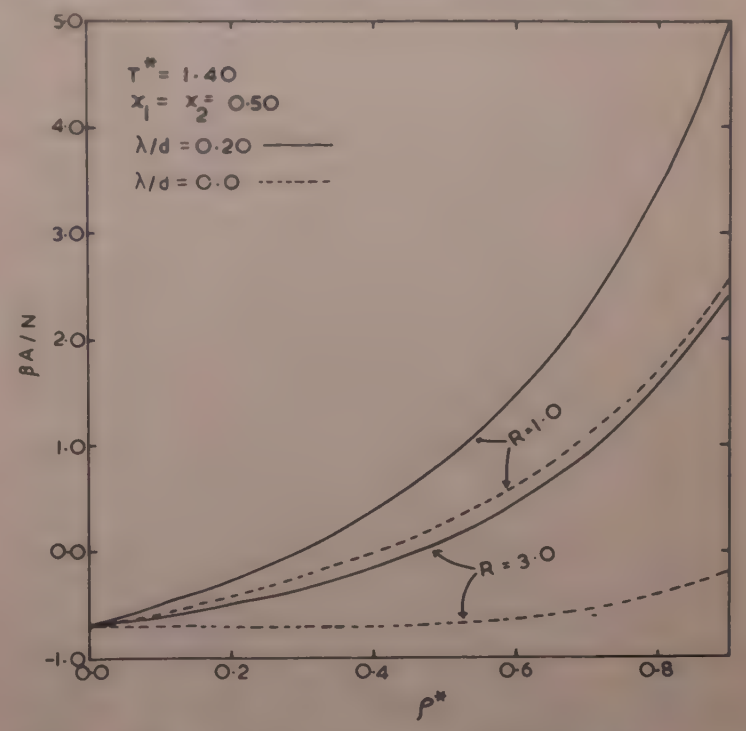

Fig. 1—Values of $\beta A/N$ of a mixture of hard-sphere and square-well molecules as a function of ρ^* for $x_1=x_2=0.5$ at $T^*=1.40$

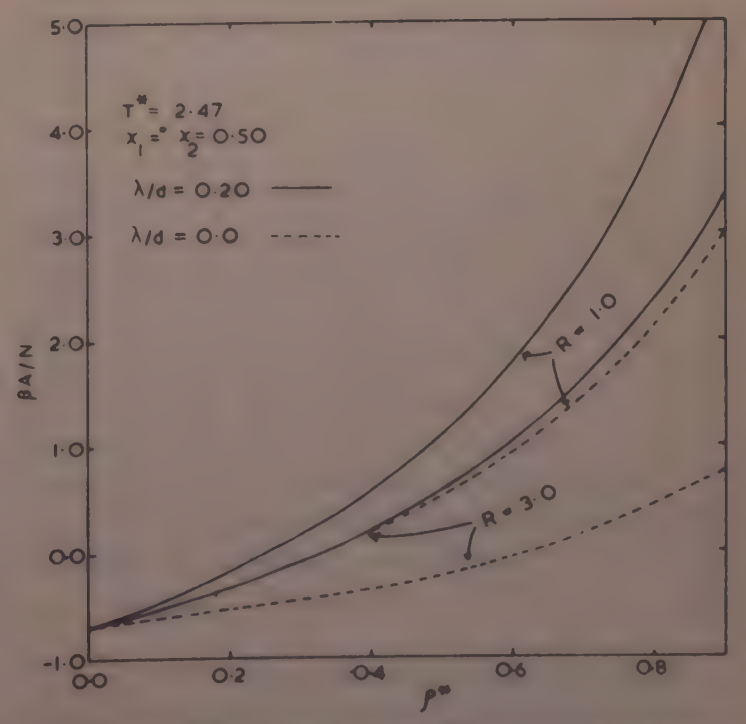

Fig. 2—Values of $\beta A/N$ for a mixture of hard-sphere and square-well molecules as a function of ρ^* for $x_1=x_2=0.5$ at $T^*=2.47$

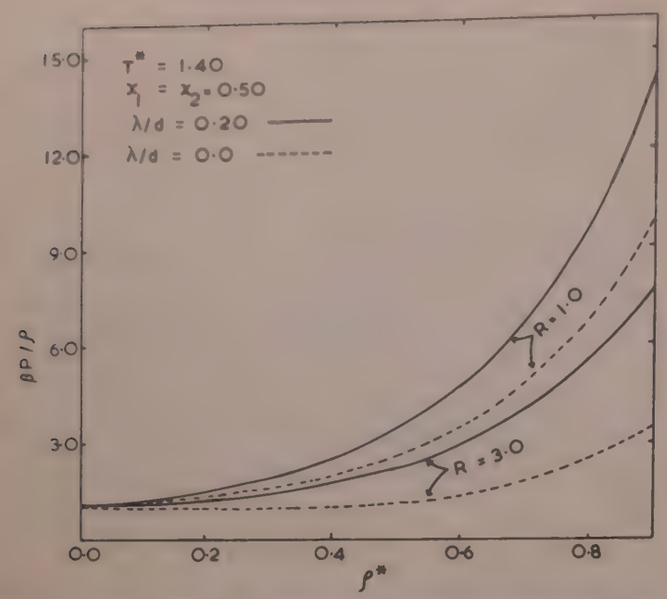

Fig. 3—Values of $\beta P/\rho$ for a mixture of hard-sphere and square-well molecules as a function of ρ^* for $x_1 = x_2 = 0.5$ at $T^* = 1.40$

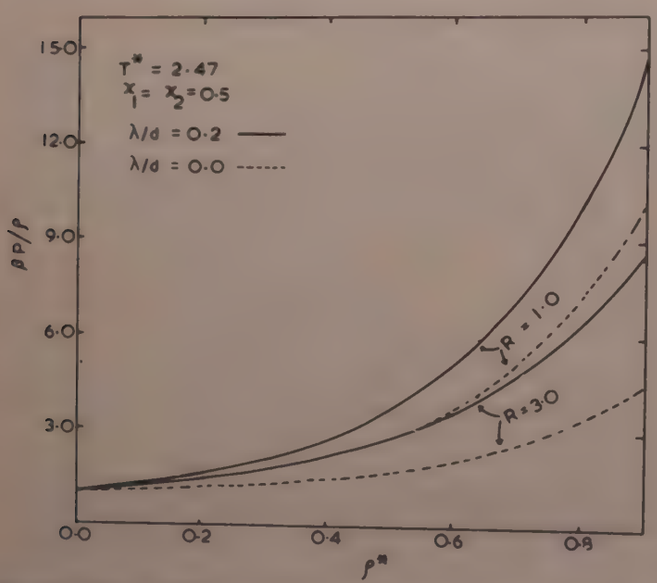

Fig. 4—Values of $\beta P/\rho$ for a mixture of hard-sphere and square-well molecules as a function of ρ^* for $x_1 = x_2 = 0.5$ at $T^* = 2.47$

$x_1 = x_2 = 0.5$ and $R = d_{22}/d_{11} = 1.0$ and 3.0. The quantity $\rho^* = \rho(\chi_1 d_{11}^3 + \chi_2 d_{22}^3)$.

The values of $\beta A/N$ for $\lambda/d = 0.0$ and 0.2 are plotted as a function of ρ^* in Figs 1 and 2 for $T^* = 1.40$ and 2.47 respectively. The values of $\beta P/\rho$ for $\lambda/d = 0.0$ and 0.2 are reported in Figs 3 and 4 for $T^* = 1.40$ and 2.47 respectively. The classical values are reported there as dashed lines. The classical values increase with decrease of R and/or increase of T^*. The quantum effect increases with the decrease of T^*. The quantum effects are minimum at $R = 1.0$ and increase as R goes away from 1.0. Further, we find that the quantum effects increase with the increase of ρ^* and λ/d.

4.2 Binary Mixture of Square-Well Molecules

The excess free-energy of a binary mixture of square-well molecules is calculated using Eq. (3.26). We use the force parameters[20] of this model for Ne and A reported in Table 2. The values of Λ^* for pure systems are obtained from the relation $\Lambda^* = h/d(m\varepsilon)^{1/2}$. To obtain d_{12} and ε_{12} for Ne-A, we use Eqs (3.1) and (3.2). For simplicity, ξ_{12} is taken to be unity. Value of Λ_{12}^* is evaluated from Eq. (3.25).

Table 2—Values of Square-Well Force Parameters

Pair	d	ε/k	Λ^*
Ne-Ne	2.382	19.5	0.9249
A-A	3.162	69.4	0.2632
Ne-A	2.772	36.79	0.3553

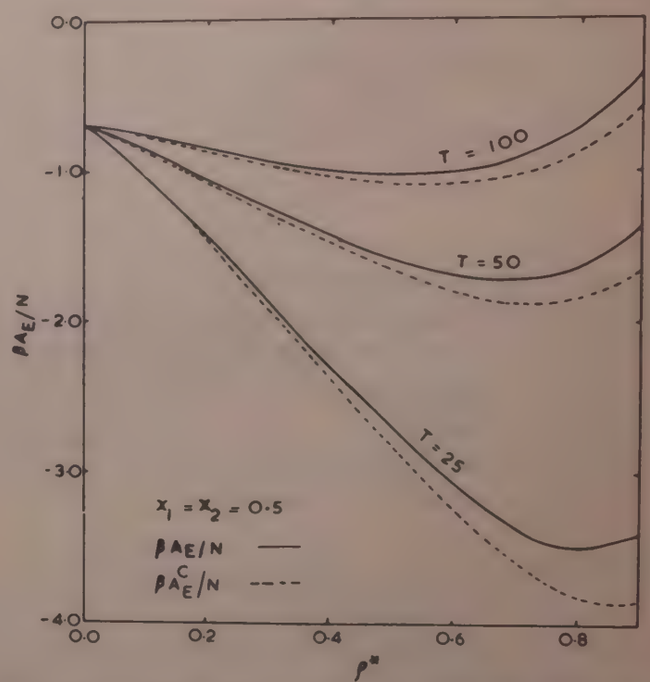

Fig. 5—Values of $\beta A_E/N$ for a mixture of square-well molecules as a function of ρ^* for $x_1 = x_2 = 0.5$

The values of $\beta A_E/N$ for this mixture are reported in Fig. 5 for temperature $T = 25$, 50 and 100 K. We find that the 'excess' quantum effect increases with increase of ρ^* and decrease of T.

References

1 Wigner E, *Phys Rev (USA)*, **40** (1932) 749.

2 Kirkwood J G, *Phys Rev (USA)*, **44** (1933) 31.

3 Derderian E J & Steele W A, *J Chem Phys (USA)*, **55** (1971) 5795; **59** (1973) 992.

4 Singh B P & Sinha S K, *J Chem Phys (USA)*, **68** (1978) 562.

5 Alder B J, *Ann Rev Phys (USA)*, **24** (1973) 325.

6 Henderson D, *J Chem Phys (USA)*, **51** (1974) 926.

7 Singh N & Sinha S K, *J Chem Phys (USA)*, **71** (1979) 3099.

8 Singh N & Sinha S K, *Indian J Pure & Appl Phys*, **18** (1980) 868.

9 Singh U N & Sinha S K, *J Chem Phys (USA)*, **77** (1982) 5784.

10 Singh U N & Sinha S K, *J Chem Phys (USA)*, **78** (1983) 3191.

11 Kalos M H, Levesque D & Verlet L, *Phys Rev (USA)*, **9A** (1974) 2178.

12 Leland T W(Jr), Rowlinson J S & Sather G A, *Trans Faraday Soc* (*GB*), **64** (1968) 1447.
13 Carnahen N F & Starling K E, *J Chem Phys* (*USA*), **51** (1969) 635.
14 Verlet L & Weis J J, *Phys Rev* (*USA*), **A5** (1972) 939.
15 Mo K C, Gubbins K E, Jacucci G & McDonald I R, *Mol Phys* (*GB*), **27** (1974) 1173.
16 Henderson D, *Ann Rev Phys Chem*, (*USA*), **25** (1974) 461.
17 Grundke E W & Henderson D, *Mol Phys* (*GB*), **24** (1972) 269
18 Barker J A & Henderson D, *Mol Phys* (*GB*), **21** (1971) 187
19 Henderson D & Leonard P J, *Physical chemistry - An advanced treatise*, edited by H Eyring, D Henderson and W Jost (Academic Press, New York), 1971, Vol VIIIB, Ch. 7.
20 Hirschfelder J O, Curtiss C F & Bird R B, *Molecular theory of gases and liquids* (John Wiley, New York), 1954, Ch. 3, 160.

Indian Journal of Pure & Applied Physics
Vol 21, September 1983, pp. 516-520

Temperature Dependence of Zero-field Splitting of Mn^{2+} in Dicalcium Barium Propionate

S V BHAT, V DHAR & R SRINIVASAN*
Department of Physics, Indian Institute of Science, Bangalore 560012

Received 4 *February* 1983; *revised received* 21 *July* 1983

The axial splitting parameter D in dicalcium barium propionate doped with Mn^{2+} has been studied from 139 to 597 K, and the temperature dependence of D of phase-I of the compound has been fitted to conform to a quadratic form in the range 265-597 K. The effect of the phase transition is to cause a slight deviation from the quadratic form above the transition temperature, over a range of about 50 K. The discontinuous change in the D-tensor at the cubic↔orthorhombic transition at 267 K is analyzed in terms of an abrupt slowing of the propionate group flipping (between its two equilibrium positions), accompanied by a static distortion. The cubic phase is seen to be the time-average of two equilibrium configurations corresponding to the low temperature phase.

1 Introduction

Dicalcium strontium propionate (DSP), dicalcium lead propionate (DLP) and dicalcium barium propionate (DBP) belong to the family of metal double-propionates. At ambient pressure, DBP undergoes two phase transitions from the room temperature cubic phase-I to phase-II at 267 K (presumed orthorhombic) and to phase-III at around 203 K (symmetry unknown).

In a previous study[1], we have analyzed the ESR spectra of Mn^{2+}-doped DBP in the crystal planes (111) and (001) and in powder samples, as a function of temperature. The zero-field axial splitting D exhibits a discontinuous change at $T_{I-II}=267$ K and a change in slope of D versus T at $T_{I-III}=203$ K corresponding to first- and second-order transitions respectively. The I ↔ II transition also shows a change in the orientation of the D-tensor axes by about ±15 K in both planes.

In the present study, we have extended the earlier preliminary results on the variation of D with temperature to cover a wide temperature range. This has warranted a new procedure of analysis of the results as we find that in phase-I, the deviation from the quadratic form,

$$D=D_0(1+\gamma T+\beta T^2) \qquad \ldots (1)$$

increases as the temperature approaches $T_{I\leftrightarrow II}$. This deviation, we attribute to the effect of the phase transition. Further, the discontinuous change at $T_{I\leftrightarrow II}$ in D, we split into two components: one static, the other dynamic. The dynamics of the propionate ion, that we utilize, are in conformity with the results of Stadnicka and Glazer[2].

2 Experimental Details

Crystals of DBP were grown from aqueous solutions of CH_3CH_2COOH, $CaCO_3$ and $BaCO_3$, in stoichiometric proportions, by slow evaporation at 313 K. Mn^{2+} was doped in the crystals by adding $MnCO_3$ to the solutions. ESR spectra were taken of powder samples. The spectra were recorded on a Varian-E-109 X-band spectrometer with 100 kHz modulation. The temperature was varied between 139 and 597 K, using a cold gas flow method (stability and resolution ±1 K).

3 Results

The axial splitting D is extracted from the ESR spectra in the same way as in our previous work[1]. The results of the D versus T plot were fitted to the quadratic form of Eq. (1). The use of this form will be justified in Sec. 4. For positive β, D shows a minimum value D_{min} at a temperature T_{min} given by:

$$D_{min}=D_0[1-\alpha^2/4\beta],\ T_{min}=\alpha/2\beta \qquad \ldots (2)$$

In our earlier work, in the temperature range 265-474 K, the results of D versus T were fitted to a single set of parameters D_0, α and β, leading to $D_{min}=84.8$ G at $T_{min}=553.9$ K.

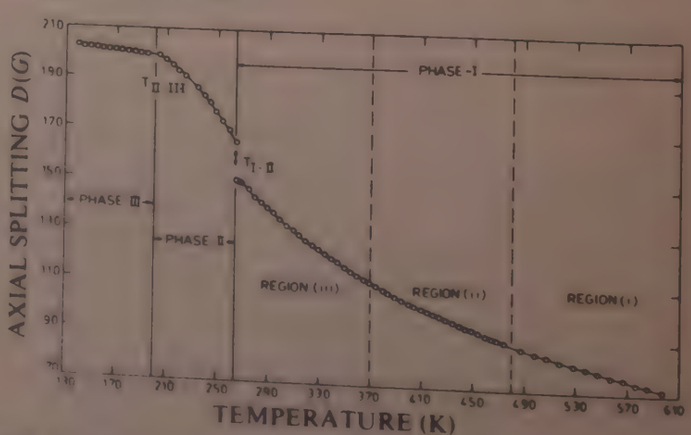

Fig. 1 Variation of the zero-field splitting parameter D with temperature. The smooth line is the theoretical fit, for phase-I. The fit is obtained with different sets of coefficients (given in Table I) for the three different regions

Table 1—Quadratic Temperature Dependence of Axial Splitting (D) in DBP

[Fitting of temperature dependence of D in different regions of phase-I with T_1 = lower temperature limit, and T_2 = upper temperature limit.]

Case	Region	T_1 (K)	T_2 (K)	D_0 (G)	($\times 10^3$ $\frac{G}{K^2}$)	($\times 10^6 \frac{G}{K^2}$)	T_{min} (K)	D_{min} (G)	rms deviation Δ
(a)	(i)	487	597	188.0	−1.4355	0.67	10.69.4	43.9	0.0919
(b)	(ii)	374	474	235.5	−1.8650	1.17	795.6	60.8	0.2677
(c)	(iii)	265	369	345.6	−2.890	2.85	506.8	92.5	0.2832
(d)	(i), (ii), (iii)	265	597	290.6	−2.332	1.82	641.6	73.2	1.0726
(e)	(i), (ii)	374	597	239.9	−1.9208	1.26	762.8	64.1	0.2482
(f)	(ii), (iii)	265	474	324.3	−2.6799	2.44	548.6	85.9	0.5109

In the present study, up to 597 K (Fig. 1), no such minimum is observed. We have re-analyzed our results, and with the new values of the parameters D_0, α and β, T_{min} lies well above the decomposition temperature of DBP (Table 1).

We have analyzed the present data, assuming that the quadratic form of Eq. (1) will be closely followed far above T_{I-II}, and that deviations from this form will occur near the transition temperature. If a single quadratic form is used for phase-I [case (d) in Table 1], the rms deviation Δ of experimental points from the theoretical values [Eq. (1)] is seen to be large. Accordingly, we have divided the data for phase-I into three regions (i), (ii) and (iii) (Fig. 1) and least-square-fitted the quadratic [Eq. (1)] to the data with the different combinations as shown in Table 1.

The rms deviation Δ was seen to be different in the different regions, being largest in region (iii).

In case (d), we also note that the value of D_{min} exceeds the lowest experimentally observed value of D. In cases (c) and (d), the values of the parameters suggest minima in D, at high temperatures, that are not observed. Also, the deviation Δ_f is larger than Δ_e while Δ_a has the smallest value. Further, the coefficient of the quadratic term (β) increases in magnitude as the temperature approaches T_{I-II} from above in sequence (i)→(ii)→(iii). The above observations support our contention that the effect of the phase transition at T_{I-II} is manifested in region (iii), and becomes larger as the transition temperature is approached from above. One may question the use of three 'regions' in phase-I, and expect that it can even be two or four regions. This choice is convenient in that one can compare the validity of the quadratic close to T_{I-II} with that far from T_{I-II}, and also with an intermediate region while retaining a sufficient number of data points to make a least-square fit meaningful. The fact that such a division of the temperature range is not entirely arbitrary and in fact is the correct thing to do is borne out by the results of the analysis in that it is shown that Eq. (1) is valid only far away from the transition [region (iii)] and as one gets closer to the transition, departures from the expected behaviour occur, largest being in region (i) which is the closest to the transition and less so in region (ii).

The quadratic form [Eq. (1)] fitting regions (i) and (ii) together (case e) was extrapolated into region (iii), and the value of D so obtained was subtracted from the experimental D value in region (iii) (Fig. 2). The difference ΔD is plotted against T in the inset (Fig. 2), representing the effect of the phase transition. The dependence is approximately linear, and we attribute it to temperature-dependent modes corresponding to phase-II.

4 Discussion

4.1 Temperature Dependence of D

There are two contributions to the temperature variation of D: one implicit—due to thermal expansion and the other explicit—due to harmonic lattice vibrations. Walsh[3] considered the explicit effect

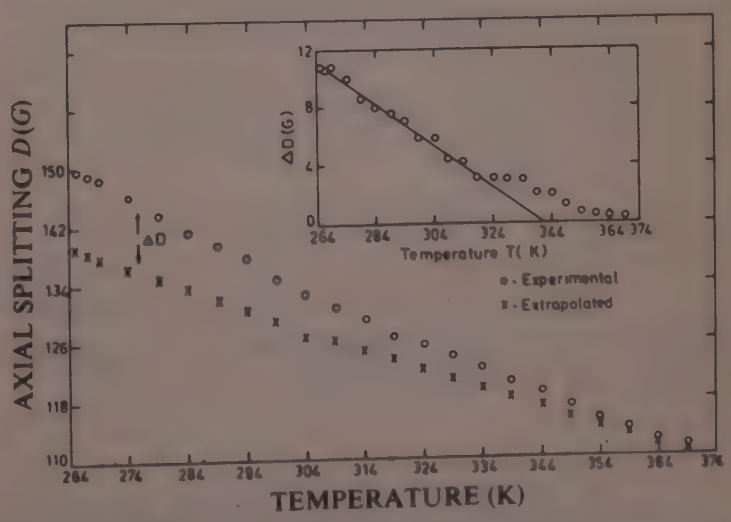

Fig. 2—Departure (ΔD), close to the transition, of experimental values of D from expected values obtained by extrapolating the curve in regions (i) and (ii)—case(e)—into region (iii). The inset shows the approximately linear dependence of ΔD on T close to T_{I-II}

and showed it to result in a temperature variation:

$$D = D_0\left(1 + B\coth\frac{h\nu}{2kT}\right) \quad \ldots (3)$$

where ν is the frequency of the lattice vibration, and D_0 the static value of D. In the high temperature approximation ($h\nu \ll kT$) this reduces to

$$D = D_0(1 + BT) \quad \ldots (4)$$

A form similar to Eq. (3) was also obtained by Serway[4] and Pfister *et al.*[5] Marshall *et al.*[6] have incorporated the effect of anharmonic potential wells to obtain a form of the type:

$$D = D_0 + \alpha\coth\frac{h\nu}{2kT} + \beta\coth^2\frac{h\nu}{2kT} \quad \ldots (5)$$

The implicit temperature variation was removed[3-5] by performing a variation of D with pressure experiment to obtain $1/D(\partial D/\partial P)$, with the thermal expansion, the compressibility and the equation of state of the material also being used. Leclerc and Manoogian[7] also used the form:

$$D = D_{\text{static}} + D_{\text{vibrational}}$$

$$= D_S^0(1 + \alpha T + \beta T^2) + D_v\coth\left(\frac{h\nu}{2kT}\right) \quad \ldots (6)$$

A possible reason for a quadratic dependence of the static contribution to D on temperature is obtained from the point-charge model, where the dependence of D on temperature is obtained from the point-charge model[8] where $D \propto (1/r^n)$. Because of thermal expansion, $r = r_0(1 + \gamma T)$, when the expression is expanded binomially, it leads to the quadratic dependence. For the vibrational contribution, D may have a quadratic dependence, from Eq. (5) in the high temperature approximation. Thus, the form of Eq. (1) may be obtained from both static and vibrational contributions. Separation of the two can only be done by means of high pressure ESR experiments. A more general form than that of Walsh[3], applicable at very low temperatures, was obtained by Shrivastava[9], using the electron-phonon interaction, but that form does not concern us here.

The pronounced nonlinearity of $D(T)$ in phase-I, as observed, makes Eq. (4) inapplicable, and one must resort to Eq. (1). It is our contention that the deviation from the quadratic form increases as $T \to T_{\text{I-II}}$, and this deviation ΔD is plotted in Fig. 2.

4.2 Discontinuous Change of D at $T_{\text{I-II}}$

According to the X-ray study of Stadnicka and Glazer[2], in phase-I the propionate groups flip between two sites ('a' and 'b') related by two-fold axes (Fig. 3). Assuming a similar dynamic model for the axial

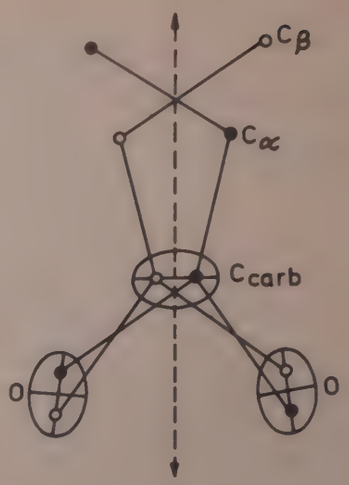

Fig. 3—Low-frequency hopping in phase-I of the propionate group between two equivalent sites (from Ref. 2)

splitting, D in phase-I is the time average, both in direction and magnitude, of two corresponding D configurations (D_a and D_b) in phase-II. The direction-averaging has been reported in our previous work[1]. These configurations correspond to our observed results of angular displacements by $\pm 15°$ in the (111) plane, and $\pm 16°$ in the (001) plane, of the D tensor axes in phase-II from those in phase-I. That is, if we associate with the D tensor, a frequency f_{obs} ($\sim 1/D$), and consider a residence time in the equilibrium configurations a and b, in phase-I, $1/t > f_{\text{obs}}$; and in phase-II, $1/t < f_{\text{obs}}$; assuming that the time required to go from configuration a to configuration b is negligible in both phases. Thus, in phase-I, the direction of the projection of D (in either plane) is the same as the coincidence direction in phase-II, because of the averaging between the two configurations above $T_{\text{I-II}}$ (Fig. 4).

In terms of the magnitude of the D tensor in the two phases, we can obtain the line position H_I (in phase-I) by assuming that it occurs at the average of the line positions in phase-II, corresponding to the two configurations:

$$H_I = \frac{H_{II}^a + H_{II}^b}{2} \quad \ldots (7)$$

for various angles of θ. The averaging is shown in Fig. 4.

From Fig. 4, we see that the principal value of D in phase-I equals the value of D at the coincidence direction in phase-II. The principal values of D just above and just below $T_{\text{I-II}}$ are related by magnitude-averaging, and the values are obtained from powder ESR spectra:

$$D_I = \frac{D_{II}(3\cos^2\theta - 1)}{2} \quad \ldots (8)$$

where $\theta = 26.6°$ is the angular separation (in space) between D_I and D_{II} (Fig. 4). This value of θ is obtained

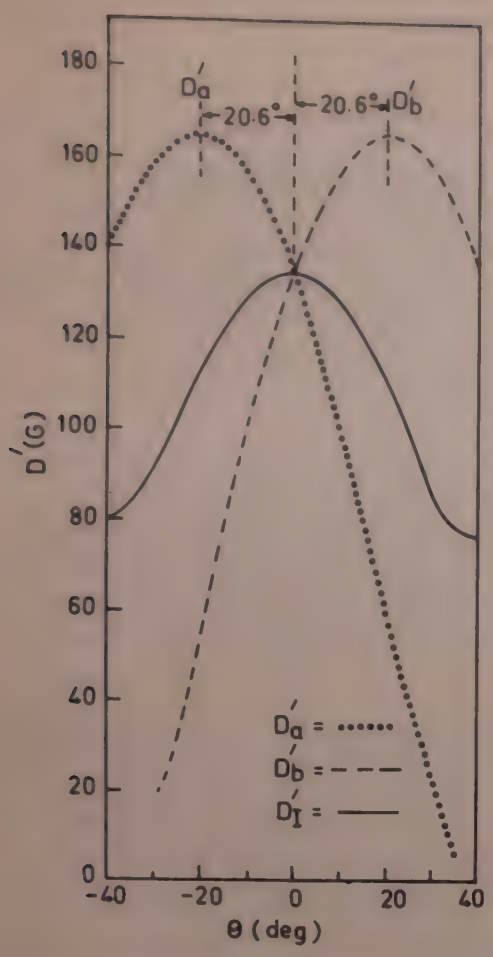

Fig. 4—Model for averaging of D corresponding to the motion of the propionate groups above the transition. $D_I = 1/2\, D_{II}(3\cos^2\theta - 1)$ is plotted as a function of θ, the orientation with respect to the magnetic field in planes defined by the two D directions in the respective phases. D_I is the time-averaged value in phase-I of D_a and D_b of phase-II

from the direction cosines previously reported[1]. From the powder spectra, D_{II} is 165.2 G, and according to Eq. (8), D_I should be 134.6 G while it is actually 149.5 G. This difference, we infer, arises because the first order I → II transition is accompanied not only by a freezing of the propionate group flipping motion, but also by a static distortion of the oxygen octahedra.

It may be noted that we have invoked a dynamic model to account (partially) for the discontinuity in D at $T_{I\to II}$, and attributed the discrepancy to the static distortion of the oxygen octahedra. On the basis of the ESR results alone, we could just as well have explained the discontinuity entirely in terms of a static deformation of the oxygen octahedron, since the propionate group flipping may be already static on the ESR time scale. However, various ^{1}H NMR second moment results[10,11] including the study of the second moment as a function both of temperature and pressure in DBP performed in our laboratory[12] show that there is certainly a slowing down of the propionate group dynamics, across the transition. Our ESR results corroborate this conclusion.

Thus, the cubic phase-I is seen to be the time average of two equilibrium configurations corresponding to phase-II, which is one of the possibilities considered by Stadnicka and Glazer[2] (in terms of the space group, $Fd3m$ of phase-I is considered as a 'dynamic' mixture of left and right-handed tetragonal space groups $P4_32_12$ and $P4_12_12$, corresponding to phase-II).

Such dynamic models, involving averaged tensors in the plane with higher symmetry, have been used by Bjorkstam[13] and Schirmer and Muller[14]. According to Bjorkstam, the averaged EFG tensor q of a deuteron in a 'close' and a 'far' configuration in an O...D−O bond in KD_2PO_4 is

$$q = \frac{q_{cl} + q_f}{2} \qquad \ldots (9)$$

This statement is analogous to the one made above for the line positions arising from the D-tensor, which transforms similarly as the EFG tensor [Eq. (8)]. Also, it is clear that the transformation of the tensors D and q is not a simple vector projection (multiplying by $\cos\theta$), but is of the form:

$$q' = q\frac{(3\cos^2\theta - 1)}{2} \qquad \ldots (10)$$

Further at T_{I-II}, the discontinuity in D may be accounted for entirely by static distortion of the oxygen octahedron or by also incorporating the freezing of the flipping (on the ESR time scale) of the propionate groups (at the transition temperature). The latter model seems to be more consistent with the model of successive arrests of the motion of the propionates proposed by Aleksandrova *et al.*[11] and with the low frequency flipping of the propionate group at room temperature reported by Stadnicka and Glazer[2].

It may be noted that the observation of symmetry change at the I-II transition has been made only by ESR methods. The T_1 versus T results of Sundaram *et al.*[15] show no change at the first-order I-II transition nor do the IR experiments of Seetharaman *et al.*[16] (although both groups detect changes at the second-order II-III transition). Probably, propionate group motions connected with the I-II transition do not fall within IR or NMR time scales. X-ray analysis of phase-II has not been reported so far.

References

1 Bhat S V, Dhar V & Srinivasan R, *J Phys Soc Jpn (Japan)*, **50** (1981) 2312.
2 Stadnicka K & Glazer A M, *Acta Crystallogr Sect B (Denmark)*, **36** (1980) 2977.
3 Walsh (Jr) W M, *Phys Rev (USA)*, **114** (1959) 1473.
4 Serway R A, *Phys Rev B (USA)*, **3** (1971) 608.
5 Pfister G, Dreybodt W & Assmus W, *Phys Status Solidi (Germany)*, **36** (1969) 351.
6 Marshall S A, Hodges J A & Serway R A, *Phys Rev A (USA)*, **136** (1964) 1024.

7 Leclerc A & Manoogian A, *J Chem Phys (USA)*, **63** (1975) 4456.
8 Geĭfman I N & Glinchuk M D, *Sov Phys Solid State (USA)*, **13** (1971) 872.
9 Shrivastava K N, *Phys Rep Phys Lett Sect C (Netherlands)*, **20C** (1975) 137.
10 Nakamura N, Suga H, Chihara H & Seki S, *Bull Chem Soc Jpn (Japan)*, **41** (1968) 291.
11 Aleksandrova I P, Zherebtsova L I & Aleksandrov K S, *Sov Phys—Crystallogr (USA)*, **12** (1968) 780.
12 Arumugam S, Bhat S V & Srinivasan R, ^{1}H high pressure NMR study of DBP, *Proc 1st Meeting on Ferroelectricity* (in Press), New Delhi, India, 1980.
13 Bjorkstam J L, *Phys Rev Lett (USA)*, **23** (1969) 780.
14 Schirmer O F & Muller K A, *Phys Rev B (USA)*, **7** (1973) 2986.
15 Sundaram C S, Ganesan K & Ramakrishna J, *Proc Nucl Phys Solid State Phys Symp (India)*, **22C** (1979) 660.
16 Seetharaman S, Bhat H L & Narayanan P S, Paper accepted for presentation in 5th European Meeting on Ferroelectricity (EMF-5), Malaga, Spain, 26 Sept.-1 Oct., 1983.

Indian Journal of Pure & Applied Physics
Vol 21, September 1983, pp. 521-524

Calibration of Makrofol Polycarbonate Plastic Track Detector Using $^{16}_{8}O$ Ions

S M FARID & A P SHARMA*
Department of Physics, Kurukshetra University, Kurukshetra 132 119

Received 27 *July* 1982; *revised received* 23 *November* 1982

The temperature dependence of etching rates of Makrofol polycarbonate plastic detectors has been studied. In the method employed, $^{16}_{8}O$-ions of energy 2.50 MeV/N (N signifies nucleon) are used as energetic ions for track formation in the detector. The experimental results indicate that the track etch rate is dependent on the energy loss rate of energetic ions; whereas the track registration sensitivity increases, the cone angle of $^{16}_{8}O$-ion tracks decreases at higher etching temperatures. The maximum etched track length agrees closely with the theoretical range. From the calibration curve, the critical energy loss is determined and is found to be 5.70 MeV $mg^{-1}cm^2$, which is in agreement with that reported in literature.

1 Introduction

The production of tracks by energetic ions in solid state nuclear track detectors (SSNTDs) and the subsequent revealing of these tracks by chemical etching is a widely used technique for detection and identification of ions. One of the most valuable features of SSNTDs is the existence of a well-defined detection threshold, i.e. a critical value of energy loss rate, $(dE/dx)_{crit}$ above which radiation damages produced on the SSNTDs by incident particles can be made into visible tracks by a selective chemical etching[1]. The critical value $(dE/dx)_{crit}$ is characteristic of detector material.

The track etch rate (V_t) along the trajectory of a particle in the track detector is an increasing function of energy deposited around the track. For all cases of particle identification with nuclear track detector, it is necessary to know the relation between V_t and the energy deposited along the trajectory of the particle under a certain etching condition. The curve of the etching rate as a function of the deposited energy is often called as the calibration curve.

The track length provides the range of the particle and hence its energy. The maximum etched track length is also a measure of the mass A and charge Z of the incident particle[2]. The bulk etching at the detector surface shortens the lengths of the tracks. To correct the observed track length, it is essential to have an accurate knowledge of bulk etch rate (V_b).

The present work was undertaken to draw the calibration curve of Makrofol-E polycarbonate plastic detector using $^{16}_{8}O$-ions of energy 2.50 MeV/N (N signifies nucleon). The critical energy loss $(dE/dx)_{crit}$ for this detector material is determined from the calibration curve. The maximum etched track length is compared with the theoretical range as well as with the range reported by earlier workers. The dependence of V_b and V_t on temperature of etching is studied.

2 Experimental Details

Samples of Makrofol-E polycarbonate plastic detectors were irradiated with $^{16}_{8}O$-ions of energy 2.50 MeV/N at an angle of 30° to the detector surface from cyclotron beams at the Joint Institute of Nuclear Research, Dubne, USSR. All etching was carried out in 6*N* NaOH solution kept at a constant temperature in a thermostatic bath. The temperature at which etching took place was maintained constant to within ±0.5°C. The temperature of the etchant varied from 50 to 90°C.

The track lengths were measured with a transmitted light microscope 'Olympus' having an eyepiece micrometer of least count 0.215 μm at a magnification of 900 ×. The total error in measurements, arising from statistical errors, diffraction of light and microscope optical resolution, was found to be ~0.5 μm.

3 Results and Discussion

3.1 Effect of Temperature on Bulk Etch Rate V_b and Track Etch Rate V_t

The bulk etch rate is measured by two techniques—(i) track diameter technique, and (ii) gravimetric technique.

From the track diameter kinetics[3,4] the relationship between track diameter (D) and V_b can be expressed by

$$D = 2V_b t\left[\frac{V-1}{V+1}\right]^{1/2} \quad \ldots (1)$$

where $V = V_t/V_b$ and t is the etching time.

If $V \gg 1$, i.e. $V_t \gg V_b$, then

$$D = 2V_b t \quad \ldots (2)$$

Eq. (2) is a linear relationship with a gradient of $2V_b$. Since $V_t/V_b \gg 1$ for full energy fission fragments in plastics[3,4], a plot of D of fission fragments versus t should approximate to a straight line having a gradient of $2V_b$.

Samples of Makrofol-E are irradiated normally with a collimated beam of fission fragments from ^{252}Cf source in vacuum ($\sim 10^{-2}$ Torr). The irradiated samples are then etched in 6 N NaOH solution at a constant temperature. A graph is then plotted for Makrofol by taking the average diameter of about 250 fission fragment tracks at various etching times. These plots are drawn for different etching temperatures. From the graphs, the values of V_b are determined for different etching temperatures.

In gravimetric technique[5], the weight of the rectangular plastic sample (foil) before and after etching is measured with a microbalance. The bulk etch rate is given by

$$V_b = \frac{\Delta m}{2S\rho t}\ 10^4 (\text{in } \mu\text{m/min}) \qquad \ldots (3)$$

where Δm (in g) is the dissolved mass in known etching time, t (in min) the etching time, S (in cm^2) the surface area of the sample, and ρ (in g/cm^3) the density of the plastic sample.

The observed (projected) track length (l) is measured from the centre of the track ellipse at the etched surface to the end of the track tip.

The corrected track length (L) is calculated by the relation[5]

$$L = \frac{l}{\cos\theta} + \frac{V_b t}{\sin\theta} - V_b(t - t_c) \qquad \ldots (4)$$

where θ is the angle of incidence, $V_b t/\sin\theta$ the surface etching correction, $V_b(t - t_c)$ the overetching correction and t_c the time required to etch the tracks completely.

The correlation between V_t and L for an etching time t is given by the relation[6]

$$L = \int_0^t V_t\, dt$$

or $$V_t = \frac{\Delta L}{\Delta t} \qquad \ldots (5)$$

Thus V_t is measured by measuring the track length increase at different etching times.

V_b and V_t are determined at 50, 60, 70, 80 and 90°C for 6N NaOH solutions.

The straight lines in Fig. 1 indicate that the dependence of V_b and V_t on etching temperature T follows the Arrhenius relationship of the forms

$$V_b = A\exp(-E_b/kT) \qquad \ldots (6)$$

$$V_t = B\exp(-E_t/kT) \qquad \ldots (7)$$

where k is the Boltzmann constant; A and B are constants, and E_b and E_t are the activation energy for bulk etching and track etching respectively. From the slopes of the straight lines, E_b and E_t have been

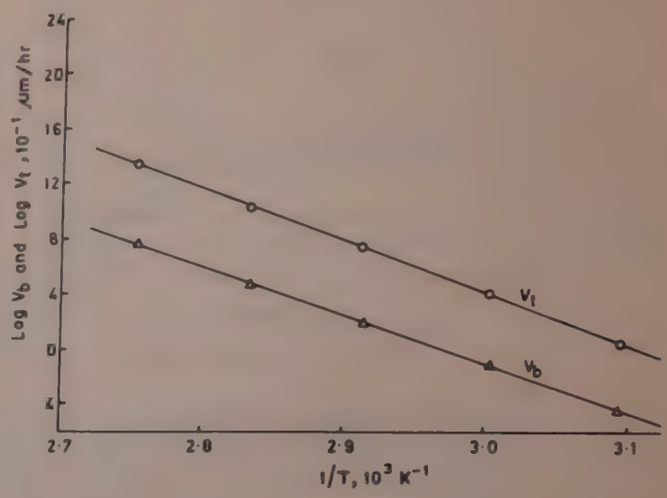

Fig. 1—V_b and V_t versus $1/T$

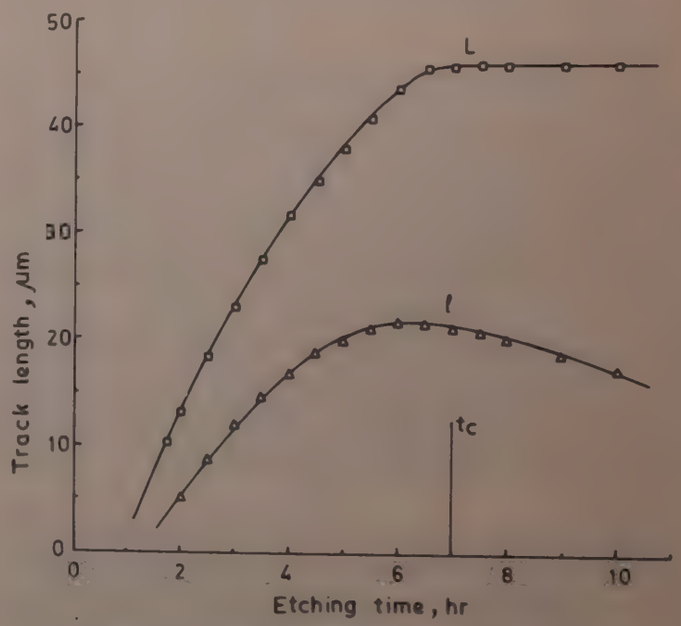

Fig. 2—L and l versus t (etching temperature, 70°C)

calculated as $E_b = (0.72 \pm 0.08)$ eV and $E_t = (0.70 \pm 0.7)$ eV. The values are in good agreement with those reported by earlier workers[7,8]. The ratio of E_t/E_b is found to be 0.97.

The variations of l and L with t for the sample etched in 6N NaOH at 70°C are shown in Fig. 2. It can be seen from Fig. 2 that l starts decreasing after complete etching time (t_c). This decrease is due to the fact that the bulk etching shortens the completely developed tracks. When bulk etching correction and overetching correction are made, L becomes constant beyond t_c.

The experimental values of V_t at different L for the sample etched in 6N NaOH at 70°C are shown in Fig. 3. Similar plots can be drawn for 50, 60, 80 and 90°C.

3.2 Dependence of Track Registration Sensitivity ($V = V_t/V_b$) and Cone Angle (φ) on Etching Temperature (T)

Taking the $V = V_t/V_b$ relationship into consideration, the values of V are calculated from the experimentally determined V_t and V_b values for

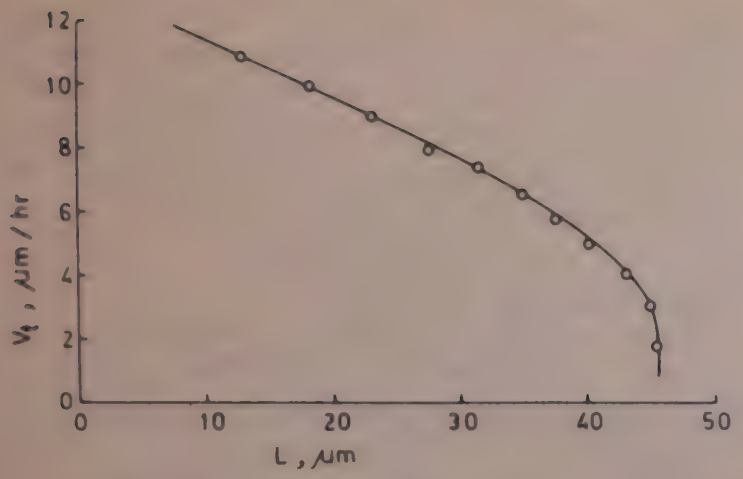

Fig. 3—V_t versus L (etching temperature, 70°C)

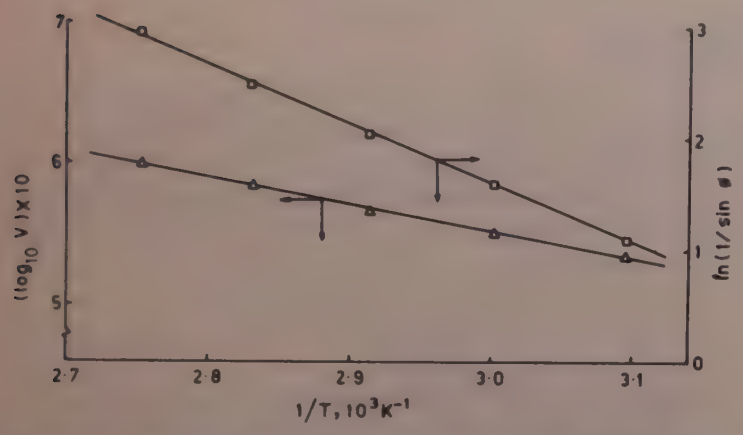

Fig. 4—Dependence of track registration sensitivity (V) and cone angle (φ) on temperature of the etchant

different temperatures. In Fig. 4, V is plotted as a function of $1/T$ and we can write

$$V=\frac{V_t}{V_b}=\frac{B}{A}\exp\left[-(E_t-E_b)/kT\right] \quad \ldots (8)$$

Thus with Makrofol-E, there is an increase in V at higher etching temperatures. Schlenk *et al.*[7] have arrived at a similar conclusion after investigating α-particle tracks in Makrofol-E.

By noting that $\sin\varphi = V_b/V_t = V^{-1}$, we can conclude that with Makrofol-E sheets the cone angles of $^{16}_{8}$O-ion tracks etched in 6N NaOH decrease at higher etching temperatures.

Using $\sin\varphi = V_b/V_t$, Eq. (8) can be written in the form.

$$\ln(1/\sin\varphi)=\frac{(E_t-E_a)}{kT}+\ln B/A \quad \ldots (9)$$

Eq. (9) shows a linear relationship between $\ln(1/\sin\varphi)$ and $1/T$. This dependence is tested by etching $^{16}_{8}$O-ion tracks in Makrofol in 6N NaOH at 50, 60, 70, 80 and 90°C and the linear relationship is confirmed (Fig. 4).

3.3 Maximum Etched Track Length Comparison with Theoretical Range

One of the exposed samples is etched in 6N NaOH at 70°C. The process is terminated when tracks developed rounded terminal ends. The track lengths are calculated using Eq. (5). The track length distribution is shown in Fig. 5. The peak position of the Gaussian curve fitted to the historgram represents the most probable length. The most probable track length of 2.5 MeV/N $^{16}_{8}$O-ion in Makrofol-E is $\langle L\rangle = 45.50$ μm.

To calculate the theoretical range of $^{16}_{8}$O- ion in Makrofol-E, the stopping power and range equations of Mukherji and Nayak[9] have been used. The range (R, mg/cm^2) of an ion in complex media is given by

$$R=\sum_{E_i}^{E_0}\frac{\delta E}{[(dE/dx)_c]_E} \quad \ldots (10)$$

where

$$[(dE/dx)_c]_E=\frac{1}{A_c}\sum_i[y_iA_i\{(dE/dx)_i\}_E]$$

is the stopping power of the complex medium at the ion energy E (in MeV), $\{(dE/dx)_i\}_E$ the stopping power of the ith atomic species at the same ion energy, $A_0(=\sum_i y_iA_i)$ the molecular mass number of the medium, A_i and Y_i are the mass number and the number of atoms per molecule of the ith atomic species respectively, δE is a small energy interval over which the stopping power remains constant, E_i is the initial ion energy and E_0 is the final energy corresponding to the ion velocity $V_0 = e^2/\hbar$.

To compute R for a heavy ion of initial energy E_i(in MeV), one has to calculate $[(dE/dx)_c]_E$ starting with $E = E_i$ at each new ion energy decreasing by a small amount $\delta E(=0.01$ MeV) over which the elemental

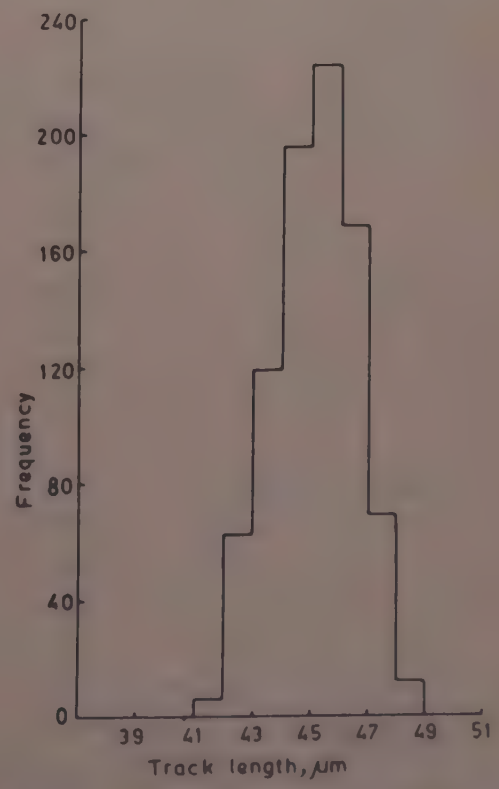

Fig. 5—Track length distribution for 30° exposure (total tracks = 856)

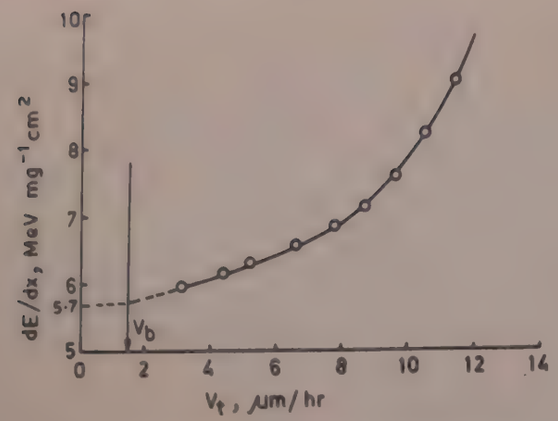

Fig. 6—Variation of V_t with the energy loss (dE/dx)

stopping power remains constant, till the final ion energy E_0 corresponding to the velocity V_0 is reached[10]. The range is then given by Eq. (10). Using the equations of Mukherji and Nayak, a computer program was made and with the help of the computer, the range and energy loss of $^{16}_{8}$O-ion in Makrofol-E($C_{16}H_{14}O_3$), ρ=(1.20 g/cm^3) were computed. The computer lists the energy loss and the penetration depth (i.e. range) for each energy until the energy reaches the value zero. The computed range of 2.50 MeV/N $^{16}_{8}$O-ion has been found to be R=48.28 μm. The maximum etched track length agrees closely (better than 6%) with the theoretical range as well as with that reported by Tripier *et al.*[11]

3.4 Calibration Curve and Critical Energy Loss

The (dE/dx) values corresponding to different track lengths (i.e. penetration depths) have been obtained from computer output and a plot of these two has been drawn (not shown). The variation of V_t with track length is shown in Fig. 3. From these two figures, we deduce that V_t is a function of energy loss rate (dE/dx), as shown in Fig. 6. The value of (dE/dx) at which V_t becomes equal to V_b is taken as the critical energy loss $(dE/dx)_{crit}$ for track etching below which no etchable track can be produced. The critical energy loss for Makrofol-E polycarbonate detector has been found to be 5.70 MeV mg^{-1}cm^2. This value is in agreement with that reported in literature[2,12].

Acknowledgement

The authors are grateful to Prof. V P Perelygin, Joint Institute of Nuclear Research, Dubna, USSR, for providing exposure facilities. One of the authors (SMF) is thankful to Dr J S Yadav for helpful discussion and to the Department of Science and Technology, New Delhi, for the award of a research fellowship.

References

1 Price P B & Walker R M, *J Apply Phys (USA)*, **33** (1962) 3400.
2 Fleischer R L, Price P B & Walker R M, *Annu Rev Nucl Sci (USA)*, **15** (1965) 1; **21** (1971) 295.
3 Somogyi G & Szalay S A, *Nucl Instrum & Methods (Netherlands)*, **109** (1973) 211.
4 Enge W, Grabisch K, Dallmeyer L, *et al.*, *Nucl Instrum & Methods (Netherlands)*, **127** (1975) 125.
5 Dwivedi K K & Mukherji S, *Nucl Instrum & Methods (Netherlands)*, **161** (1979) 317.
6 Fleischer R L, Price P B & Walker R M, *Nuclear tracks in solids* (University of California Press, Berkeley), 1975.
7 Schlenk B, Somogyi G & Valek A, *Radiat Eff (GB)*, **24** (1975) 247.
8 Frank A L & Benton E V, *Radiat Eff (GB)*, **2** (1970) 269.
9 Mukherji S & Nayak A K, *Nucl Instrum & Methods (Netherlands)*, **159** (1979) 421.
10 Mukherji S & Srivastava B K, *Phys Rev (USA)*, **B9** (1974) 3708; **A14** (1976) 718.
11 Tripier J, Remy G, Ralarosy J, *et al.*, *Nucl Instrum & Methods (Netherlands)*, **159** (1979) 421.
10 Mukherji S & Srivastava B K, *Phys Rev (USA)*, **B9** (1974) 3708; **A14** (1976) 718.
11 Tripier J, Remy G, Ralarosy J, *et al.*, *Nucl Instrum & Methods (Netherlands)*, **115** (1974) 29.
12 Debeauvais M, Stain R, Ralarosy J & Cuer P, *Nucl Phys A (Netherlands)*, **90** (1967) 186.

Indian Journal of Pure & Applied Physics
Vol 21, September 1983, pp. 525-528

Spatial Correlation & Isothermal Compressibility in Interacting Bosons at Low Temperatures

A N PHUKAN*
Department of Physics, Dirugarh University, Dibrugarh 786 004

and

P N BORA
Department of Physics, North Lakhimpur College, North Lakhimpur 787 001

Received 27 *September* 1982

Properties of interacting bosons have been studied using the formalism of the theory of many-body systems. Results obtained for the isothermal compressibility show remarkable agreement with the experimental values on liquid ^{4}He. The mean square relative fluctuation in the number density of the system at temperatures below the lambda-transition temperature of liquid He^4 and the degree of correlation amongst the bosons at such temperatures are also studied using the standard methods of statistical mechanics.

1 Introduction

Calculations on the thermodynamic properties and the energy excitation spectrum of interacting bosons and comparison of such theoretical results with those of liquid ^{4}He had been a subject of a number of rigorous studies[1-5] in recent years. Of the various forms of the ^{4}He-^{4}He interaction potential, the Gaussian equivalent of the Lennard-Jones potential developed by Khanna and Das[2] could be quite successfully used in calculating the energy excitation spectrum for the interacting bosons. Kebukawa *et al.*[4] calculated the excitation energy by considering the phonon-phonon interaction to be through the Morse potential. But their calculations led to a perceptible difference between theory and experiment in the extremely low momentum region and also in the higher momentum region above the roton dip in the excitation energy spectrum for liquid ^{4}He. Commenting on such discrepancies between theory and experiment Kebukawa *et al.* hinted[4] upon the necessity of taking account of a long tail of attractive potential and also put forward the idea that the best realistic potential would be that of Lennard-Jones instead of the Morse potential. But the main difficulty with the Lennard-Jones potential, in such a theory, was the nonavailability of its Fourier transform. Khanna and Das[2], however, built the Gaussian equivalent of the Lennard-Jones potential, having the required Fourier transform and calculated the energy excitation spectrum for interacting bosons resembling, both qualitatively and quantitatively, the experimental energy excitation spectrum for liquid ^{4}He.

Using this potential from Ref. 2, we have, in this work, studied the connection between density fluctuations and spatial correlations of the bosons. We have used the expression for the space integral of the correlation function $C(r)$ in terms of the means square relative fluctuation in density. The isothermal compressibility χ_T is then brought in to enable us to study the correlation function (or for that matter, the mean square relative fluctuation in density). The theory to obtain the isothermal compressibility for the system of bosons is then incorporated and an expression is derived for the isothermal compressibility, involving, in the process, the ground state reaction matrix. We have seen that the mean square relative fluctuation can be written as kT times the isothermal compressibility, where k is the Boltzmann constant and T is the absolute temperature and thus we have studied the isothermal compressibility and the mean square relative fluctuation in density for the system of bosons interacting via a potential composed of a hard core plus two gaussians.

The results obtained by us in our present calculations, for the isothermal compressibility bear very good agreement with the experimental values for liquid ^{4}He. In some of our earlier works (Ref. 6 for example), we have calculated the isothermal compressibility for the bosons assuming them to interact via a potential composed of a hard core followed by a square well. Comparing our present calculations with these earlier results we observe that better agreement between theory and experiment results, when the inter-particle potential is assumed to

be composed of a hard core followed by two gaussians, than when it is of the hard core followed by a square well type.

As regards the mean square relative fluctuation in density we observe that in our present calculations, it is of the order of about one-tenth of $1/N$, where N is the Avogadro number, at temperatures below about 1 K; while it becomes of the order of $1/N$ at and above $T = 1$ K. This result may be interpreted as indicating some sort of phase transition in the system around $T = 1$ K, corresponding thereby to the second phase transition observed experimentally in liquid ^{4}He at around 0.6 K.

2 Basic Theoretical Formulations

The measure of the degree of spatial correlation in an interacting system of N particles enclosed in a volume V is given by the pair correction function $C(r)$ defined by

$$C(r)=\eta^2(r)-1; \quad r=r_1-r_2 \qquad \ldots (1)$$

where $\eta^2(r)$ is the pair distribution function. The product $\eta^2(r)d^3r$ determines the probability of finding a particle in the volume element d^3r around the point r when there is already a particle at the point $r=0$. The case of a classical gas composed of non-interacting particles is characterized by absence of spatial correlations and in such cases $\eta^2(r)$ is identically equal to unity and consequently the pair correlation function becomes identically equal to zero.

Considering a macroscopic region V_m in the assembly, let there be N_m number of particles in this region and defining the number N_m which is fluctuating as a result of the switching on of the interaction by

$$N_m=\sum_{i=1}^{N}\mu(r_i) \qquad \ldots (2)$$

where the function $\mu(r)$ is such that $\mu(r)=1$ when r lies inside the region V_m and zero when r lies outside of it, the mean square relative fluctuation in density is given by[7]

$$F=\frac{\langle N_m^2\rangle-\langle N_m\rangle^2}{\langle N_m\rangle^2}=\frac{1}{\rho}\left[1+\rho\int_{V_m}C(r)d^3r\right] \qquad \ldots (3)$$

where $C(r)$ is the pair correlation function.

Again, the space integral of the pair correlation function $C(r)$ is related to the isothermal compressibility χ_T through the well known relation (Ref. 6)

$$\overline{C(r)}\,d^3r=kT\chi_T-\frac{1}{\rho} \qquad \ldots (4)$$

This means that the mean square relative fluctuation in density is given by

$$F=\frac{1}{\rho}[1+\rho kT\chi_T-1]=kT\chi_T \qquad \ldots (5)$$

To calculate χ_T we proceed from the known relation

$$\chi_T=-\frac{1}{\rho}\left(\frac{\partial P}{\partial\rho}\right)^{-1} \qquad \ldots (6)$$

To calculate χ_T from Eq. (6) one has to know the pressure P. The equation of state is given by

$$\frac{P}{\rho kT}-1=2\pi\rho\int_0^\infty r^2dr \times[\exp\{-V(r)/kT\}-1]g(r) \qquad \ldots (7)$$

The radial distribution function (RDF), $g(r)$, is related to the pair distribution function (PDF), $\eta^2(r)$, by the relation:

$$g(r)=\frac{\eta^2(r)}{\rho^2}$$

where ρ is the particle density.

The PDF is the inverse Fourier transform of the structure factor $S(k)$ and is given by

$$\eta^2(r)=\frac{1}{(2\pi)^3}\int S(k)\exp(-ik.r)\,d^3k \qquad \ldots (8)$$

This structure factor, in its turn, determines the excitation energy spectrum $E(k)$ given by

$$S(k)=\frac{\hbar^2k^2}{2m^*E(k)} \qquad \ldots (9)$$

This means that, when $E(k)$ is known for an interacting system, Eq. (9) can be used to determine $S(k)$ and then substituting for $S(k)$ in Eq. (8), the PDF can be calculated to know the pressure P required for calculating χ_T from Eq. (6). This method of calculating the RDF from $E(k)$ has been followed in our present calculations.

Our earlier work[1] gives a method of calculating $E(k)$ in terms of the matrix elements t_{0000} of the ground state reaction matrix, and we have:

$$E(k)=\left(\frac{\hbar^2k^2}{2m^*}\right)\left[1+\frac{4m^*}{\hbar^2k^2}N_0t_{0000}\frac{\sin ka}{ka}\right]^{1/2} \qquad \ldots (10)$$

which gives[6]

$$\eta^2(r)=\delta(r)-\frac{2m^*N_0t_{0000}}{(2\pi)^3\hbar^2}\left[\frac{4\pi}{ar}\begin{cases}\pi r/2 & 0<r\leq a\\ \pi a/2 & r>a>0\end{cases}\right] \qquad \ldots (11)$$

Now when the system of bosons interact through a two-body potential composed of a hard core followed by a combination of both repulsive and attractive Gaussian potential (which is the equivalent of Lennard-Jones potential) given by

$$U(r)=\left\{4V_0\left[\exp\left(-\frac{r-a}{\mu_R}\right)^2-\exp\left(-\frac{r-a}{\mu_A}\right)^2\right]\right. \quad r<a\,r>a \qquad \ldots (12)$$

the ground state reaction matrix t_{0000} is given[2] by

$$N_0 t_{0000} = \frac{\lambda^2 \hbar^2}{2m^* a^2} + 4\pi^{3/2} \rho V_0 (\mu_R^3 - \mu_A^3) \quad \ldots (13)$$

where μ_R and μ_A are the repulsive and attractive ranges respectively after the hard core.

Using Eqs (13), (11), (10) and (7) the equation of state for the presently considered system of bosons is given by

$$\frac{P}{\rho kT} - 1 = \frac{\lambda^2}{6} - \frac{\lambda^2 V_0}{a^2 kT}[(\mu_A^2 - \mu_R^2) + a\sqrt{\pi}(\mu_A - \mu_R)]$$
$$- \frac{4\pi^{3/2} m^* V_0 (\mu_A^3 - \mu_R^3) \rho a^2}{3\hbar^2}$$
$$+ \frac{8\pi^{3\ 2} m^* V_0^2 \rho (\mu_A^3 \mu_R^3)}{\hbar^2 RT}$$
$$\times [(\mu_A^2 \mu_R^2) + a\sqrt{\pi}(\mu_A - \mu_R)] \quad \ldots (14)$$

From the above equation and using Eq. (6) one can calculate χ_T from the following expression

$$\chi_T = -\frac{1}{\rho}\left\{ kT + \frac{\lambda^2 kT}{6} - \frac{\lambda^2 V_0}{a^2} \right.$$
$$\times [(\mu_A^2 - \mu_R^2) + a\sqrt{\pi}(\mu_A - \mu_R)]$$
$$- \frac{8\pi^{3/2} m^* \rho V_0 a^2 kT (\mu_A^3 - \mu_R^3)}{3\hbar^2}$$
$$+ \frac{16\pi^{3\ 2} m^* \rho V_0^2 (\mu_A^3 - \mu_R^3)}{\hbar^2}$$
$$\left. \times [(\mu_A^2 - \mu_R^2) + a\sqrt{\pi}(\mu_A - \mu_R)] \right\}^{-1} \quad \ldots (15)$$

When, however, the bosons are assumed to interact through a two-body potential composed of a hard core followed by a square well, i.e. a potential of the type,

$$U(r) = \begin{cases} +\infty & r < a \\ -V_0 & a < r < b \\ 0 & r > b \end{cases} \quad \ldots (16)$$

the expression for χ_T becomes

$$\chi_T = -\frac{1}{\rho}\left\{ kT + \frac{\lambda^2 kT}{6} - \frac{8\pi m^3 \rho V_0 a^2 kT}{9\hbar^2} \right.$$
$$- (e^{\beta V_0} - 1)\frac{\lambda^2 kT(b^2 - a^2)}{4a^2}$$
$$\left. + (e^{\beta V_0} - 1)\frac{4\pi m^* \rho V_0 kT (b-a)^3 (b^2 - a^2)}{3\hbar^2} \right\}^{-1} \quad \ldots (17)$$

3 Numerical Calculations and Results

Using Eqs (16), (3) and (4), the values of χ_T and F at different temperatures T are evaluated, taking the numerical values of the following parameters as:

$\lambda^2 = 33$
$\mu_A^2 = 0.2206 \text{Å}^2$
$\mu_R^2 = 0.1103 \text{Å}^2$
$a = 2.1 \text{Å}$

$$\frac{m^*}{m} = 1.6$$

$V_0 = 14.11 \times 10^{-16}$ erg
$k = 1.38 \times 10^{-16}$ erg/deg

The reason for our choosing these values of the parameters lies in the fact that the potential considered in our present calculations could very nicely bring in qualitative and quantitative agreement between the theoretical values of the excitation energy of the interacting bosons and the experimental energy excitation graph for liquid ^{4}He, as shown in Ref. 2. Table 1 gives the values of χ_T and F (the mean square relative fluctuation in density) of a condensed system of interacting bosons for the potential composed of a hard core plus two gaussians at different temperatures below the λ-transition temperature of liquid ^{4}He.

In Table 2 are recorded the values of χ_T versus T and F versus T, for a system of bosons interacting with a two-body potential composed of a hard core followed by a square well using Eqs (17), (3) and (4). In these

Table 1—Variation of χ_T and $F(=kT\chi_T)$ with Temperature, for Hard Core + Two Gaussians-Type of Potential

T, K	$\chi_T 10^{-6}$ cm^2/dyn	$F(=\chi_T kT) \times 10^{T22}$
2.2	0.0108	0.0327
2.0	0.0104	0.0287
1.8	0.0100	0.0248
1.6	0.0096	0.0213
1.4	0.0093	0.0179
1.2	0.0090	0.0149
1.0	0.0087	0.0120
0.8	0.0084	0.0002
0.6	0.0082	0.0067
0.4	0.0080	0.0044
0.2	0.0077	0.0021

Table 2—Variation of χ_T and $F(=kT\chi_T)$ with Temperature for Hard Core + Square Well-Type of Potential

T, K	χ_T, cm^2/dyn	$F(=kT\chi_T)$
2.2	-95.0×10^{-13}	$-288.42 \times 10^{-}$
2.0	-67.0×10^{-13}	-184.92×10^{-13}
1.8	-42.0×10^{-13}	-104.33×10^{-13}
1.6	-23.0×10^{-13}	-50.78×10^{-13}
1.4	-11.0×10^{-13}	-21.25×10^{-13}
1.2	-37.0×10^{-14}	-61.27×10^{-14}
1.0	-80.0×10^{-15}	-110.40×10^{-15}
0.8	-74.0×10^{-16}	-81.70×10^{-16}
0.6	-15.0×10^{-17}	-12.42×10^{-17}
0.4	-40.0×10^{-21}	-22.08×10^{-21}
0.2	-15.0×10^{-32}	-4.14×10^{-32}

calculations we use the following numerical values for the different parameters appearing in Eq. (17),

$V_0 = 14.11 \times 10^{-16}$ erg; $b = 6$ Å; $a = 2.1$ Å;
$m^*/m = 1.6$; $\lambda^2 = 33$

These values were earlier used in our calculations on the thermodynamics of interacting boson system[1,6,8]

4 Discussion

Comparing our calculations shown in Fig. 1. with the experimental results[9] for liquid ^{4}He for its isothermal compressibility we see that very good qualitative agreement between theory and experiment is obtained in our present calculations. Further, from Table 1 it is seen that in our present calculations the mean square relative fluctuation in density for a condensed system of bosons increases as the temperature increases but nowhere in the temperature region $0.4\,\text{K} < T < 2.2\,\text{K}$, the density fluctuation becomes unity. This makes the system quite stable and also means that very few particles go to the excited levels from the ground state when a two-body potential, composed of a repulsive hard core followed by two gaussians is applied to the system. In other words, this predicts quite a strong correlation amongst the bosons in the ground state and also the presence of stronger attractive interactions amongst them. This result was also obtained earlier by Khanna *et al.*[5] when they studied the properties of interacting bosons using the same type of potential but with a different formalism.

As regards the order of the fluctuation in density, we see that for the present potential the order of fluctuation in the number density is very much smaller than $1/N$ in the extremely low temperature region, where N is the Avogadro number, and it becomes of the order of $1/N$ only at and above about 1 K. This might mean the existence of a transition in phase of the assembly at about 1 K, thereby corroborating the existence of a second phase transition in liquid He II at about 1 K, as was observed experimentally.

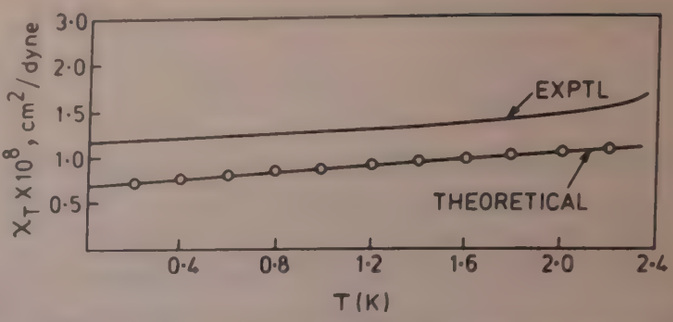

Fig. 1—Plot of isothermal compressibility χ_T versus temperature (T)

Acknowledgement

The authors are thankful to Prof. K M Khanna for inspiring comments and constructive criticism. One of the authors (PNB) is thankful to the Dibrugarh University for providing the facilities to carry out this research programme.

References

1 Khanna K M & Phukan A N, *Physica A (Netherlands)*, **58** (1972) 263; **60** (1972) 438.

2 Khanna K M & Das B K, *Physica A (Netherlands)*, **69** (1973) 611.

3 Brown G V & Cooperswmith M H, *Phys Rev (USA)*, **178** (1969) 327.

4 Kebukawa T, Yamasaki S & Sunakawa S, *Prog Theor Phys (Japan)*, **44** (1970) 565.

5 Khanna K M, Singh S C & Sinha O P, *Indian J Pure & Appl Phys*, **19** (1981) 955.

6 Khanna K M, Phukan A N & Sarmah N C, *Indian J Pure & Appl Phys*, **15** (1977) 498.

7 Pathria R K, *Statistical mechanics*—International Series in Natural Philosophy, Vol 45 (Pergamon Press, London) 1977, 499.

8 Khanna K M & Phukan A N, *Indian J Pure & Appl Phys*, **9** (1971) 156.

9 Donnelly R J, *Experimental superfluidity : Chicago LLectures in Physics* (Chicago University, Press, Chicago, USA) 1967, 233.

Indian Journal of Pure & Applied Physics
Vol 21, September 1983, pp. 529-533

Effect of Interstitial Gas-Pressure & Particle Size on the Effective Thermal Conductivity of Two-phase (Gas-Solid) System

R N PANDEY*† N S SAXENA & D R CHAUDHARY
Department of Physics, University of Rajasthan, Jaipur

Received 20 *August* 1982; *revised received* 30 *May* 1983

An attempt has been made to explain the behaviour of the effective thermal conductivity of two-phase gas-solid systems at different interstitial gas pressures, using kinetic theory. Dependence of gas and solid conduction upon porosity and particle size has also been estimated. Calculated values of the effective thermal conductivity have been compared with reported experimental results. On using the proposed theory in Russel's expression and Hashin's lower bound, we find a fair agreement with experimental results.

1 Introduction

Experimentally, variation of the effective thermal conductivity (K_E) at different interstitial gas pressures of lunar materials[1,2] has been widely studied. The effective thermal conductivities of glass beads[3,4] and fibrous silica[5-7] have recently been studied under changing interstitial gas pressure. In the references[1-7] cited above one finds that behaviour of interstitial gas has been treated qualitatively and some empirical expressions of K_E for silica[5,6] have been suggested. However, the available expressions lack the generality and quantitative character. In the present work, expressions for gas conduction and K_E of a two-phase gas-solid system under changing interstitial gas pressure are suggested. The behaviour of solid conduction at reduced pressure is also explained.

2 Theory

The thermal conductivity (K_{g_0}) of an unconfined gas having mean free path λ_0, density ρ_0, mean molecular velocity $\bar{u}$, specific heat c_v and specific heats' ratio γ at a gas pressure P_0 is estimated[8,9] by

$$K_{g_0}=\frac{1}{4}(9\gamma-5)\bar{u}c_v\lambda_0\rho_0 \qquad \ldots (1)$$

In a gas-solid two-phase system the interstitial gas is mainly confined inside pores and it behaves differently than an unconfined gas. When pore diameter d is comparable to the mean free path λ, at the interstitial gas pressure, P, the collisions of gas molecules with the absorbed molecules at the pore surface occur frequently. The total path length for N collisions is thus affected by the presence of a pore. The consideration of total probability of intermolecular collisions for all values of molecular displacement gives an expression[1,6,10] for effective mean free path (λ_e). The effective mean free path λ_e as derived earlier is given by

$$\frac{1}{\lambda_e}=\frac{1}{\lambda}+\frac{1}{d} \qquad \ldots (2)$$

The interstitial gas of mean free path λ, thus becomes equivalent to a free gas with a mean free path λ_e. Thus, analogous to Eq. (1), the thermal conductivity of interstitial gas at the interstitial pressure P may be written as

$$K_g=\frac{1}{4}(9\gamma-5)c_v\bar{u}\lambda_e\rho_e \qquad \ldots (3)$$

Here it has been assumed that γ, $\bar{u}$, c_v and temperature of interstitial gas are constant at different interstitial gas pressures.

Gas conduction—A significant variation in K_E occurs in moderate pressure region where mean free path λ is comparable to pore diameter d. The thermal conductivity K_g of the gas, using Eqs (1) and (3), is

$$K_g=K_{g_0}\left(\frac{\lambda_e\rho_e}{\lambda_0\rho_0}\right) \qquad \ldots (4a)$$

From the kinetic theory, for a free gas

$$\frac{\lambda_0}{\lambda}=\frac{\rho_e}{\rho_0}=\frac{P}{P_0} \qquad \ldots (4b)$$

As such Eq. (4a) can be written as

$$K_g=K_{g_0}\left(\frac{\lambda_e P}{\lambda_0 P_0}\right) \qquad \ldots (5)$$

Now, consider a gas pressure P_c when the mean free path of free gas λ_c is equal to pore diameter d. Using Eqs (4b) and (5)

$$\lambda P=\lambda_0 P_0=\lambda_c P_c \qquad \ldots (6)$$

We thus have

$$K_g=K_{g_0}\left(\frac{\lambda_e P}{dP_c}\right) \qquad \ldots (7)$$

---

* Present address: Teacher fellow, Govt College, Dholpur

Since $\frac{\lambda_e}{dP_c}=\left(\frac{\lambda d_g}{\lambda+d}\right)\frac{1}{dP_c}$

$$=\frac{1}{P_c+\left(\frac{d}{\lambda}\right)P_c}$$

and as $\lambda_c=d$, using Eq. (6) we have

$$\left(\frac{\lambda}{\lambda+d}\right)\frac{1}{P_c}=\left(\frac{1}{P_c+P}\right)$$

Therefore,

$$K_g=K_{g_0}\left(\frac{P}{P+P_c}\right) \quad \ldots (8)$$

Eq. (8) predicts the behaviour of gas conduction at interstitial gas pressure near to P_c. The characteristic pressure P_c may be defined from Eq. (8) as $P\to P_c$, $K_g \to \frac{1}{2}K_{g_0}$, i.e. the pressure where thermal conductivity of a pore-confined gas is reduced to half of its unconfined free gas value (K_{g_0}). In addition, since λ and d are equal at $P=P_c$, the molecular density will be uniform inside all the pores and on an average there will be at least one molecule per pore. The gas molecules accumulate inside the pore at $\lambda < d$, while a few of the pores are vacant at $\lambda > d$. Therefore, molecular density is optimized at $P = P_c$. As the convective heat transfer is proportional to molecular density, the convection effects are also optimized at this pressure (P_c). The radiative heat transfer is minimum at this pressure for this mode is much more predominant in a vacated pore, whence $\lambda \gg d$. This indicates that thermal conductivity measured at the characteristic pressure P_c would be solely an outcome of conduction process.

High pressure region—When the interstitial gas pressure is much larger than P_c, the mean free path λ becomes much smaller than d. Using Eq. (2), the thermal conductivity of gas approaches its maximum value (K_{g_0}), i.e. as $\lambda \ll d$,

$\lambda_e \to \lambda$

and

$K_g \to K_{g_0}$ ... (9)

Low pressure region—When interstitial pressure is much lower than P_c, the mean free path λ becomes much larger than d. Using Eq. (2), we have, as $\lambda \ll d$,

$\lambda_e \to d$

and $K_g \to K_{g_0}\left(\frac{P}{P_c}\right)$ ... (10)

Nevertheless, the adsorbed gas molecules at the pore surface will always contribute to gas conduction. Therefore, K_g cannot be made zero as allowed by Eq. (10).

Characteristic pressure—According to Eq. (6), the characteristic pressure is a function of pore size only. As mentioned above in Eq. (6)

$$P_c \propto \frac{1}{d}$$

and the pore size d is proportional to D, the solid grain size[6]. Therefore, we may write

$$P_c \propto \frac{1}{D}$$

Thus it is indicated that characteristic pressure P_c of an interstitial gas in a powder should be larger than P_c of the same gas in beads of a solid material.

Solid conduction—The solid conduction in an evacuated two-phase porous system is due to grain to grain contact. This can be accounted through area of contact of a solid grain[2,11]. The area of contact is proportional to the number of solid grains and area of a single grain. When grains under consideration are spheres of diameter D and φ_s is the volume fraction of solid phase present in a two-phase system, we then have the number of grains $\propto(\varphi_s/D^3)$ and the area of a single grain $\propto D^2$. Hence solid conduction K_{s_1} is given by

$$K_{s_1}=\beta\frac{\varphi_s}{D} \quad \ldots (11)$$

where β is a proportionality constant depending upon the nature of the solid material.

Radiative transfer—The second important mechanism of heat transfer in evacuated porous systems is radiative transfer of heat within the pore. This contribution should be proportional to the pore area and the number of pores. The pore size d is proportional[6] to grain size D. Hence if φ_g be the volume fraction of gas in a two-phase system, we have,

number of pores $\propto \frac{\varphi_g}{D}$

and pore area $\propto D^2$

Hence radiative contribution to heat transfer is

$$K_{r_1}=\delta\varphi_g D \quad \ldots (12)$$

where δ is a proportionality constant depending upon the nature of the gas. It is assumed here that temperature of the two-phase system is constant.

In practice, the measured values of the effective thermal conductivity at very low pressure comprise both solid conduction and radiative transfer. Eqs (11) and (12) when added may estimate effective thermal conductivity at very low pressure ($P \ll P_c$) i.e.

$K_E = K_{s_1} + K_{r_1}$

$$=\beta\frac{\varphi_s}{D}+\delta\varphi_g D \quad \ldots (13)$$

Effective thermal conductivity—In the literature we find a number of expressions[12-20] for the prediction of effective thermal conductivity (K_E) of a two-phase system. These expressions are meant for the system where gas is at a constant pressure, generally at normal pressure. These expressions for K_E may be used under varying interstitial gas pressure provided the thermal conductivities of gas and solid phases are inferred at those gas pressures. It is relevant to assume here that the thermal conductivity of solid phase (K_s) is invariant at different interstitial gas pressures. On substituting the appropriate values of K_{g_0}, P and P_c in Eqs (8), (9) and (10), the thermal conductivity of the gas phase (K_g) at different interstitial gas pressure may be evaluated. The variation in K_E occurs only due to the variation in K_g. Therefore, the effective thermal conductivity K_E of the two-phase porous system may now be evaluated by substituting K_s, φ and K_g at related interstitial gas pressure. Here the porosity φ is assumed constant and independent of gas pressure. However, the value of K_E at very low pressure ($P \ll P_c$) may be evaluated by using Eq. (13). In general, K_E is a function of K_s, K_g, P, P_c and φ. Using functional form, we may write

$$K_E = f(K_s, K_g, P, P_c, \varphi) \quad \ldots (14)$$

The behaviour of K_E near characteristic pressure P_c may be estimated by differentiating Eq. (14) with respect to P and φ respectively. Thus we have,

$$\left(\frac{\partial K_E}{\partial P}\right)_{P=P_c} = f'(K_s, K_g, P_c \text{ and } \varphi)$$

$$= f'\left(K_s, \frac{1}{2}K_{g_0}, \varphi\right) \text{ as } \frac{P}{P+P_c} \to \frac{1}{2} \text{ at } P = P_c$$

or

$$\left(\frac{\partial K_E}{\partial P}\right)_{P=P_c} = \text{constant (if } \varphi \text{ is constant)} \quad \ldots (15)$$

and

$$\left(\frac{\partial K_E}{\partial \varphi}\right)_{P=P_c} = f'(K_s, K_g, P_c)$$

(when K_g is a linear function of φ)

or

$$\left(\frac{\partial K_E}{\partial \varphi}\right)_{P=P_c} = f'\left(K_s, \tfrac{1}{2}K_{g_0}\right)$$

$$= \text{constant (if } P_c \text{ is constant)} \quad \ldots (16)$$

Eqs (15) and (16) are equivalent expressions. Eq. (15) indicates that variation in K_E with respect to interstitial gas pressure is uniform near the characteristic pressure P_c of a given two-phase system, provided the porosity (φ) remains constant. Similarly, Eq. (16) implies that variation in K_E with respect to porosity is also constant provided the change in porosity does not affect the grain size. These two expressions qualitatively predict the behaviour of K_E near P_c.

3 Comparison with Experimental Values

We have tried to find the suitability of various expressions for the effective thermal conductivity of gas-solid two-phase system. Table 1 shows a comparison of the calculated [using Eq. (8)] and reported values of K_E of glass beads (size 50 μm) at two different interstitial gas pressures (10^{-2} and 10^3 mm of mercury). It is seen that Hashin-Shtrikman's lower bound[14] and Russel's expressions[19] fairly agree with the observed value of K_E of the glass beads (size 50 μm) system. The effective thermal conductivities (K_E) of fibrous silica (fibre diameter 1.2 μm) and glass beads (size 50 and 150 μm) at varying interstitial gas pressures have been calculated using these two expressions[14,19] only. Predictions of K_E from Lichtnecker's expression[16] are also satisfactory in case of fibrous silica (fibre diameter 1.2 μm). Therefore, this expression has also been considered for further calculations. Figs 1-3 show the calculated values of K_E along with the reported experimental values at different interstitial gas pressures.

It is evident from Figs 1-3 Lichtnecker's expression[16] predicts K_E values nearly two times the experimental value of K_E for 50 and 150 μm sizes of glass bead systems. However, the same expression

Table 1—Experimental & Calculated Values of K_E (in $Wm^{-1}K^{-1}$) from Various Expressions Using Eq. (8) at Two Values of Interstitial Air Pressure for Glass Beads-Air System

[Porosity = 0.42; K_s = 1.04; K_g = 0.026; T = 300 K; and size, 50 μm]

Expressions	$K_E \times 10^2$ at 10^{-2} mm of H_g		$K_E \times 10^2$ at 1000 mm of H_g	
	Reported	Calculated	Reported	Calculated
Wiener's expression[20] (For parallel resistors)	0.5	58	13	60
Wiener's expression[20] (for series resistors)	do	0.005	do	6.5
Lichtnecker's expression[16]	do	0.75	do	22.9
Landau's expression[17]	do	20	do	36
Kumar & Chaudhary's expression[15]	do	30	do	37
Maxwell's expression[18]	do	49.5	do	51.5
Hashin-Shtrikman's lower bound[14]	do	0.4	do	11.7
Brailsford and Major's expression[12]	do	49.8	do	51.5
Russel's expression[19]	do	0.05	do	13.2
Bogomolov relation[13]	do	0.01	do	30.7

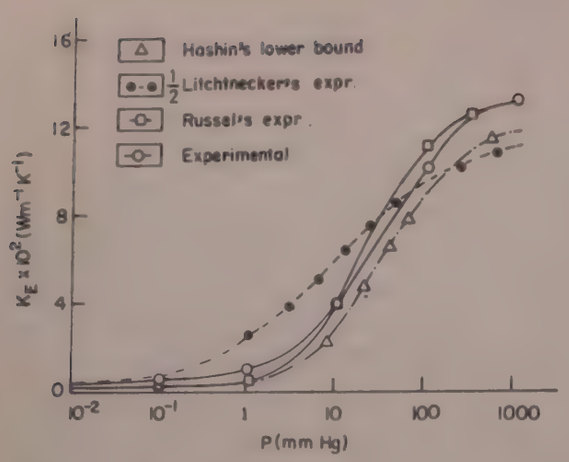

Fig. 1 -Variation in K_E of glass beads (size 150 μm and porosity 0.38) with change in interstitial air pressure [The characteristic pressure is 6.5 mm of mercury.]

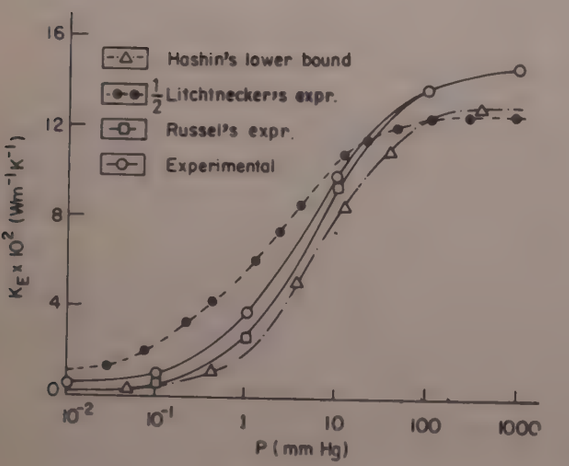

Fig. 2—Variation in K_E of glass beads (size 50 μm and porosity 0.42) with change in interstitial air pressure [The characteristic pressure is 31 mm of mercury.]

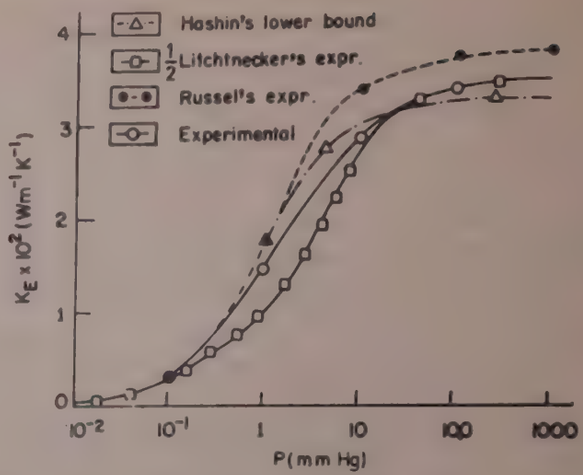

Fig. 3—Variation in K_E of fibrous silica (fibre diameter 1.2 μm and porosity 0.95) with interstitial air pressure [The characteristic pressure is 1.2 mm of mercury.]

gives K_E very close to experimental value of K_E for highly porous fibrous silica (fibre diameter 1.2 μm).

It is also indicated that Hashin-Shtrikman's lower bound[14] predicts K_E values with a maximum error of 10% for the considered systems. It is further noted that predictions by Russel's expression[19], using the proposed expression for K_g are closest to the observed values of K_E. The maximum error from this expression is 8%.

The variation in observed value of K_E near characteristic pressure is uniform in all the three systems as predicted by Eqs (15) and (16). The solid-to-solid conduction and radiative heat transfer coefficients β and δ have been estimated from the measured values of K_E for basalt powder[2,4,11] and glass beads[2,4,11]. We find β and δ to be constant (having only a variation of 7%). These are given in Table 2. These are material constants and as such these

Table 2—Dependence of Solid Conduction (K_{s_1}) and Radiative Transfer of Heat (K_{T_1}) upon Particle Size and Porosity in Evacuated Two-Phase System at 300 K

Material	Size (D) μm	$\bar{D}$ μm	ρ g/cc	φ_s	φ_g	$K_{s_1} \times 10^4$ Wm^{-1}K^{-1}	$\beta \times 10^7 \left(=\frac{K_{s_1}\bar{D}\times 10^7}{\varphi_s}\right)$ WK^{-1}	$K_{r_1} \times 10^4$ Wm^{-1}K^{-1}	$\delta \left(=\frac{K_{r_1}}{\varphi_g \bar{D}}\right)$ Wm^{-2}K^{-1}	$\bar{\beta} \times 10^7$ WK^{-1}	$\bar{\delta}$ Wm^{-2}K^{-1}
Basalt powder[2,11]	10-37	24	1.36	0.45	0.55	15.5	0.835	2.34	17.70	0.764	17.5
	44-74	59	1.43	0.48	0.52	6.1	0.756	5.75	18.50		
	37-62	49.5	1.10	0.37	0.63	5.1	0.701	5.16	16.40		
Glass beads[2,11] (A)	10-37	24	1.35	0.54	0.46	9.5	0.424	1.70	15.40		
	38-53	45.5	1.50	0.60	0.40	4.5	0.341	—	—	0.408	13.2
	53-74	63	1.60	0.64	0.36	—	—	3.10	13.60		
	250-350	300	1.55	0.62	0.38	0.95	0.459	12.06	10.60		
Glass beads[2,11] (B)	53-74	63	1.6	0.64	0.36	7.00	0.689	—	—		
	88-125	106	1.5	0.60	0.40	3.20	0.565	7.60	17.90	0.625	22.90
	590-850	615	1.7	0.68	0.32	0.66	0.597	55.00	27.90		

Values unavailable in the References mentioned in Col. 1.

values may be applied to systems made of the same materials having different porosities and grain sizes.

4 Results and Discussion

In a two-phase system comprising air and glass (silica) the ratio K_g/K_s is 10^{-2} at normal gas pressure. We find that only a few of the expressions of K_E of a two-phase system are capable of predicting K_E at low K_g/K_s value. The ratio K_g/K_s further decreases with the reduction in interstitial gas pressure [also obvious through Eqs (8)-(10)]. This further reduces the number of useful expressions for K_E for the present purpose. All those expressions which are linear sum of thermal conductivities of phases would not lead to observed values of K_E at largely reduced pressures, because an appreciable change in the volume fraction of solid affects very little the experimental value of K_E at very low pressures (Figs 1-3). On the other hand, expressions which employ the product K_gK_s account satisfactorily. Therefore, Russel's expression[19] and Hashin-Shtrikman's lower bound[14] under the governing Eqs (8), (9) and (10) are found to be the only suitable expressions for the evaluation of K_E of a two-phase porous system at different interstitial gas pressures.

An increase in characteristic pressure with a decrease in particle size (Figs 1-3) indicates that a two-phase system consisting of microfined powdered material and air may behave as a good insulator even at the atmospheric pressure.

Acknowledgement

We are thankful to Mr. Veerendra Kumar for giving valuable suggestions. One of us (RNP) is grateful to the University Grants Commission, New Delhi for the award of a teacher fellowship.

References

1 Keshok E, *Technical report* 72-T4, *for NASA*, contract NAS1-9034 (Old Dominion University, Norfolk, Virginia, USA 1972, pp 5-6.
2 Wechsler A E, Glaser P E & Fountain A J, *Progress in astronautics and aeronautics*, Vol 28: *Thermal characteristics of moon* (MIT Press, Massachusetts, USA) 1972, pp 215-241.
3 Beroes C S & Hatters H D, *Report on glass-steel beads* (Chemical and Petroleum Engineering Department, University of Pittsburgh, USA) 1969, pp 721-728 (private communication).
4 Wechsler A E, *Report on glass beads* by the Engineering Science Research and Experiment Group (Arthur D Little Inc, Cambridge, Massachusetts, USA) 1966, pp 89-96 (private communication).
5 Pettyjohn R R, *Report on fibrous silica* (General Dynamics Corporation, Sandiego, California, USA) 1971, pp 729-736 (private communication).
6 Pratt A W, *Research (GB)*, **15** (1962) 214.
7 Verschoor J D & Greebler P, *Trans ASME* (Materials Science) (USA), **74** (1952) 961.
8 Eucken, *Phys Z (Germany)*, **14** (1913) 324.
9 Tye R P, *Thermal conductivity*, Vol 2 (Academic Press, London) 1969, 26.
10 Sweet J N, *Energy Report* (Sandia Laboratories, New Mexico, USA) February 1979, pp 27-28.
11 Wechsler A E, *Powder Technol (Switzerland)*, **3** (1969) 163.
12 Brailsford A D & Major K G, *J Appl Phys (USA)*, **15** (1964) 313.
13 Bogomolov V Z, *Trans Phys-Astron Inst*, Vol 3 (Agriculture Press, USSR) 1941, p 13.
14 Hashin Z & Shtrikman S, *J Appl Phys (USA)*, **33** (1962) 3125.
15 Kumar V & Chaudhary D R, *Indian J Pure & Appl Phys*, **18** (1980) 984.
16 Lichtnecker K, *Phys Z (Germany)*, **27** (1926) 115.
17 Landau L D, *Dielectrics of continuous media* (Pergamon Press, London) 1960, 46.
18 Maxwell J C, *Treatise on electricity and magnetism*, Vol 1 (Clarendon Press, Oxford) 1904, 435-441.
19 Russel H W, *J Am Ceram Soc (USA)*, **18** (1935) 1.
20 Wiener O, *Phys Z (Germany)*, **5** (1904) 332.

NOTES

Indian Journal of Pure & Applied Physics
Vol 21, September 1983, pp. 534-536

Thermally Stimulated Current in Thermomagnetically-treated Naphthalene

A K BHATNAGAR, M S QURESHI & C S BHATNAGAR*
Department of Physics, M A College of Technology, Bhopal 462 007

Received 25 *September* 1982; *revised received* 8 *June* 1983

Thermally stimulated current in naphthalene electrets prepared in presence of thermal excitation (T_f=23, 55, 60, 65 and 70°C) and magnetic field (H_f=14.50 kOe) is analyzed using three methods, viz. (a) Garlick and Gibson initial rise method, (b) Bucci plot method and (c) Cowell and Woods curve fitting method. Trap depths from 1.024 to 1.206 eV and reciprocal of trap escape frequency (τ_0) from 1.52×10^{-17} to 2.24×10^{-14} sec are obtained. The spread in the value of trap depth shows that the traps are distributed and closely spaced.

Persistent internal polarization in naphthalene thermoelectret has been studied by Shrivastava and Ranjit Singh[1]. According to them the phenomenon is due to trapping of both holes and electrons. The decay of charge is supposed to be due to retrapping in shallow impurity levels. Campos *et al.*[2] have suggested the presence of pseudo dipoles to explain the thermo-electret effect in naphthalene. Thermally stimulated current (TSC) in naphthalene has been reported by Campos and Mergulhao[3], and they have obtained the value of 1.26 eV for activation energy for a TSC maximum at 38°C. They concluded that trapping is taking place in deep as well as in shallow traps.

Surface charge decay of naphthalene magneto-electrets has been studied by Agrawal and Bhatnagar[4]. It is suggested that, trapping of charge carrier in structural defects and grain boundaries, and pseudo dipoles caused by nearby trapping of an electron-hole pair, may be the cause of the observed magnetoelectret state in naphthalene.

Thermally stimulated current technique, being a powerful tool to study the internal mechanism, is used in the present communication for the first time to study naphthalene polarized in presence of magnetic field and thermal excitation.

Experimental Details

Polycrystalline naphthalene obtained from M/s Reidel De Haen AG Seelze Hannovek, Germany was moulded into discs of 1.36 cm diameter and 0.16 cm thick by the method of Agrawal[5]. Tin foils having a diameter equal to that of the disc were stuck to both the faces of it by 'melted-on' method[1] for better electrical contact. A series of magnetoelectrets were prepared at various temperatures (T_f) (23, 55, 60, 65 and 70 C) and a magnetic field (H_f) of 14.50 kOe by the usual method[5]. Magnetic field was kept on for 1.5 hr, 1 hr of which was at constant forming temperature and half an hour during the cooling phase.

Keithley electrometer 610 C was used to study the TSC thermogram. The arrangement for TSC was the same as used by Verma and Bhatnagar[6] and was enclosed in a chamber which was heated by Tempo Flexotherm heating tape. A linear heating rate of 1°C/min was used to record the TSC. The whole experimental procedure was carried out in dark. Only red safe-light was used for taking observations.

Thermally stimulated current is explained by the equation[7]

$$i(T)=A\exp\left[-\frac{E}{kT}-\frac{1}{\beta\tau_0}\int_{T_0}^{T}\exp\left(-\frac{E}{kT}\right)dT\right] \quad \ldots (1)$$

where $i(T)$ is the measured current, E the trap depth, k the Boltzmann constant, T the temperature in Kelvin, β the heating rate, τ_0 the inverse of the trap escape frequency and A a constant which depends on trapping parameters. The experimental results can be analyzed using the following three methods:

(a) *Garlick and Gibson method*[8]

According to this method the low temperature tail of Eq. (1) is given by

$$\ln(i)=C-\frac{E}{kT} \quad \ldots (2)$$

where C is a constant. Slope of the straight line plot of $\ln(i)$ versus $1/T$ leads to the value of E/k and hence E.

On differentiating Eq. (1) to get the maximum value of current, one obtains

$$\tau_0=\frac{kT_m^2}{\beta E\exp(E/kT_m)} \quad \ldots (3)$$

The time constant for any other temperature can be obtained by the equation

$$\tau=\tau_0\exp(E/kT) \quad \ldots (4)$$

(b) *Bucci plot method*[9]

In the derivation of Eq. (1)

$$\tau=\frac{n(T)}{i(T)}$$

where $n(T)$ is the number of electrons remaining in traps at temperature T. The numerator can be obtained from the integration of the TSC graph as shown in Fig. 1.

$$\text{Therefore } \tau=\frac{\int_{nT}^{\infty}i(t)\,dt}{i(T)} \quad \ldots (5)$$

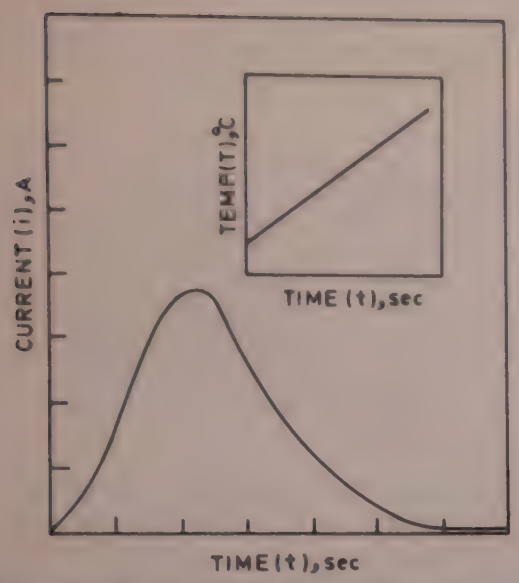

Fig. 1—Demonstration graph for Bucci plot method, i.e. plot of current $i(t)$ versus time (t) [Inset time (t) versus temperature (T)]

and Eq. (4) yields

$$\ln \tau = \ln \tau_0 + \frac{E}{kT} \qquad \ldots (6)$$

Values of τ at different temperatures can be obtained from Eq. (5). And slope of the Bucci plot between $\ln \tau$ and $1/T$ gives E and intercept on $\ln \tau$ axis gives $\ln \tau_0$ and hence τ_0.

(c) *Cowell and Woods curve fitting method*[10]

Substitution of $x = E/kT$ and $dx = -E/kT^2 dT$ in Eq. (1) and on subsequent approximation gives a simplified equation

$$i(x) \approx A \exp[-x - B \exp(-x).x^{-2}] \qquad \ldots (7)$$

When Eq. (7) is differentiated and equated to zero for the maximum in the curve, it gives

$$B' = \frac{(\exp x^*)(x^*)^3}{x^* + 2} \qquad \ldots (8)$$

Here $x^* = E/kT_m$, T_m = temperature at the maximum current value and B' an approximate value of B obtained by replacing the approximation of Eq. (7) by an equality.

Eqs (7) and (8) are used for the curve fitting technique. The value of T_m is obtained from the experimental curve. The method described in (a) and (b) are used to calculate an approximate value of E with T_m; this leads to an approximate value of x^*. This value on substituting in Eq. (8) yields B'. Value of $i(x)$ is then calculated from Eq. (7). A is used as an adjustable parameter to normalize the theoretical curve with the experimental one at the maximum, that is

$$A = i(x)/\exp[-x^* - B' \exp(-x^*).x^{*-2}] \qquad \ldots (9)$$

Any error in the initial value of E chosen is indicated by a failure to obtain a good fit between the experimental and theoretical curve. If the fit is not good a new value of E is chosen and the procedure is repeated, until an excellent fit is obtained. The value of E corresponding to this fit is taken to be the correct value of trap depth. Value of τ_0 can be calculated from the value of B, obtained with the help of the equation $B = 1/\tau_0 . E/\beta T$. The value of τ at any other temperature is given by Eq. (4).

Results and Discussion

A representative TSC curve is shown in Fig. 2. For this sample, the forming temperature (T_f) was 60°C and forming magnetic field (H_f) was 14.50 kOe.

A single peak has been observed at 40.0 ± 0.5°C. The peak currents for the various samples are given in Table 1, which also gives the value of trap depth E and τ_0 obtained by Garlick and Gibson's method.

Straight line plot between $\ln(i)$ and $1/T$ of Garlick and Gibson's initial rise method for the sample $T_f = 60$°C and $H_f = 14.50$ kOe is shown in Fig. 3. Trap depth for the various samples varies from 0.764 to 0.977 eV and τ_0 varies from 3.23×10^{-10} to 9.41×10^{-14} sec.

Bucci plot between $\ln(\tau)$ and $1/T$ for the same sample ($T_f = 60$°C and $H_f = 14.50$ kOe) is shown in Fig. 4. For different samples the values of E and τ_0 are given in Table 1.

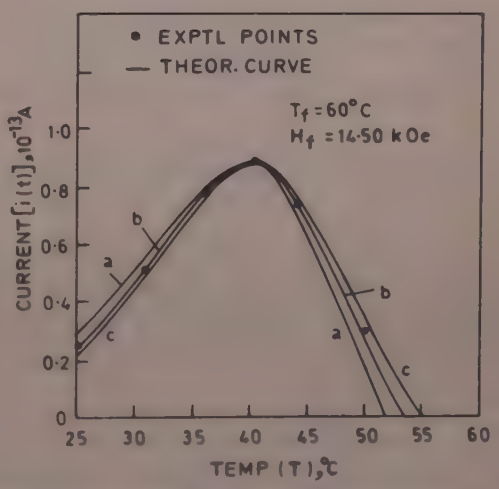

Fig. 2—Demonstration of Cowell and Woods curve fitting method, i.e. plot of thermally stimulated current $i(t)$ versus temperature (T). [• Experimental points and —, theoretical curve for: (a) $E = 1.079$ eV (b), $E = 1.081$ eV and (c), $E = 1.083$ eV]

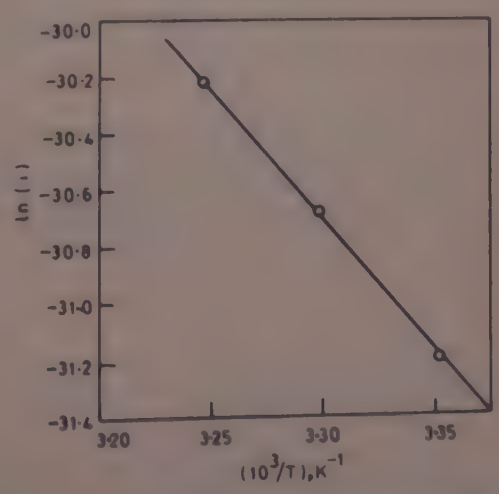

Fig. 3— ln(i) versus 1 T plot of Garlick and Gibson

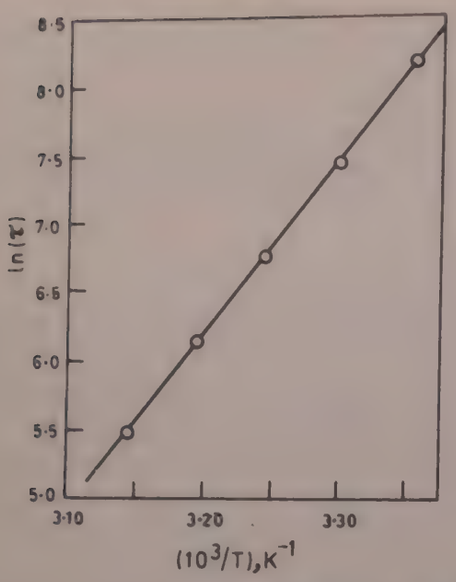

Fig. 4— ln τ versus $1/T$ curve by Bucci plot method

The trapping parameters obtained by Cowell and Woods method are given in Table 2. This table also includes value of τ_{300} and τ_{max}, the value of τ corresponding to room temperature and the temperature at the maximum of the TSC peak is obtained. The curve fitting technique of Cowell and Woods is demonstrated in Fig. 2. As seen from Fig. 2 when E is less than the value of trap depth corresponding to the experimental curve, the curve at the initial stage lies above the experimental one and vice-versa.

Garlick and Gibson method can give only a rough estimate of trap depth (E) because very few experimental points are available for the plot of ln (i) versus $1/T$. The slope of straight line plot so obtained is quite ambiguous. The values of trap depths calculated by this method deviate a lot from the results obtained by other methods as shown in Tables 1 and 2.

The Bucci plot method gives better result, as the whole TSC curve is utilized to get the straight line plot between ln τ and $1/T$. The values of E so obtained from Bucci method are used in Cowell and Woods curve fitting method as described earlier. The value of trap depth (E) corresponding to the best fit is taken to be the correct value (Fig. 2b). Trap depth calculated by this method varies from 1.024 to 1.206 eV and τ_0 from 1.52×10^{-17} to 2.24×10^{-14} sec.

This distribution of trap depths suggests that instead of a single trap level, there are a number of closely spaced traps. The traps may be due to inhomogeneities at the grain boundaries of the polycrystalline naphthalene.

Table 1—Values of Peak Current, E and τ_0 for the Samples Prepared at 14.50 kOe

T_f	I_{max}	Garlick & Gibson method		Bucci plot method	
C	10^{-13}A	E, eV	τ_0, sec	E, eV	τ_0, sec
23	1.12	0.800	8.99×10^{-11}	1.077	2.50×10^{-15}
55	0.90	0.960	1.81×10^{-13}	1.209	1.13×10^{-17}
60	0.90	0.844	1.51×10^{-11}	1.080	1.88×10^{-15}
65	0.72	0.764	3.23×10^{-10}	1.025	1.92×10^{-14}
70	1.10	0.977	9.41×10^{-14}	1.048	7.72×10^{-15}

Table 2—Values of E, τ_0, τ_{300} and τ_{max} for the Samples Prepared at 14.50 kOe by Cowell & Woods Method

T_f	E, eV	τ_0, sec	τ_{300}, sec	τ_{max}, sec
23	1.078	2.26×10^{-15}	3.03×10^{3}	4.72×10^{2}
55	1.206	1.52×10^{-17}	2.91×10^{3}	4.19×10^{2}
60	1.081	1.81×10^{-15}	2.66×10^{3}	4.68×10^{2}
65	1.024	2.24×10^{-14}	2.54×10^{3}	4.98×10^{2}
70	1.052	5.39×10^{-15}	2.61×10^{3}	4.81×10^{2}

The authors are thankful to the Principal, M.A. College of Technology, Bhopal for providing necessary facilities. They are also thankful to Dr M L Khare for valuable suggestions. One of the authors (AKB) is thankful to the University Grants Commission, New Delhi for awarding him a Teacher Research Fellowship. He is also thankful to the Government of Madhya Pradesh for sponsoring him to avail of the opportunity of carrying out the research work.

References

1 Shrivastava A P & Ranjit Singh, *Indian J Pure & Appl Phys*, **10** (1972) 266, 811.

2 Campos M, Ferreira G L & Mascarenhas S, *J Nonmetals (GB)*, **2** (1974) 123.

3 Campos M & Mergulhao S, *J Appl Phys (USA)*, **3** (1980) 1619.

4 Agrawal B M & Bhatnagar C S, *Indian J Pure & Appl Phys*, **13** (1975) 370.

5 Agrawal B M, *Studies of magnetic field polarization on naphthalene*, Ph D thesis, Bhopal University, 1976.

6 Verma D & Bhatnagar C S, *Indian J Pure & Appl Phys*, **14** (1976) 93.

7 Perlman M M, *J Appl Phys (USA)*, **42** (1971) 2645.

8 Garlick G F J & Gibson A F, *Proc Phys Soc London (GB)*, **60** (1948) 574.

9 Bucci C & Fieschi R, *Phys Rev (USA)*, **148** (1966) 816.

10 Cowell T A T & Woods J, *Br J Appl Phys (GB)*, **18** (1967) 1045.

Indian Journal of Pure & Applied Physics
Vol 21, September 1983, pp. 537-539

Effects of Electric and Magnetic Fields on Propagation Characteristics of Microwaves in InSb

P N GUPTA*, M RAM & S K TOLPADI

Electronics & Radio Physics Laboratory, Department of Physics, Banaras Hindu University, Varanasi 221005

Received 29 *June* 1982; *revised received* 25 *November* 1982

Characteristics of electromagnetic waves, propagating through a semiconductor plasma in the presence of external electrostatic and magnetostatic fields, have been investigated. Dispersion relation is obtained for the case in which the applied magnetic field is in the direction of propagation and the electric field in a direction perpendicular to the magnetic field. From the dispersion relation, expressions for attenuation and phase constants have been derived. Sample calculations have been made for the case of InSb under different conditions and the results obtained are discussed. It is suggested that such investigations are useful in obtaining information about transport properties of semiconductors.

The study of the propagation of electromagnetic waves through a semiconductor plasma has gained importance because of its possible application to study the transport property of semiconductors. Pioneering work in this direction was done by Bok and Noziers[1] and Steele and Vural[2]. Recently, Pic and Ligeon[3] have made a study of the effect of transverse current on helicon wave propagation through InSb. In this note, we present the results of an investigation of the propagation of electromagnetic waves through a semiconductor plasma in the presence of external electrostatic and magnetostatic fields. Expressions for attenuation and phase constants have been obtained from the dispersion relation, and a sample calculation has been made for InSb under a wide variety of conditions.

Theoretical consideration and dispersion relation— Consider a plane wave propagating in the z-direction through a homogeneous semiconducting medium of infinite extent in the direction of propagation. The external dc magnetic field is applied in the z-direction parallel to the direction of propagation and the electric field is applied in the x-direction. We assume that all field variables have a time and space dependence given by $\exp j\ (\omega t - Kz)$, where K is the propagation constant, ω is the wave frequency. From Maxwell's equations governing the field vectors of the electromagnetic wave for a semiconductor medium and linearized equations of carriers under the influence of applied electric and magnetic fields, the dispersion relation [Pic and Ligeon[3]] is obtained as

$$(A_1 + jA_2)K^4 + (B_1 + jB_2)K^2 + (C_1 + jC_2) = 0 \qquad \ldots (1)$$

where

$$A_1 = -1$$

$$A_2 = \frac{\sigma_l}{\omega}\left(1 - \frac{v_d^2}{v_1^2}\right)$$

$$B_1 = \frac{\omega^2}{v_1^2}\left[2 + \left(\frac{\sigma_l}{\omega}\right)^2 \cdot \frac{1}{1+\lambda_e^2}\left\{\frac{v_d^2}{v_1^2} - 2\right\}\right]$$

$$B_2 = \frac{\omega^2}{v_1^2}\left(\frac{\sigma_l}{\omega}\right)\left[\frac{v_d^2}{v_1^2} - 2\left\{\frac{2+\lambda_e^2}{1+\lambda_e^2}\right\}\right]$$

$$C_1 = \frac{\omega^4}{v_1^4}\left[3\left(\frac{\sigma_l}{\omega}\right)^2 \cdot \frac{1}{1+\lambda_e^2} - 1\right]$$

$$C_2 = \frac{\omega^4}{v_1^4}\left(\frac{\sigma_l}{\omega}\right)\left[\frac{3+\lambda_e^2}{1+\lambda_e^2} - \left(\frac{\sigma_l}{\omega}\right)^2 \frac{1}{1+\lambda_e^2}\right]$$

with

$$\sigma_l = \frac{\sigma_0}{\varepsilon_0 \varepsilon_l}$$

$\sigma_0 = ne\mu_e$, static electronic conductivity $\lambda_e = \mu_0 B_0$

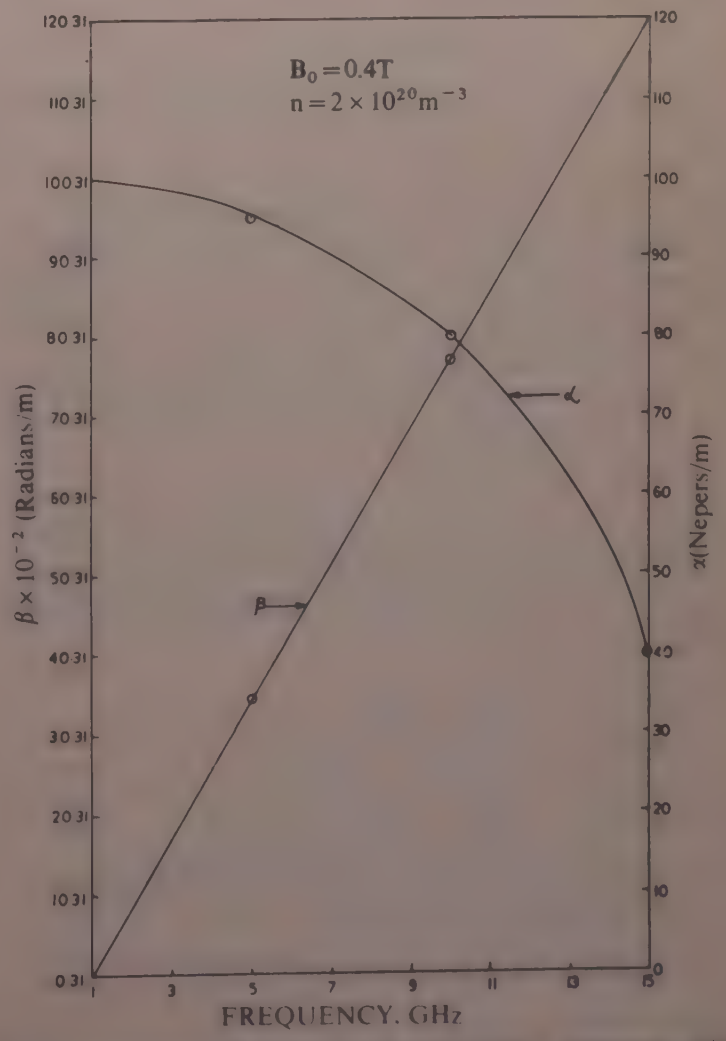

Fig. 1—Variation of phase and attenuation constants with frequency at $B_0 = 0.4$ T, $n = 2 \times 10^{20}$ m^{-3}

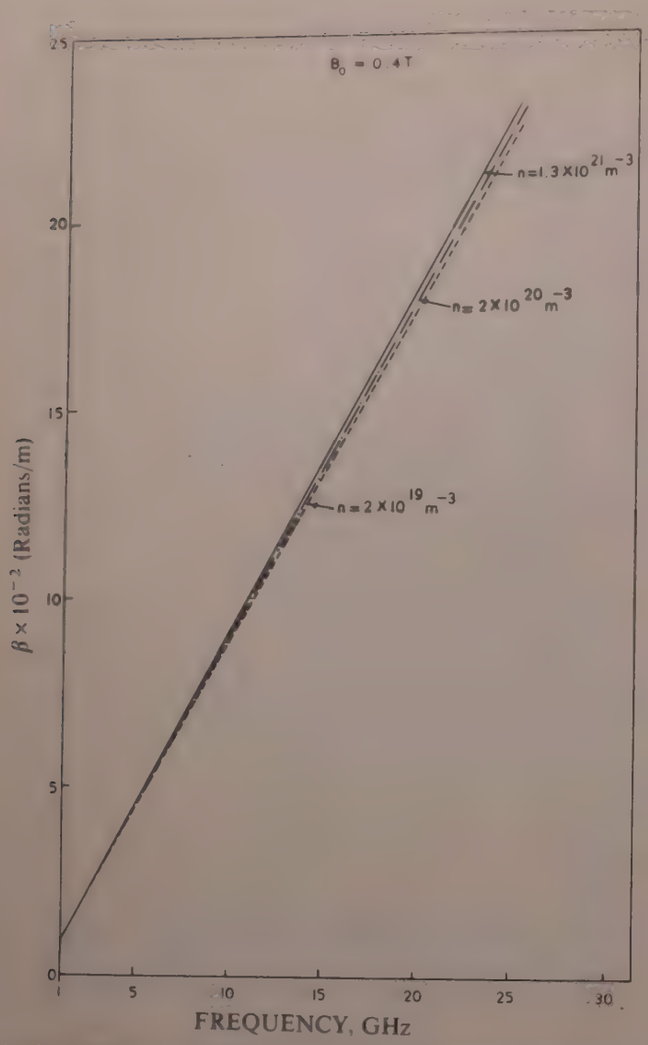

Fig. 2—Variation of phase constant with frequency for different carrier concentrations at $B_0 = 0.4$ T

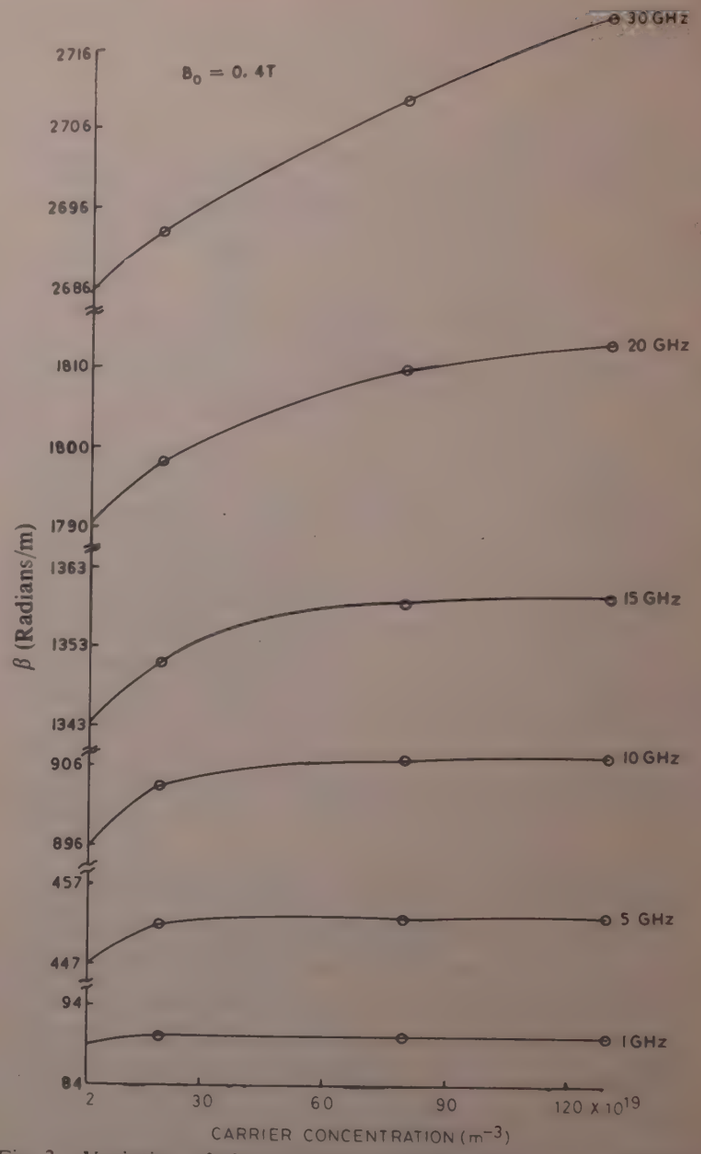

Fig. 3—Variation of phase constant with carrier concentration for different frequencies at $B_0 = 0.4$ T

$v_1 = (\mu_0 \varepsilon_0 \varepsilon_l)^{-1/2}$, wave velocity in the semiconductor, ε_1 is the lattice dielectric constant of the semiconductor, ε_0 the permittivity of the free space, μ_0 = the permeability of the semiconductor (assumed to be of free space), n the electron concentration, e the electronic charge, μ_e the electron mobility, B_0 the static magnetic field, and v_d the drift velocity.

In Eq. (1), $K = \beta - j\alpha$ where α and β are the attenuation and phase constants for the electromagnetic wave as it travels in the semiconductor. From Eq. (1), one obtains a coupled equation in terms of α and β, as

$$4\beta(A_2^2 + 1)\alpha^3 + (A_2B_1 + B_2)\alpha^2 + [-4\beta^3(A_2 + 1) + 2(B_1 - B_2A_2)]\alpha + [-\beta^2(A_2B_1 + B_2) - (A_2C_1 + C_2)] = 0 \quad \ldots (2)$$

The dispersion relation for the propagating wave ($\alpha = 0$) from Eq. (1) is given as

$$A_1\beta^4 + B_1\beta^2 + C_1 = 0$$
$$A_2\beta^4 + B_2\beta^2 + C_2 = 0 \quad \ldots (3)$$

and the expression for the phase constant is given by

$$\beta = \pm\left[\frac{A_1C_2 - A_2C_1}{A_2B_1 - A_1B_2}\right]^{1/2} \quad \ldots (4)$$

Results and discussion—In order to demonstrate the effect of magnetic field and electrostatic field on the propagation characteristics, sample calculations have been made for the case of p-type InSb. Attenuation and phase constants have been computed using Eq. (2). The parameters used in the calculation are given in Table 1. [Pic and Ligeon[3], Kruse[4]].

In the temperature range under consideration (−80 C to −60 C), the p-type InSb behaves nearly like an intrinsic semiconductor in which the concentration of holes and electrons are nearly the same. Since the electron mobility in InSb is about two orders of magnitude higher than the hole mobility, the contribution of holes to the conductivity is neglected.

The results of calculation are presented in Figs 1-3. Fig. 1 represents the variation of attenuation and phase constants with frequency. The parameters chosen are $n = 2 \times 10^{20}$/m^3, $B_0 = 0.4$T and $\mu_e = 0.5$ m^2/V sec. The

Table 1—Parameters Used in the Calculation

S. No.	n m^{-3}	B_0 T	μ_e m^2 V_s
1	2×10^{19}	0.4	8.00
2	2×10^{20}	0.4	0.50
3	1.3×10^{21}	0.4	0.02
4	1.3×10^{21}	0.3	10.50
5	1.3×10^{21}	0.2	12.50
6	1.3×10^{21}	0.1	14.50
7	1.3×10^{21}	0.0	15.10

$v_d = 10^5$ m/sec; $e = 1.602 \times 10^{-16}$C; $\varepsilon_i = 18.7$;
$\mu_0 = 1.257 \times 10^{-6}$H/m; $\varepsilon_0 = 8.854 \times 10^{-12}$F/m

value of β is found to increase linearly with the frequency in the range 1 to 15 GHz while the attenuation constant (α) decreases with the increase of frequency.

Fig. 2 shows the variation of β with carrier concentration and frequency at a constant static magnetic field of 0.4 T. From Fig. 2 it is evident that the phase constant is practically independent of carrier concentration and that it varies linearly with frequency.

Fig. 3 depicts the variation of phase constant with concentration at constant signal frequency and magnetic field. It is observed that the variation is very small.

Effects of drift velocity and magnetic field have been also considered and it is found that phase constant is nearly unaffected by the drift velocity. This result agrees with the experimental result obtained by Pic and Ligeon[3]. Variation in phase constant is negligible as the magnetic field varies from 0.1 to 0.4 T.

Thus, the study of the phase and attenuation constants in the microwave region in the presence of the external static electric and magnetic fields can be used to explore the properties of semiconductors like InSb.

One of the authors (PNG) wishes to acknowledge the constant encouragement from Prof. Suresh Chandra.

References

1 Bok J & Noziers P, *J Phys & Chem Solids (GB)*, **24** (1963) 709.

2 Steele M C & Vural E, *Wave interactions in solid state plasma* (McGraw-Hill, New York) 1968, 39.

3 Pic E & Ligeon M, *Phys Status Solidi a (Germany)*, **23** (1974) 409.

4 Kruse P W, *Semiconductors and semimetals*, Vol 5, edited by R K Willardson & A C Beer (Academic Press, New York) 1970, 18.

Indian Journal of Pure & Applied Physics
Vol 21, September 1983, pp. 540-541

A Two-state Thermodynamical Model for Ultrasonic Energy Loss in Liquid Metals

B V S MURTHY*
Department of Physics, S J College of Engineering, Mysore 570 006
&
O N AWASTHI
Department of Physics, Regional College of Education, Mysore 570 006

Received 5 March 1983

Liquid metals show the existence of an excess ultrasonic absorption over the classical theoretical value. We suggest a two-state thermodynamical model for liquid metals which explains this excess ultrasonic absorption observed in eight liquid metals.

The excess ultrasonic absorption observed in liquid metals by the absorption measurements[1,2] has been assumed to be caused by the existence of the structural bulk viscosity as in associated liquids. An ultrasonic wave passing through the medium causes periodic changes of pressure due to which the molecules of the liquids fall into the vacancies in the lattice during the compression phase and return to their original position during the rarefaction phase. This process gives rise to the structural relaxation which is responsible for the loss of ultrasonic energy.

A linear relationship between $\ln(\eta_b/\eta_s)$ and ΔS is observed in liquid metals as in the case of associated liquids[3], where η_b is the bulk viscosity, η_s is the shear viscosity and ΔS is the entropy of melting. Also (η_b/η_s) is fairly independent of temperature around the melting point. This suggests a strong Coulomb interaction between the ions and the electrons which may cause them to behave like associated liquids This guides us to propose a two-state thermodynamical model for the acoustical energy loss in liquid metals. The existence of a double structure has already been confirmed by diffraction experiments[4].

The thermodynamic states of the atoms in the liquid under thermodynamic equilibrium can be characterized by the difference in the structural arrangements corresponding to the difference in the free-energy states. A fraction of the total number of atoms will be in state I and the remaining in state II, at a particular temperature and pressure. The acoustic waves passing through the medium disturb the population densities of both these states. The equilibrium will be established after the lapse of a finite time called the relaxation time τ. The states I and II above correspond to the condensed state and the liquid state, respectively.

Employing the Stokes and Kirchhoff's relations for classical absorption and Hall's theory[5,6] the following relation is obtained for the absorption of ultrasonic energy due to structural causes:

$$\left(\frac{\alpha}{f^2}\right)_{str.} = \frac{2\pi^2}{c_l}\frac{\beta_r \tau}{\beta_0} \qquad \ldots (1)$$

where β_r is the relaxational compressibility, c_l is the ultrasonic velocity of longitudinal waves in the liquid and β_0 is the compressibility in the liquid state at the concerned temperature and pressure. For the calculation of $(\alpha/f^2)_{str.}$ using Eq. (1), it is necessary to estimate β_r and τ independently of the ultrasonic measurements. A relaxation treatment is applied to the configurational component of compression to derive the expressions for β_r and τ:

$$\beta_r = V(\Delta V/V)^2/2RT\{1+\cosh(\Delta F/RT)\} \qquad \ldots (2)$$

where V represents the average molar volume, ΔF the difference in free-energy between states I and II, R the

Table 1—The Experimental and Theoretical Values (from the Proposed Model) of the Ultrasonic Absorption (α/f^2) in Eight Liquid Metals

Metal	T(K)	$(\Delta V/V)$	τ	α/f^2			
				Exptl	Classl.	Excess*	Present theory†
Na	373	0.29	0.71	11.40	9.20	2.20	2.43
K	348	0.29	1.04	31.90	27.20	4.70	4.86
Rb	316	0.29	2.16	75.50	54.40	17.10	18.32
Cs	308	0.29	2.66	110.30	87.07	23.23	23.21
Cd	633	0.30	0.35	14.50	11.28	3.22	2.17
Sn	513	0.28	0.28	5.63	4.29	1.34	1.23
Pb	613	0.28	0.41	9.40	7.57	1.83	1.93
Bi	553	0.26	0.51	8.05	5.73	2.32	2.95

* Difference of values given in columns 5 and 6.
† Values same as in col 7 but according to present theory.

gas constant, T the temperature and $(\Delta V/V)$ the relative change in molar volume.

The relaxation time is evaluated using Eyring's theory of reaction rates[7] and is given as:

$$\tau=(V\eta_s/RT)[1+\exp(\Delta F/RT)] \quad \ldots (3)$$

The relative change in volume $(\Delta V/V)$ is estimated employing the concept of open packed structure in the condensed state and the close packed structure for the liquid metals concerned. The details for evaluation of $(\Delta V/V)$ for liquid metals have been discussed elsewhere[5]. With the knowledge of the basic parameters and the equations discussed above, the theoretical values of $(\alpha/f^2)_{str.}$ due to structural cases are calculated. The values agree fairly well with the experimental results[1,2] for the eight liquid metals studied by us (Table 1)

One of the authors, B V S Murthy, would like to thank H H Sri Shivarathri Rajendra Swamiji and Prof. M H Dhananjaya for their help.

References

1 Kim M G, Kemp K A & Letcher S V, *J Acous Soc Am (USA)*, **49** (1971) 706.
2 Plass K G, *Acoustica (Germany)*, **13** (1963) 240.
3 Higgs W & Litovitz T A, *J Acous Soc Am (USA)*, **32** (1960) 1108.
4 Richter H & Breitling G, *Adv Phys (GB)*, **16** (1967) 293.
5 Murthy B V S & Awasthi O N, *Phys Lett A (Netherlands)*, (1981) in press.
6 Hall L, *Phys Rev (USA)*, **73** (1948) 775.
7 Eyring H, *J Chem Phys (USA)*, **4** (1936) 283.

Indian Journal of Pure & Applied Physics
Vol 21, September 1983, pp. 542-543

Equilibrium Geometry of AH_2, AHF & AF_2 Molecules by NDDO Method

A N DIXIT*
Chemistry Department, M B P G College,
Haldwani (Nainital)

Received 22 *March* 1982; *revised received* 4 *January* 1983

The all valence NDDO-MO method, after correction by *S*-function, is used to calculate the bond angle and bond length for the equilibrium configuration of some radicals and molecules. The results so obtained are in good agreement with the experimental values. Unlike in CNDO or INDO method no rotational averaging of repulsion integrals is done at the expense of information about the directional properties of orbitals. Hence, this method should be able to handle the problem of electronic structure in molecules possessing one or more lone pairs and also in molecules in which *d*-orbitals play vital role in bonding.

The NDDO approximation was subjected to considerable theoretical analysis, but very few numerical calculations were attempted. Roby formulated a theoretical NDDO-MO scheme which did not seriously jeopardize the simplicity of Pople's scheme[1]. We have presently calculated equilibrium geometry of a number of molecules using Roby's formulation with a view to ascertaining its capabilities and limitations and to prove the effects of several refinements which have been suggested. To provide a consistent interpretation for the results, a minimum basis set of Slater-type orbitals, expanded in terms of three Gaussians each by a variational fit[2], was employed in the calculation. Clementi-Raimondi exponents[3] were used for the orbital exponents of atoms of the first row of periodic table. The exponent for hydrogen was taken as 1.2. The integrals occurring in such computations can be evaluated to a high degree of accuracy with considerable ease using GTO basis[4]. In the scheme formulated, the atomic orbital basis set $\{\psi\}$ is transformed into Lowdin symmetry orthogonalized (OAO) set $\{\lambda\}$, using the transformation[5].

$$\lambda = \psi S^{-1/2} \qquad \ldots (1)$$

The secular equation to be solved over the $\{\lambda\}$ basis then becomes:

$$F^{\lambda} C^{\lambda} = C^{\lambda} E \qquad \ldots (2)$$

$$F^{\lambda} = H^{\lambda} + G^{\lambda} \qquad \ldots (3)$$

where, H^{λ} and G^{λ} are respectively the one- and two-electron parts of Fock matrix F^{λ}. The MO-coefficients C^{λ} and F^{λ} may be expressed in terms of their non-orthogonal counterparts as follows:

$$F^{\lambda} = S^{-1/2} F S^{-1/2} \qquad \ldots (4)$$

$$C^{\lambda} = S^{1/2} C \qquad \ldots (5)$$

where S is overlap matrix over the non-orthogonal basis set. The OAO basis does not pose any difficult problem because it is easily evaluated over the non-orthogonal basis. However, Roby and Sinanoglu[1] have effected a simplification by proving the following interesting theorem.

The electron repulsion in integral supermatrix over the OAO basis may be equated to that over the non-orthogonal basis in which the NDDO approximation has been made, provided the Ruedenberg expansion[6] is sufficiently valid. In mathematical form

$$G^{\lambda} = G_{\text{NDDO}} \qquad \ldots (6)$$

$$\text{i.e.} \quad (\mu_A^{\lambda} V_B^{\lambda} / \sigma_C^{\lambda} \rho_D^{\lambda}) = (\mu_A V_A / \sigma_C \rho_C) \delta_{AB} \delta_{CD} \qquad \ldots (7)$$

The truncated Ruedenberg expansion for a minimum basis set of atomic orbital is obviously far from correct. However, the source of error may easily be pinpointed in Roby's scheme, and hence the method may be subjected to systematic refinements.

The scale factors[7] are employed for Coloumb repulsion integrals in the present work. They are evaluated using the S-expansion technique, correct through second order in overlap[8]. For one-centre Coulomb repulsion integrals, the corrections are given by

$$^{\lambda}V_{\mu\nu}^{AA} = V_{\mu\mu}^{AA} + \sum_{B \neq A} \sum_{\delta}^{B} \tfrac{1}{4} [S^2{}_{\mu\delta}^{AB} (V_{\mu\nu}^{AA} V_{\mu\delta}^{AB}) + (S^2)_{\nu\delta}^{AB} (V_{\mu\nu}^{AA} - V_{\mu\delta}^{AB})] \qquad \ldots (8)$$

$$^{\lambda}V_{\mu\delta}^{AB} = V_{\mu\delta}^{AB} + \sum_{\nu}^{A} \tfrac{1}{4} (S^2)_{\delta\nu}^{BA} (V_{\mu\delta}^{AB} - V_{\mu\nu}^{AA}) + \sum_{\varepsilon}^{B} \tfrac{1}{4} (S^2)_{\mu\varepsilon}^{AB} (V_{\mu\delta}^{AB} - V_{\delta\varepsilon}^{BB}) + \sum_{C \neq AB} \sum_{\omega}^{C} \tfrac{1}{4} [(S^2)_{\delta\omega}^{BC} (V_{\mu\delta}^{AB} - V_{\mu\omega}^{AC}) + (S^2)_{\mu\omega}^{AC} (V_{\mu\delta}^{AB} - V_{\delta\omega}^{BC})] \qquad \ldots (9)$$

The core-valence separation was carried out closely along the lines suggested by Lykos and Parr[8]. The total wavefunction is written in the form

$$\psi = \mathscr{A} (\psi^{\text{core}} \psi^{\text{val}}) \qquad \ldots (10)$$

wher ψ^{core} and ψ^{val} are antisymmetrized functions for tne core and valence electrons respectively. $\mathscr{A}$ is an antisymmetrization operator which interchanges electrons between the core and valence shells. The core orbitals are taken to be the original unpolarized atomic orbitals of the neutral atom.

The expectation value of electronic energy may be written as

$$E_T = E_{\text{core}} + E_{\text{val}} \qquad \ldots (11)$$

where $E^{\circ}_{core} = \int \psi^{core} \mathscr{H}^{\circ}_{core} \psi^{core} d\tau$ ... (12)

$E_{val} = \int \psi^{val} \mathscr{H}_{val} \psi^{val} d\tau$ ... (13)

In Eqs (11) & (12)

$$\mathscr{H}_{core}\ (1,2, \ldots n_c) = \sum_{k=1}^{n_c} \mathscr{H}_N^{(k)} + \tfrac{1}{2} \sum_{k,\lambda}^{n_c} \frac{1}{\gamma_{k,\lambda}} \quad \ldots (14)$$

and

$$\mathscr{H}_{val}(n_c+1 \ldots, n_c+n_v) = \sum_{\mu=n_c+1}^{n_c+n_v} \mathscr{H}_{core}^{(b)} + \tfrac{1}{2} \sum_{\mu,\nu=n_c+1}^{n_c+n_v} \frac{1}{\gamma_{\mu,\nu}} \quad \ldots (15)$$

with

$$\mathscr{H}_{core}^{(b)} = K_N^{(\mu)} + \sum_{J=1}^{n_c} [2J_J(\mu) - k_J(\mu)] \quad \ldots (16)$$

In Eqs (12-16) $\mathscr{H}_N$ is the kinetic energy plus the nuclear attraction terms, the remaining term representing the Coulomb and exchange potentials from the core electrons.

This procedure of core-valence separation is justified only if all valence orbitals are kept orthogonal to all core orbitals. In the present set of calculations, the 2*s* orbital has been made orthogonal to the 1*s* core on the same atom by the Schmidt procedure. The valence orbitals on any atom have not been orthogonalized to the core on another atom but the overlap is expected to be too small to have any contribution. The conventional and more convenient way of treating the core as a point charge collapse at the nucleus has also been studied.

The theoretical calculation of the equilibrium geometry for a molecule involves systematically minimizing the total energy of the system with respect to all independent internal displacement coordinates of the molecule. The binding energy of a molecule is then the difference between the total energy of a molecule at equilibrium geometry and the sum of the atomic energies of the component atoms. Actually the position of the absolute minimum in the total energy of the system is specified by the equilibrium geometry[9].

A systematic study has been made of molecules containing the atoms H, C, N and F with NDDO theory with only one or two polyvalent atoms (C or N). If we denote polyvalent atoms by symbol A and other atoms (H or F) by X and Y, the class of molecules considered is AX_2, AXY and AY_2 molecules. The following constraint is placed on the nuclear configuration:

$$AX_2, AXY, AY_2 : C_{2v} \text{ symmetry.}$$

We preferred here the Schoenflies notation[10] expressing point symmetry.

The calculations were performed by starting with an initial guess of the nuclear configuration and varying individual parameters, bond angle in turn, until a minimum in the total energy was found. In all these cases, bond angles were varied initially in steps of 1° and bond length in steps of 0.1 Å. After one complete cycle through all parameters, the step sizes were decreased by a factor of 10 for a second cycle.

Table 1—Calculated & Experimental Geometries for AH_2, AHF & AF_2 Molecules

	RAH, Å		RAF, Å		θ_{angle}	
	Calc	Exptl	Calc	Exptl	Calc	Exptl
Singlet states						
CH_2	1.14	1.12	—	—	105.0	103.2
CHF	1.13	1.12	1.29	1.31	104.1	101.8
CH_2	1.11	—	1.30	1.30	103.8	104.9
OH_2	1.02	0.88	—	—	104.5	104.3
OHF	1.06	—	1.19	—	107.0	—
OF_2	—	—	1.27	1.41	105.9	103.3
Doublet states						
NH_2	1.05	1.02	—	—	104.8	103.3
NHF	1.07	—	1.24	—	106.6	—
NF_2	—	—	1.26	1.37	103.0	104.2
Triplet states						
CH_2	1.08	1.04	—	—	160.0	180.0
CF_2	——	—	1.33	—	129.8	—

For the carbon compounds CH_2, CHF and CF_2 all calculated bond lengths agree well with the experimental values, and the valence angles for the singlet states are also in good agreement. The bond angle in triplet state of CH_2 is correctly predicted to be larger than that in the singlet; however, the NDDO optimized calculations still lead to a bent triplet form rather than the linear form suggested on the basis of spectroscopic evidence.

For the oxygen compounds, we may note that the experimentally observed geometry of water is well reproduced. However, the theory incorrectly predicts the FOF angle in F_2O to be larger than in water. The NDDO gives small values for O−F bond length. The calculated angle in OHF is probably also too large for similar reasons. All these results are presented in Table 1.

References

1 Roby K R & Sinanoglu O, *Int J Quantum Chem (USA)*, III S (1969) 223; Roby K R, *Chem Phys Lett (Netherland)*, **11** (1971) 6.

2 Huzinaga S, *J Chem Phys (USA)*, **42** (1965), 1293.

3 Clementi E & Raimondi D L, *J Chem Phys (USA)*, **38** (1963) 2686.

4 Kern C W & Karplus M, *J Chem Phys (USA)*, **43** (1965) 415.

5 Löwdin P O, *J Chem Phys (USA)*, **18** (1950) 365.

6 Ruedenberg K, *J Chem Phys (USA)*, **19** (1951) 1433.

7 Brown R D & Roby K R, *Theor Chim Acta (Germany)*, **16** (1970) 175.

8 Lykos P G & Parr R G, *J Chem Phys (USA)*, **24** (1956) 1166.

9 Wilson H B (Jr), Decius J C & Cross P C, *Molecular vibrations* (McGraw Hill, New York), 1955.

10 Clyde M, Day J R & Selbin J, *Theoretical inorganic chemistry* (Van Nostrand, New York), 1980.

Indian Journal of Pure & Applied Physics
Vol 21, September 1983, pp. 544-545

A Force Field Study of Nitrogen Dioxide

S MOHAN* & K G RAVIKUMAR

Division of Applied Sciences, Anna University,
Madras Institute of Technology, Chromepet,
Madras 600 044

Received 25 *November* 1982; *revised received* 8 *March* 1983

A fresh study of vibrational molecular constants of nitrogen dioxide molecule has been carried out following Wilson's *F-G* matrix method using a general quadratic potential function and kinetic constants. The complete vibrational analysis of NO_2 is presented and the results are briefly discussed.

Analysis of absorption spectrum of nitrogen dioxide in the visible region has been difficult for many decades because of its complexity[1]. Several authors attempted to elucidate the complexity of NO_2 spectrum. Some groups investigated small details of the whole spectrum, like the rotational analysis of different vibronic bonds. Other groups measured fine and hyperfine structures of specific vibronic levels. But no satisfactory analysis of the coarse vibrational structure of the NO_2 is available in the literature. Recently, Bolduan and Jodl[1] used the matrix isolation technique to investigate the vibrational structure of the NO_2 molecule in the ground state as well as in the excited electronic state. They reported the complete vibrational frequencies of this molecule in rare gas solids Ar, Kr and Xe. Using the ground state frequencies in the present investigation, the molecular constants, viz. potential constants, compliance constants, vibrational mean amplitudes, Coriolis coupling constants, centrifugal distortion constants, inertia defect and thermodynamic functions for nitrogen dioxide have been studied. The structural parameters used in the present investigation have been taken from Ref. 2. The symmetry coordinates and the other details of the procedure of the calculations are the same as those given in the earlier papers[3-5].

The evaluated molecular constants are reported in Table 1. The interesting observation in this molecule is that the major potential constants as well as the interaction potential constants are positive. The N-O potential constant obtained in the present work is in the expected range. Further, the values obtained by the present method agree satisfactorily with the values reported by Arakawa and Nielsen[2] ($f_d = 10.927$; $f_{dd} = 2.038$; $f_\alpha = 1.125$; $f_{d\alpha} = 0.930$). The compliance constants are evaluated by the Decius method[6]. They naturally exhibit trends opposite to those relating to the potential constants. It may be noticed that the bond-bond interaction and bond-angle interaction compliance constants are negative in this molecule. Using the potential constants in Cyvin's secular equation[7], the symmetrized mean square amplitude elements and hence the mean amplitudes are obtained at 298.16 K. It may be seen that the mean amplitude for the bonded as well as the non-bonded distances obtained in the present work is in the characteristic range for N−O vibration.

Table 1—Molecular Constants

Kinetic constants (10^{-23}g)

	$(X)NO_2$
k_d	1.4598
k_{dd}	0.9150
k_z	0.5448
k_{dz}	0.4691

Force constants (mdyn/Å)

	$(Ar)NO_2$	$(Kr)NO_2$	$(Xe)NO_2$
f_d	10.6942	10.7026	10.6480
f_{dd}	2.3102	2.3290	2.2589
f_z	1.0928	1.0896	1.0856
f_{dz}	0.9410	0.9382	0.9347

Compliance constants $(mdyn/Å)^{-1}$

	$(Ar)NO_2$	$(Kr)NO_2$	$(Xe)NO_2$
n_d	0.1007	0.1006	0.1009
n_{dd}	−0.0186	−0.0188	−0.0183
n_z	0.9759	0.9784	0.9824
n_{dz}	−0.0706	−0.0704	−0.0712

Coriolis coupling constants

	$(X)NO_2$
ζ_{11}	−0.4124 (−0.49092)
ζ_{11}	0.9110 (0.87121)
$(\zeta_{11})^2$	0.1700 (0.241 0.009)

Centrifugal distortion constants (MHz)

	$(Ar)NO_2$	$(Kr)NO_2$	$(Xe)NO_2$
$-\tau_{xxxx}$	318.5032	319.1683 (299.4)	320.6801
$-\tau_{zzzz}$	0.0398	0.0398 (0.0414)	0.0401
τ_{xxzz}	1.7707	1.7804 (1.843)	1.7817
$-\tau_{xzxz}$	0.2601	0.2604 (0.245)	0.2599

Mean amplitudes (Å) at 298.16K

	$(Ar)NO_2$	$(Kr)NO_2$	$(Xe)NO_2$
l_d	0.0387	0.0387	0.0387
l_q	0.0459	0.0459	0.0459

Inertia defect (amu Å in the ground state)

$(Ar)NO_2$	$(Kr)NO_2$	$(Xe)NO_2$
0.0972	0.0973 (0.0970)	0.0975

*Values in parentheses are the observed values.

The Coriolis coupling constants which may be determined experimentally can, however, be evaluated from a reliable set of potential constants and the values can be used for a detailed interpretation of the vibrational spectrum. The Coriolis coupling constants are obtained according to the vector method of Meal and Polo[8]. As expected, the value of ζ^{C}_{13} is negative. Further, ζ-values obey the sum rule:

$$\zeta^{2}_{13} + \zeta^{2}_{23} = 1$$

The Coriolis coupling constants when compared with the values available in the literature[9] agree satisfactorily.

The centrifugal distortion constants evaluated by Kivelson and Wilson's[10] method are presented in Table 1 and they are also in the expected range. The present values of centrifugal distortion constants are compared with the observed values[11] in Table 1. The close agreement between the present values and the observed values points out the significance of the method of kinetic constants.

The calculated values of the inertia defect of nitrogen dioxide molecule using Coriolis coupling constants and centrifugal distortion constants are also given in Table 1, along with the experimental values[5,11]. It is interesting to note that the calculated value agrees quite well with the experimental value indicating the significance of the present method.

Lastly, the thermodynamic functions of nitrogen dioxide are calculated for the ideal gas state at 1 atm pressure assuming a rigid rotor harmonic oscillator model. The effects of spin contribution, anharmonicity and non-rigidity are neglected. The contribution to the vibrational part of these thermodynamic functions has been calculated from the tables given by Johnson *et al*[12]. The values thus obtained form the thermodynamic functions are available with the authors. These constants are useful in the interpretation of the experimental results on thermodynamic properties.

The authors are thankful to Prof S Sathikh, Director of the Madras Institute of Technology, for his encouragement and the facilities given to carry out this research work. One of the authors (KGR) is thankful to the CSIR, New Delhi, for the award of a junior research fellowship which enable him to pursue this investigation.

References

1 Bolduan F & Jodl H J, *J Mol Spectrosc (USA)*, **91** (1982) 404.

2 Arakawa E T & Nielsen H H, *J Mol Spectrosc (USA)*, **2** (1968) 413.

3 Thirugnanasambandam P & Mohan S, *J Chem Phys (USA)*, **61** (1974) 470.

4 Mohan S, *Acta Phys Pol Ser A (Poland)*, **57** (1980) 433.

5 Mohan S & Manickavachagam R, *Indian J Pure & Appl Phys*, **16** (1978) 55.

6 Decius J C, *J Chem Phys (USA)*, **38** (1963) 241.

7 Cyvin S J, *Molecular vibrations and mean square amplitude* (Universitetsforlaget, Oslo and Elsevier, Amsterdam) 1968.

8 Meal J H & Polo S R, *J Chem Phys (USA)*, **24** (1956) 1119, 1126.

9 Oka T & Morino Y, *J Mol Spectrosc (USA)*, **8** (1962) 9.

10 Kivelson D & Wilson E B (Jr), *J Chem Phys (USA)*, **20** (1953) 1575.

11 Bird G R, Bird J C, Jache A W, *et al.*, *J Chem Phys (USA)*, **40** (1964) 3378.

12 Johnson H L, Savadoff L & Belyer J, *Contribution to thermodynamic functions* (Office of Naval Research, Washington, USA) 1949.

Indian Journal of Pure & Applied Physics
Vol 21, September 1983, pp. 546-549

Lifetimes of ^{28}Si States

V K MITTAL*, D K AVASTHI & I M GOVIL
Department of Physics, Panjab University, Chandigarh 160014

Received 1 *May* 1981; *revised received* 9 *May* 1983

Levels of ^{28}Si were populated using ^{27}Al(p, γ) reaction at $E_p = 2.05$ MeV. Decay from the resonance at 13.6 MeV in ^{28}Si was studied. The lifetimes of the levels were measured using DSA technique. The lifetime of 13.56 MeV state as 27 ± 5 fs is being reported for the first time. The measured lifetimes have been compared with the previous experimental values and are found to be in good agreement. Further, the present experimental lifetimes are compared with the theoretical predictions using PW, KLS and ASDI interactions.

There has been a considerable difficulty in understanding the spectrum of ^{28}Si. The nuclei at the beginning of the *s-d* shell exhibit characteristic rotational spectra ($0^+, 2^+, 4^+$); however, this structure breaks down towards the middle of the shell. Therefore, the structure of ^{28}Si has been studied in recent years by various authors[1-9] by means of ^{27}Al(p,γ) ^{28}Si reaction to obtain information about the energy, spin, parity, lifetimes, etc. of various excited states. The recent experimental information about ^{28}Si has been compiled by Endt and van der Leun[10]. A 13.56 MeV level in ^{28}Si corresponding to the proton resonance at 2.046 MeV was investigated by Kennedy *et al.*[11] They assigned 2^+, 3^+, 4^+ as probable spins to this level. However, no measurement of the lifetime of this level was reported. Therefore, we decided to investigate the lifetime of this level in the present study. The lifetimes of other levels are also compared with the theoretically calculated lifetimes to see the effectiveness of various interactions employed in the description of this nucleus.

Experimental details—The reaction ^{27}Al (p,γ) ^{28}Si was used to populate states in ^{28}Si at proton bombarding energy of 2.05 MeV corresponding to the resonance at 13.56 MeV[11]. The proton beam was obtained from the Chandigarh cyclotron. The target was 5 keV thick for 2 MeV protons. The γ-rays were detected by a 50 cc Ge(Li) detector having resolution of

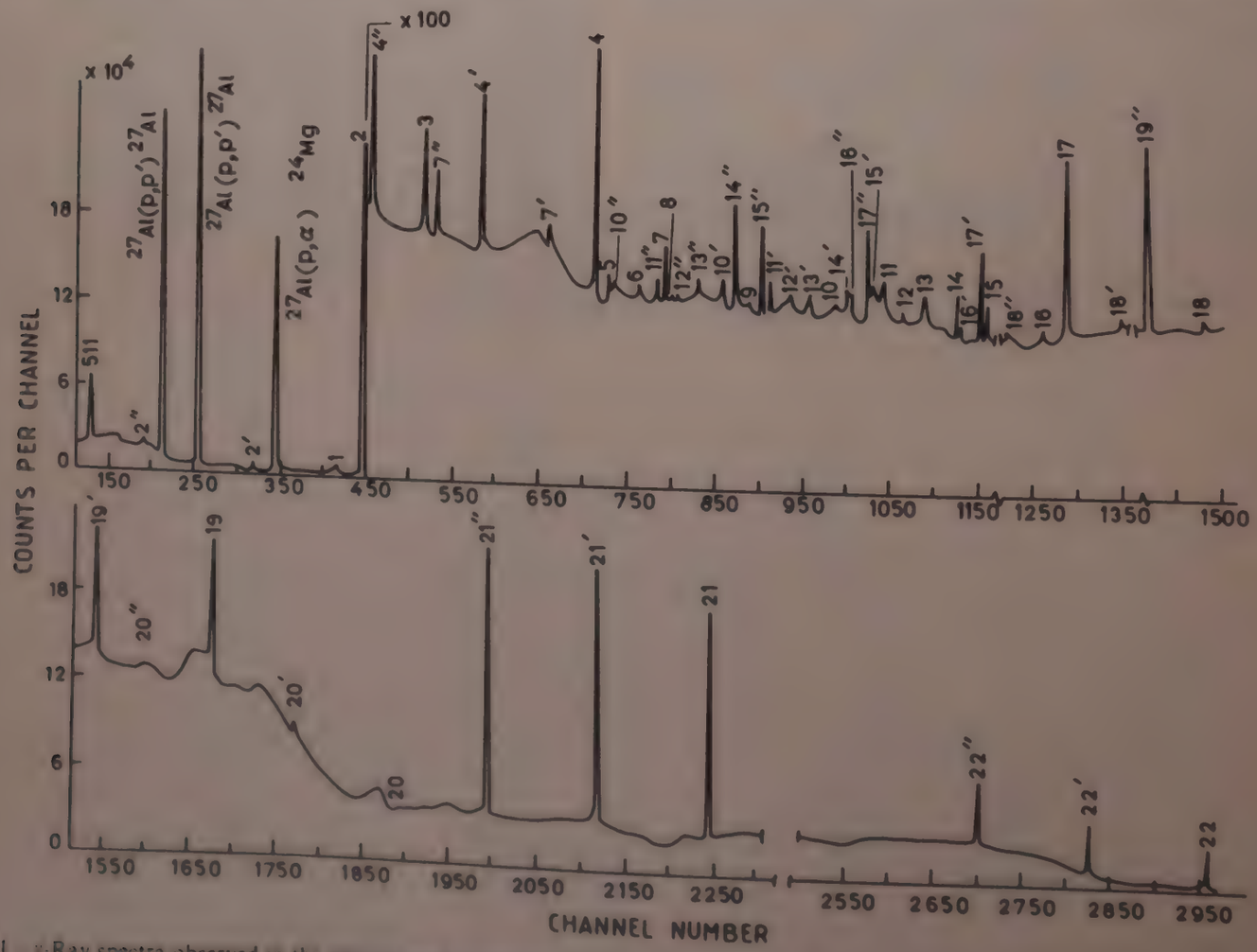

Fig 1 — γ-Ray spectra observed in the present work [Number on the peak represents the corresponding transition in Table 1. Single and double primes represent first and second escape peak]

≈2 keV at 1.33 MeV. A typical spectrum is shown in Fig. 1. The numbers marked on the peaks in Fig. 1 correspond to the transitions shown in Table 1 and the corresponding level scheme is shown in Fig. 2. The detector system was calibrated for energy and efficiency using γ-rays from ^{152}Eu, ^{154}Eu and ^{56}Co. The drift in the detecting system was checked periodically using ^{60}Co source and observing the γ-rays from ^{19}F (p, $\alpha\gamma$) ^{16}O reaction along with the well known background peaks. Centroid positions of γ-rays' full energy photo peaks were measured with the help of first moment method.

Analysis—The lifetimes were calculated using DSA technique from the positions of the centroid using the equation[12]

$$F(\tau)=\frac{\Delta E}{(\cos\theta_1-\cos\theta_2)\beta.E_{90}}$$

where $F(\tau)$ is the attenuation coefficient, ΔE the energy difference at angles θ_1 and θ_2, E_{90} the energy of γ-ray and β the Z component of the velocity of recoiling ^{28}Si atoms.

Since the cross-section for the capture reaction was low, the spectrum at each angle was recorded for more than 20 hr to get sufficient statistics on the relevant peak.

From 13.56 MeV level, there were three major transitions as shown in Fig. 3. Lifetimes were measured for all the three transitions. Experimental $F(\tau)$ was calculated using Doppler shift equations and was found to be almost same in all γ-rays from this level.

Table 1—Transitions and γ-ray Energies for Various Peaks Corresponding to Numbers shown in Fig. 1

Peak No.	Transition From→To	Energy (keV)
1	6276.4→4617.7	1658.7
2	1779.1→0	1779.1
3	8944.5→6888.8	2055.7
4	4617.7→1779.1	2838.6
5	13555→10666.2	2889.4
6	9315.8→6276.4	3039.4
7	13555→10417.0	3138
8	13555→10375	3180
9	10417→6838.2	3578.2
10	8543.2→4617.7	3925.5
11	10417→6276.4	4140.6
12	13555→9315.8	4239.0
13	8944.8→4617.8	4328.8
14	6276.4→1779.1	4497.3
15	13555→8944.9	4610.1
16	13555→8544.5	5011.55
17	6888.8→1779.1	5109.7
18	10417→4617	5800
19	13555→6888.8	6666.2
20	9315.8→1779.1	7536.7
21	13555→4617.7	8938.3
22	13555→1779.1	11775

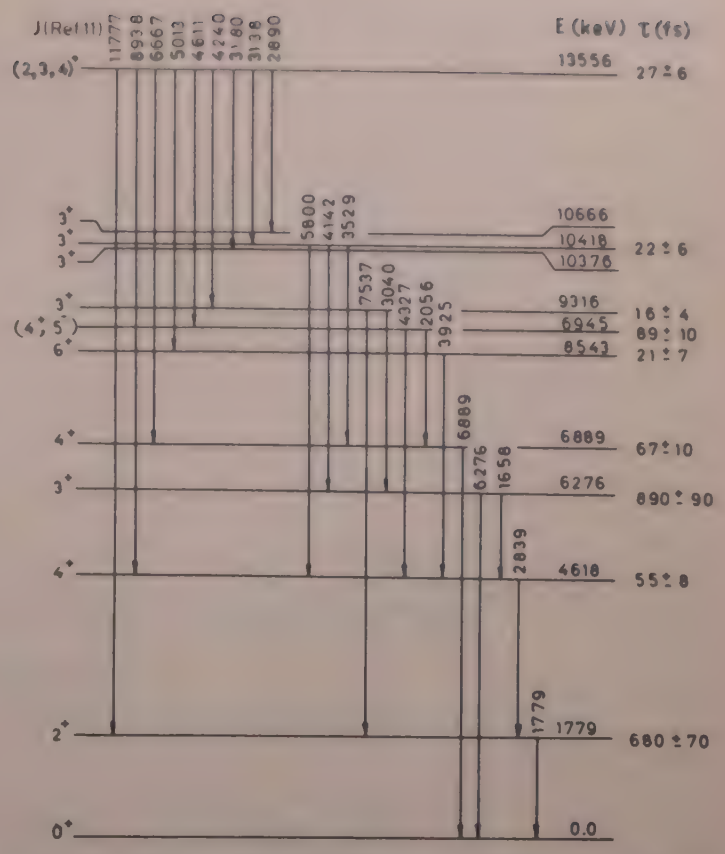

Fig. 2—Decay scheme of ^{28}Si observed in the present work corresponding to the resonance at E_p=2.046 MeV

Theoretical attenuation factor was calculated using a computer code based on the nuclear stopping approximation of Blaugrund[13] and the stopping theory of Lindhard *et al.*[14] The target thickness was taken into account explicitly in calculating the theoretical values of $F(\tau)$. The target was divided into 10 layers of equal thickness and $F_i(\tau)$ was calculated for each layer and the average value of $F\tau$) was calculated from the values of $F_i(\tau)$. A theoretical $F(\tau)$ versus τ curve was constructed and the values of lifetimes were extracted from these values using the experimental values of $F(\tau)$.

Results and discussion—Experimental lifetimes of various levels are shown in Table 2. The lifetime of the level at 13.56 MeV being reported for the first time is the weighted average of the values of lifetimes for the three transitions from this level as discussed above. The present value of lifetime of this level supports the spin assignment $(2,3,4)^+$ to this level[11].

^{28}Si is a nucleus having doubly closed proton and neutron shell, hence several shell model calculations of positive and negative parity states have been performed. Recently, two different interactions have been used for the calculations. The first is Preedom-Wildenthal[15] (PW), which is based on an effective *d-s* interaction with two-body matrix elements adjusted to fit the ^{22}Ne and ^{22}Na data. The other is Kahana-Lee-Scott[16] (KLS) interaction which is renormalized interaction based on a realistic bare NN potential and among the several renormalized *d-s* interactions.

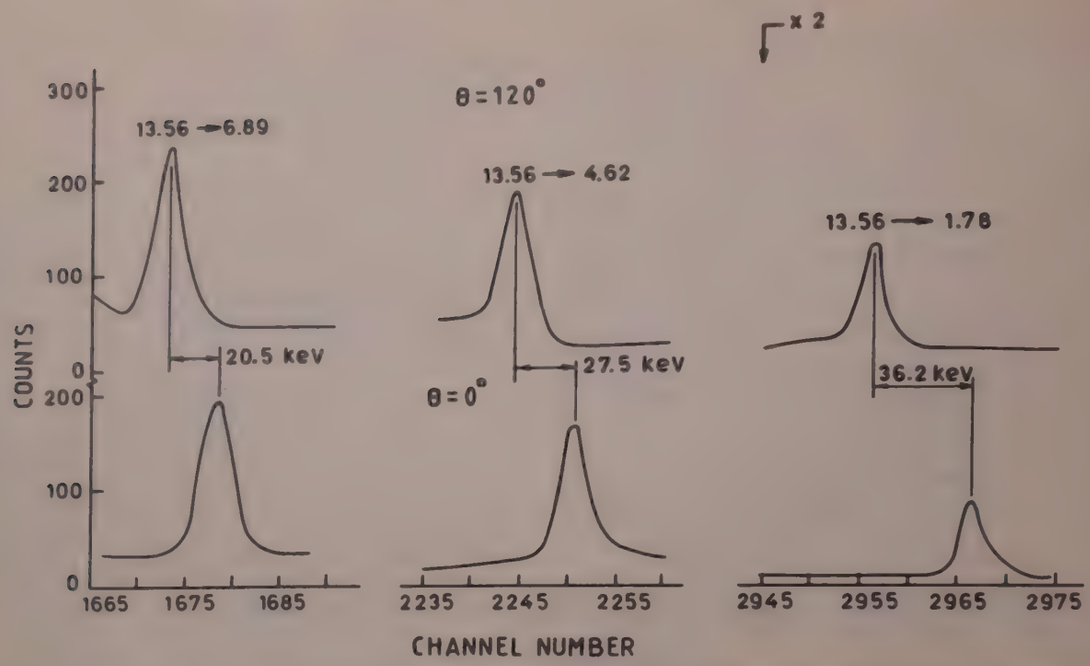

Fig. 3—Shift in the centroid position for 13.56→6.89, 13.56→4.62 and 13.56→1.78 transitions at 120° and 0°

Table 2—Various Levels with Values of Excitation Energy and Lifetime

Level keV	E_γ keV	Lifetime (fs)					
		Experimental			Theoretical		
		Present	Ref. 8	Ref. 10	PW[15] interaction	ASDI[17] interaction	KLS[16] interaction
1779.1±0.1	1779.1	680±70	—	700±20	727	790	817
4617.7±0.3	2838.6	55±8	40±7	63±6	55	57	51
6276.4±0.4	4497.3	890±90	—	1200±120	1230	780	9150
6888.8±0.5	5109.7	67±10	45±9	50±7	28.6	27	937
8543.2±0.7	3925.5	31±7	<5	18±5	18.6	13.5	9.5
8944.9±0.6	2055.7	89±10	100±8	85±15	—	—	—
9315.8±0.7	3039.4	16±4	<5	10±5	—	—	—
10417.6±1.8	4141.2	22±6	27±8	26±5	—	—	—
13555.6±3.1	11776.5	27±5	—	—	—	—	—

The shell model calculations by Van Eijkern[17] for this nucleus have been performed using adjusted surface δ interactions (ASDI) in $1d_{5/2}$, $2s_{1/2}$ and $1d_{3/2}$ configuration space. The calculated results from ASDI wavefunctions have been obtained with bare nucleon Ml single-particle matrix elements and an isoscaler effective charge $e^\circ = 2.15e$; the isovector effective charge has been kept equal to unity.

Table 2 also shows the values of lifetimes obtained in the present experiment along with the theoretically calculated lifetimes using the above three different approaches, viz. PW, ASDI and KLS. It is evident from Table 2 that the theoretical lifetimes obtained using PW and ASDI interactions are almost of the same order and they agree well with the experimental values. However, KLS interaction results are not supported by our experiment. The theoretical calculations of the several high energy levels are still missing; the calculations of these levels will be useful to verify the above conclusion.

References

1 Gibson E F, Battleson K & McDaniels D K, *Phys Rev (USA)*, 172 (1968) 1004.

2 Meyer M A & Wolmarans N S, *Nucl Phys A (Netherlands)*, 136 (1968) 663.

3 Meyer M A, Wolmarans N S & Reitmann D, *Nucl Phys A (Netherlands)*, 144 (1970) 261.

4 Roush M L, West L A & Narion J B, *Nucl Phys A (Netherlands)*, 147 (1970) 235.

5 Forsblom I, *Commentat Phys-Math (Finland)*, 40 (1970) 65.

6 Muang F C D, Gibson E F & McDaniels D K, *Phys Rev C (USA)*, 3 (1971) 1222.

7 Neal C F & Lam S T, *Phys Lett B (Netherlands)*, 45 (1973) 127.

8 Meyer M A, Venter I & Reitmann D, *Nucl Phys A (Netherlands)*, 250 (1975) 235.

9 Mass J W, Somorjai E, Graber H D *et al.*, *Nucl Phys A* (*Netherlands*), **301** (1978) 213.

10 Endt P M & van der Leun C, *Nucl Phys A* (*Netherlands*), **310** (1978) 1.

11 Kennedy D L, Heggie J C P, Davies P J & Bolotin H H, *Nucl Instrum & Methods* (*Netherlands*), **140** (1977) 519.

12 Warburton E K, Olness J W & Poletti A R, *Phys Rev* (*USA*), **160** (1967) 938.

13 Blaugrund E A, *Nucl Phys* (*Netherlands*), **88** (1966) 501.

14 Lindhard J, Scharff M & Schiott, *Kgl Danske Videnskab Selskab, Mat-Fys Medd* (*Denmark*), **33** (14), (1963) 1.

15 Preedom B M & Wildenthal B H, *Phys Rev C* (*USA*), **6** (1972) 1633.

16 Kahana S, Lee H C & Scott C K, *Phys Rev* (*USA*), **185** (1969) 1378.

17 Van Eijkern F E H, *Experimental studies on* ^{32}P *and shell model calculations in* $A=28$-32 *nuclei*, Ph D thesis, Utrecht University, Netherlands, 1975.

Indian Journal of Pure & Applied Physics
Vol 21, September 1983, pp. 550-551

Uranium Estimation in Some Indian Toothpastes

SURINDER SINGH & H S VIRK*
Department of Physics, Guru Nanak Dev University, Amritsar

Received 23 *October* 1982; *revised received* 24 *January* 1983

The fission track technique has been used to estimate uranium concentration in some toothpastes manufactured in India. Uranium content varies from 0.91 to 3.56 ppm in selected varieties of toothpastes.

The solid state nuclear track detector (SSNTD) technique, because of its simplicity and applicability, has attracted many users in diverse fields such as anthropology, archaeology, biology, medical sciences and industrial technology[1]. The heaviest naturally occurring trace element, uranium, plays an important role in these investigations. The technique has already been exploited by various workers[2-5] for the trace determination of uranium in semiconductors, water, milk powders, human blood, plants, soils, Indian cigarettes (tobacco), tea leaves, portland cement, detergents and soaps, coal, flyash, steel, etc. In our laboratory, we have applied this technique for the trace determination of uranium in some toothpastes manufactured by various agencies in India. The aim of this particular work is to estimate the level of uranium content in toothpastes for the studies of radiation health hazards.

We followed the external detector method as suggested by Fleischer *et al.*[1] and Fisher[6] for bulk determination of uranium in homogeneous solids. The procedure is well-established. Toothpastes were dried in an oven at 200°C for 24 hr. The dried powder (50 mg) was homogeneously mixed with 100 mg of methyl cellulose used as a binding material. The mixture was pressed into a pellet by a specially designed hand-pressing machine. These pellets were then covered on both sides with lexan plastic discs of the same diameter as the pellet. One such pellet was made of the standard glass dosimeter. The pellets covered with lexan discs were enclosed in an aluminium capsule and were irradiated with a thermal neutron dose of 5×10^{15} (nvt) from the CIRUS Reactor of Bhabha Atomic Research Centre, Trombay. After irradiation, the lexan discs were etched in 6N NaOH at 70°C for 30 min and were scanned for fission track density. A blank lexan detector was irradiated along with the samples and checked for background tracks. It was found almost devoid of background tracks.

Table 1—Uranium Estimation in Some Indian Toothpastes

[U Content of glass dosimeter = 20 ppm; thermal neutron dose = 5×10^{15} (nvt)]

Trade name of the tooth-paste	Manufacturing agency	U content (ppm)
Signal	Hindustan Lever Ltd, Bombay	0.91
Closeup	Hindustan Lever Ltd, Bombay	1.04
Promise	Balsara Hygiene Products, Bombay	1.48
Cosmo	Hindustan, Rimmer, Delhi	1.78
Colgate	Colgate Palmolive Ltd, Bombay	1.82
Flash	Flash Laboratories (Pvt) Ltd, Bombay	2.41
Forhans	Geoffrey Manners & Co Ltd, Bombay	2.71
Binaca	Ciba-Geigy of India Ltd, Bombay	2.76
Neem	Calchemico, The Calcutta Chemical Co Ltd, Calcutta	2.76
Vicco vajradanti	Vicco Laboratories, Bombay	3.56

The uranium concentration was calculated using a simple relation for external detector method[1]:

$$U_x = U_s\left(\frac{T_x}{T_s}\right)\left(\frac{I_s}{I_x}\right)\left(\frac{R_s}{R_x}\right) \quad \ldots (1)$$

where the subscripts x and s stand for unknown and standard respectively, U, the uranium concentration, T the fission track density, I the isotopic abundance ratio of ^{235}U and ^{238}U and R the range of fission fragments in mg/cm^2. The correction factor (R_s/R_x) approaches unity for most of the silicate materials and plastics[1].

Toothpastes consist of various agents such as polishing agents or abrasive materials, humectants, binders, sweetening agents, flavouring agents, surfactants, flourides which act as a germicide and water. Materials used under these subheadings may vary from one manufacturer to another depending upon their formulation. Minerals, inorganic and organic matters present in the toothpastes are generally contaminated with minor amounts of uranium.

The uranium content of various toothpastes calculated by using Eq. (1) is given in Table 1. The uranium content has been found to vary from 0.91 to 3.56 ppm. Signal toothpaste manufactured by Hindustan Lever Ltd., Bombay, has a minimum uranium content of 0.91 ppm, whereas Viccovajradanti manufactured by Vicco Laboratories, Bombay, has yielded a maximum content of 3.56 ppm. Higher value of uranium in Viccovajradanti paste may

be due to the presence of minerals derived from the plant sources. The uranium content in the toothpastes is quite low and is not harmful for society.

References

1 Fleischer R L, Price P B & Walker R M, *Nuclear tracks in solids, principles and applications* (University of California Press, Berkeley, USA), 1975.

2 Abdullaev Kh, Zakhavataev B B & Perelygin V P, *Radiobiology (USA)*, **8** (1969) 765.

3 Carpenter B S & Cheek C H, *Anal Chem (USA)*, **44** (1970) 600.

4 Chakarvarti S K, Lal N & Nagpaul K K, *Proc 10th Int Conf on Solid State Nuclear Track Detectors*, held in Lyons, 2-6 July 1979, 701.

5 Suri P S, Singh S & Virk H S, *Indian J Pure & Appl Phys*, **19** (1981) 1131.

6 Fisher D E, *Anal Chem (USA)*, **42** (1970) 414.

Indian Journal of Pure & Applied Physics
Vol 21, September 1983, pp. 552-554

Calculation of Specific Gravity of Cobalt & Copper Complexes from X-ray Chemical Shifts

V KUMAR*†, K S SRIVASTAVA‡ & A R CHETAL
Department of Physics & Mathematics
Indian School of Mines, Dhanbad 826004

Received 4 *January* 1982; *revised received* 21 *February* 1983

The specific gravities of copper and cobalt complexes have been calculated from their X-ray chemical shifts. The calculated values of specific gravities of cobalt sulphide (CoS), cobalt disulphide (CoS_2), cobalt oxalate (CoC_2O_4), cobalt sulphate ($CoSO_4.7H_2O$), copper oxide (CuO) and copper sulphate ($CuSO_4.5H_2O$) are in fair agreement with their observed values. The specific gravities of piperidinium pentamethylene dithiocarbonatocobalt (II) (Co-PPD); 5,5′-thiodisalicylatocobalt (II) (Co-TDSA); 1-phenyltetrazoline-5-thionocobalt (II) (Co-PhTT); dimethylaminoethanethiolatocobalt (II) (Co-DMAET); α-mercaptopropionatocobalt (II) (Co-TLA); potassium deacyanocobalt (II) $K_6[Co(CN)_{10}]$; tetra-aminocarbonatocobalt (III) nitrate $[Co(NH_3)_4(CO_3)]NO_3$; tetra-aminodinitrocobalt (III) nitrate $[Co(NH_3)_4(NO_2)_2]NO_3$; tri-aminotrinitrocobalt (III) $[Co(NH_3)_3(NO_2)_3]$; 5,5′-thiodisalicylatocopper (II) (Cu-TDSA); piperidinium pentamethylene dithiocarbonatocopper (II) (Cu-PPD); diacetylacetonatocopper (II) hydride (Cu-AcAcH); diacetylacetonatocopper (II) chloride (Cu-AcAcCl); diacetylacetonatocopper (II) bromide (Cu-AcAcBr); diacetylacetonatocopper (II) nitrite (Cu-AcAcNO_2); and α-mercaptopropionatocopper (II) (Cu-TLA) have been calculated for the first time.

X-ray absorption spectroscopy has been effectively used[1-3] to determine bond length, effective ionic charge and coordination number of solids. Chemical shifts of the X-ray absorption edges have been studied by several workers in compounds[4-7], complexes[8-10] and spinels[11,12] and various possible physico-chemical qualitative explanations have been put forward from time to time. Recently, the authors' group[13,14] have calculated the chemical shifts with the help of plasmon shifts for several compounds. In the present note, we report the specific gravities of some cobalt and copper complexes using the experimental values of chemical shifts of X-ray absorption edges. The calculations are based on plasma oscillations theory of solids.

In the X-ray absorption process, the inner electron is ejected and goes to the first unoccupied state above the Fermi level giving rise to an absorption peak. The ejected electron produces an interaction[15,16] of suddenly created or annihilated core holes with conduction electrons, in such a way that electrons oscillate collectively. In the Bohm and Pines[17] theory of plasma oscillations, the formation of energy loss and structural dependence has been ascribed to such interaction. Couchois[18], Lewis *et al.*[19] and Borovskii and Shmidt[20] have also shown such a possibility in X-ray absorption spectra. In this case the mean electronic neutrality is formed from free crystal electrons and from the lattice ions. Plasma can be stimulated to collective vibrations and fluctuations of charge density by means of a falling electron. The primary electrons suffer characteristic energy losses which correspond to natural frequency of collective density vibrations of free electrons or valence electrons. So it is quite plausible to explore such vibrations for the calculation of the density of compounds and complexes.

On lines similar to our earlier[13,14] calculations, the 'plasmon shift' or chemical shift of X-ray absorption edge of a compound or a complex is given by

$$\delta E = (\hbar\omega_p)_C - (\hbar\omega_p)_M \quad \ldots (1)$$

where $(\hbar\omega_p)_C$ = plasmon energy of compounds or complexes, $(\hbar\omega_p)_M$ = plasmon energy of metal and

$$\hbar\omega_p = \hbar(4\pi ne^2/m)^{1/2} \quad \ldots (2)$$

In Eq. (2) n is the density of free electrons, e and m are the electron charge and mass respectively. Further, for the electron density we get the following equation:

$$n = \frac{L\sigma Z}{A} \quad \ldots (3)$$

where L is the Loshmidt number, σ is the density, Z is the valency (effective number of valence electrons taking part in plasma oscillations) and A is the atomic weight (molecular weight W in case of molecule or compound). Putting the numerical values for plasmon energy in Eq. (2), we get the expression:

$$\hbar\omega_p = 28.8(Z\sigma/W)^{1/2} \quad \ldots (4)$$

Eq. (4) is valid for free electron-like metals but to a fairly good approximation, it can also be used for semiconductors and insulators[21]. The plasmon energy for dielectric is given by [16,22]

$$\hbar\Omega_p = \frac{\hbar\omega_p}{(1-\delta\varepsilon_0)^{1/2}} \quad \ldots (5)$$

where $\delta\varepsilon_0$ is a very small correction to the free electron plasmon energy ($\hbar\omega_p$) and, to a first approximation, can be neglected.

Using Eqs (4) and (5), Phillip and Ehrenreich[16] have calculated plasmon energies for various compounds and compared them with their experimental values. They found that within the limits of experimental error

†Present address: Instrumentation Section, Central Mining Research Station, Barwa Road, Dhanbad 826001
‡Physics Department, Lucknow University, Lucknow 226007

Table 1—Calculated Specific Gravities of the Complexes

Complex	Molecular formula	$(\delta E)_{obs}$ eV	Z_C	W_C	$(\sigma_C)_{calc}$	$(\sigma_C)_{obs}$ (Ref. 24)
		Co-Complexes				
	CoS	7.41 ± 1.0 (Ref. 25)	7	91.01	5.4229	5.45
	CoS_2	18.99 ± 1.0 (Ref. 25)	13	123.03	4.6465	4.268
	CoC_2O_4	5.47 ± 0.3 (Ref. 26)	17	146.96	2.8928	3.021
	$CoSO_4.7H_2O$	10.4 Ref. 27)	87	281.12	1.8159	1.94
Co-PPD	$[Co(C_{11}H_{22}N_2S_2)Cl_2.(H_2O)]$	4.5 (Ref. 27)	115	412.331	1.0642	—
Co-TDSA	$H_2[Co(C_{14}H_8O_6S).4H_2O]$	7.6 (Ref. 27)	129	437.304	1.4430	—
Co-PhTT	$[Co(C_7H_5N_4S)_2]$	7.7 (Ref. 27)	103	413.37	1.7266	—
Co-DMAET	$Na_2[Co(C_4H_{10}NS)_2(OH)_2].2H_2O$	8.6 (Ref. 27)	103	283.366	1.2990	—
Co-TLA	$Na_2[Co(C_3H_4O_2S).2H_2O]$	8.9 (Ref. 27)	53	245.085	2.2503	—
	$K_6[Co(CN)_{10}]$	14.5 (Ref. 27)	77	533.73	5.7220	—
	$[Co(NH_3)_4(CO_3)].NO_3$	10.8 (Ref. 27)	68	247.087	2.1184	—
	$[Co(NH_3)_4(NO_2)_2].NO_3$	11.7 (Ref. 27)	76	281.092	2.3364	—
	$[Co(NH_3)_3(NO_2)_3]$	15.1 (Ref. 27)	64	248.06	3.2298	—
		Cu-Complexes				
	CuO	3.87 ± 0.6 (Ref. 28)	3	79.54	6.8699	6.40
	$CuSO_4.5H_2O$	13.4 (Ref. 27)	71	249.69	2.481	2.284
Cu-TDSA	$H_2[Cu(C_{14}H_8O_6S).4H_2O]$	8.0 (Ref. 27)	133	417.95	1.3376	—
Cu-PPD	$Cu_2[(C_{11}H_{22}N_2S_2)Cl_4.4H_2O]$	7.5 (Ref. 27)	154	587.317	1.5381	—
Cu-AcAcH	$Cu(C_5H_7O_2)_2$	12.3 (Ref. 27)	79	261.762	2.1298	—
Cu-AcAcCl	$Cu(C_5H_6O_2Cl)_2$	10.9 (Ref. 27)	91	330.660	2.0610	—
Cu-AcAcBr	$Cu(C_5H_6O_2Br)_2$	10.4 (Ref. 27)	91	419.578	2.4960	—
$AcAcNO_2$	$Cu(C_5H_6O_2NO_2)_2$	8.8 (Ref. 27)	106	351.762	1.5354	—
Cu-TLA	$H_3[Cu_3(C_3H_4O_2S)_3].3H_2O$	15.6 (Ref. 27)	144	563.085	3.2833	—

the calculated and experimental values agreed fairly well. Thus Eq. (4) can also be applied for dielectrics. In the present work, the calculated values of the plasmon energy for Co and Cu have been taken as 11.19 and 10.79 eV respectively from our earlier papers[13,14].

With the help of Eqs (1) and (4), we have obtained the following expression for the specific gravity:

$$\sigma_C = \frac{W_C[\delta E + (\hbar\omega_p)_M]^2}{Z_C 829.44} \quad \ldots (6)$$

where suffix C stands for complexes or compounds.

Eq. (6) help us in calculating the specific gravity of any complex or compound from its known chemical shifts δE. Using this equation, we have first calculated the specific gravities for the compounds CoS, CoS_2, CoC_2O_4, $CoSO_4.7H_2O$, CuO and $CuSO_4.5H_2O$ whose specific gravities are known. Within the limits of the experimental error of chemical shifts, the calculated values for these compounds agree fairly well with their known values of specific gravity. The present study indicates that plasmons do exist in the above insulating complexes and their energy can be calculated by the nearly free valence electron theory[23]. This would mean that the plasma frequency is much larger than that derivable from the band gaps in these insulating complexes. Therefore, Eq. (6) has been used to calculate the specific gravities of the complexes Co-PPD, Co-TDSA, Co-PhTT, Co-DMAET, Co-TLA, $K_6[Co(CN)_{10}]$, $[Co(NH_3)_4(CO_3)]NO_3$, $[Co(NH_3)_4(NO_2)_2]NO_3$, $[Co(NH_3)_3(NO_2)_3]$, Cu-TDSA, Cu-PPD, Cu-AcAcH, Cu-AcAcCl, Cu-AcAcBr, Cu-$AcAcNO_2$ and Cu-TLA whose specific gravities are unknown.

In these calculations, the effective value of Z for cobalt and copper has been taken as one[13,14]. The effective values of Z for oxygen, sulphur, chlorine, bromine, hydrogen, carbon and nitrogen have been taken as 6, 6, 7, 7, 1, 4 and 3 respectively. These values of Z are their usual valencies.

The calculated values of the specific gravities for cobalt and copper complexes are listed in Table 1 from which it can be seen that the error between the calculated and observed values for the specific gravity is in between 0.5 and 8%. This, as mentioned earlier, may be due to the experimental error which is of the order of 1 eV in the measurement of chemical shifts.

In conclusion, we would like to point out that the specific gravities of unknown compounds and complexes can be determined from their chemical shifts. This method, however indirect it may be, has the advantage of being free from the effects of macroscopic porosity and thus gives intrinsic specific gravity. The accuracy of the values of the specific gravity calculated by this method will depend upon how accurately the chemical shift is determined.

The authors are grateful to Dr B Singh, Director, Dr S C Srivastava, Assistant Director, Central Mining Research Station, Dhanbad and Prof. G S Marwaha, Director, Indian School of Mines, Dhanbad, for inspiration and continuous cooperation.

References

1 Deshmukh P, Deshmukh P & Mande C, *J Phys C (GB)*, **14** (1981) 531.

2 Koul P N, Padalia B D & Ghatikar M N, *J Phys Soc Jpn (Japan)*, **50** (1981) 246.

3 Ballal M M & Mande C, *J Phys & Chem Solids (GB)*, **38** (1977) 1383; *J Phys C (GB)*, **11** (1981) 837.

4 Kawata S & Maeda K, *J Phys F (GB)*, **3** (1973) 167; *J Phys C (GB)*, **11** (1978) 2391.

5 Adhyapak S V & Nigavekar A S, *J Phys & Chem Solids (GB)*, **39** (1978) 127.

6 Salem S I, Chang C N & Nash T J, *Phys Rev B (USA)*, **18** (1978) 5168.

7 Salem S I, Chang C N, Lee P L & Severson V, *J Phys C (GB)*, **11** (1978) 4085.

8 Mehta S & Anikhindi R G, *Phys Lett A (Netherlands)*, **70** (1979) 158.

9 Kumar A, Nigam A N & Srivastava B D, *J Phys C (GB)*, **13** (1980) 3523.

10 Nigam H L, Srivastava B D & Prasad J, *Solid-State Commun (USA)*, **28** (1978) 1001.

11 Nayak R M & Padalia B D, *Phys Status Solidi b (Germany)*, **96** (1979) 259.

12 Ballal M M & Mande C, *J Phys & Chem Solids (GB)*, **38** (1977) 843.

13 Srivastava K S, Shrivastava R L, Harsh O K & Kumar V, *J Phys & Chem Solids (GB)*, **40** (1979) 489.

14 Srivastava K S, Kumar V & Harsh O K, *Indian J Pure & Appl Phys*, **19** (1981) 398.

15 Marton L, Leader L B & Mendlowitz H, in *Advances in electronics and electron physics*, Vol 7, edited by L Marton (Academic Press, New York) 1955, 225.

16 Phillip H R & Ehrenreich H, *Phys Rev (USA)*, **129** (1963) 1550.

17 Bohm D & Pines D, *Phys Rev (USA)*, **92** (1953) 609; Pines D, *Phys Rev (USA)*, **92** (1953) 626.

18 Couchois Y, *Acta Crystallogr (Denmark)*, **5** (1952) 351.

19 Lewis B, Leader L B, Mendlowitz H & Marton L, *Phys Rev (USA)*, **101** (1956) 1460.

20 Borovskii I B & Shmidt V V, *Soviet Phys Dokl (USSR)*, **4** (1959) 855.

21 Srivastava K S, Shrivastava R L, Harsh O K & Kumar V, *Phys Rev B (USA)*, **19** (1979) 4336.

22 Raether H, *Ergeb Exakten Naturwiss (Germany)*, **38** (1965) 84.

23 Mott D E, *Fine structure in X-ray absorption spectra*, Ph D thesis, New Mexico State University, USA, August 1963.

24 *Handbook of chemistry and physics* (The Chemical Publishing Co, CRC Press Inc, USA), 58th Edn, 1977-78.

25 Kondawar V K & Mande C, *J Phys C (GB)*, **9** (1976) 1351.

26 Nigam A K & Gupta M K, *J Phys F (GB)*, **3** (1973) 1251.

27 Krishna V, *Studies in coordination compounds: X-ray absorption spectroscopic investigations on some cobalt and copper complexes*, Ph D thesis, Allahabad University, Allahabad, 1973, pp. 60, 62.

28 Verma L P & Agarwal B K, *J Phys C (GB)*, **2** (1968) 1658.

INSTRUCTIONS TO AUTHORS

SCOPE

The journal welcomes, for publication, full papers and short notes, reporting significant new results of research, in all areas of physics except space physics. The applied fields covered are electronics, electrical engineering, instrumentation and applied mathematics. However, papers in applied mathematics with emphasis on only derivation and proofs and having no direct physical significance, will not be considered. Review articles are not published normally.

SUBMISSION OF MANUSCRIPT

Manuscripts for consideration should be submitted, *in duplicate*, to Editor, Indian Journal of Pure & Applied Physics, Publications & Information Directorate, Hillside Road, New Delhi 110012. They should neither have been already published nor be under consideration elsewhere.

Manuscripts should be in English and typewritten on only one side of good quality paper, in double space, with adequate margin on all four sides. One original and one carbon or photo-copy, each complete in all respects including abstract, illustrations, appendixes, etc. are to be submitted.

PREPARATION OF MANUSCRIPT

Authors may consult recent issues of the Journal to familiarize themselves with the general style and practices adopted in regard to the various elements of a paper.

General

Manuscript should be presented in as concise a form as possible. Good attention should be given to spelling and grammar. In giving names of chemical compounds and structures, abbreviations of units of measurements, symbols and notations, the style and practices recommended by the IUPAP and IUPAC, should be followed.

Frequently repeating combinations of words, e.g. electric field gradient (EFG), junction field effect transistor (JFET), stimulated Raman emission (SRE), should be abbreviated subsequently, indicating the abbreviated form in parenthesis, as shown, at the place of their first occurrence.

Pages should be numbered consecutively and arranged in the following order: Title, authors' names with their institutional affiliations and abstract, along with relevant footnotes whenever necessary (on a separate sheet); introduction; experimental details/theory/method/analysis; results; discussion; conclusion(s); acknowledgement; references and appendixes. Tables, captions for figures (with legends) and appendixes should be typed *on separate sheets* and attached at the end of the manuscript.

Title

The title should be neither too brief/general nor unnecessarily long. It should reflect the content of the paper so as to derive the maximum advantage in indexing. If a paper forms part of a general series, a specific subtitle, indicating the particular aspect of the work covered in the paper, should be provided.

A short running title for the paper, the broad subject heading under which it should be classified in the contents page (authors may consult recent numbers of the journal for this purpose), and the author (indicated by an asterisk on the relevant author's name) and address for correspondence, should also be provided on the title page.

Abstract

The abstract, usually not exceeding 200 words, should indicate the scope and significant content of the paper, highlighting the principal findings and conclusions. It should be in such a form that abstracting periodicals can use it without modification.

Introduction

Long and elaborate introduction should be avoided. It should be brief and state the exact scope of the study in relation to the present status of knowledge in the field. Literature review should be limited strictly to what is necessary to indicate the essential background and the justification for undertaking the study.

Materials, methods, apparatus, etc.

The sources of materials and their purity, methods of preparation, procedure for measurements and their accuracies, etc. should be clearly stated to enable any other worker to repeat the work if necessary. New methods, techniques, theories, etc. should be described in adequate detail; but if they are well known, a mere literature reference to them will do; differences from standard ones, improvements or innovations should, however, be clearly mentioned.

Results

Only such primary data as are essential for understanding the discussion and main conclusions emerging from the study should be included. All secondary data as are of interest to a specific category of readership *should not be included* in the paper. Such data should be retained by the authors for supply, on request, to any interested research worker. A footnote to this effect may be inserted at the relevant place in the paper.

The results must be presented in a coherent sequence in a unified logical structure, avoiding repetition or confusion. Limitations of the results should be clearly stated.

The same data should not be presented in both tabular and graphic forms. Only such tables and figures as are essential should be included. Simple linear plots that can easily be discussed in the text, should not be included. Infrared, ultraviolet, NMR and other spectra, DTA curves, etc. should be included only if they pertain to new compounds and/or are essential to the discussion; otherwise only significant numerical data should be given in the text or in a table.

Discussion

Long rambling discussion should be avoided. The discussion should deal with the interpretation of results without repeating information already presented under results. It should relate new findings to the known and include logical deductions. A separate section on 'conclusions' can be given only when they are well established and of outstanding significance. Mere observation of qualitative trends of results should be distinguished from firm conclusions. Also, limitations, if any, to the conclusions should be clearly pointed out.

Mathematical portions

Special attention should be given to the mathematical portions of the paper. Equations must be well separated from the text and written clearly with good separation between the successive lines. The usual norms of breaking long mathematical expressions should be adhered to. Equations should be numbered consecutively in Arabic numerals with the number in parenthesis near the right hand margin. Superscripts and subscripts should be clearly indicated in pencil by V and Λ sign respectively. Capital and small letters,

particularly of the same letter when both occur, as well as letters or *symbols likely to be confused* one for the other, *should be* clearly *distinguished*. Special characters (e.g. Greek, script, vector, tensor, etc.) required must be indicated by marginal notes. Letters and symbols which should appear in bold face must be clearly indicated. To simplify typesetting: (i) long and complicated mathematical expressions which are frequently repeated should be replaced with single letter/symbol, *without clashing with the others used* in the paper; (ii) the "exp" form of complex exponential functions should be used; and (iii) to simplify fractions, the solidus (/) is to be used and fractional exponents are to be used instead of root signs, e.g.

write $\exp\{-i\omega_0(t_1-t_2)/2\}$ and *not* $e^{-i\omega_0(t_1-t_2)/2}$

write $(4\omega_{pl}\,K_{3\lambda}^2/\tilde{\omega}\,K_D^2)^{1/2}$ and *not* $\sqrt{\dfrac{4\,\omega_{pl}\,K_{3\lambda}^2}{\tilde{\omega}\,K_D^2}}$

Tables

Tables should be numbered consecutively in Arabic numerals and *should bear brief titles. Column headings should be brief.* Units of measurement should be abbreviated and placed below the headings. Nil results should be indicated and distinguished clearly from absence of data. Inclusion of structural formulae inside the tables should be avoided as far as possible. Tables should be referred to in the text by numbers and not by terms like 'above', 'below', 'preceding' or 'following'. Results should not be presented to a greater accuracy than that of the method employed.

Illustrations

The number of illustrations should be kept to the minimum. Wherever possible, e.g. a number of individual analogous figures referring to different variables, substances, molecules, etc. may be combined into one composite figure. All illustrations should be numbered consecutively in Arabic numerals. *Captions and legends* to the figures should be *self-explanatory*. Line drawings should be made with Indian ink on white drawing paper/cellophane sheet/tracing cloth, and drawn to approximately twice the printed size.

The lettering should be uniform, preferably in stencil, so as to be *not less than* 1.5 *mm after reduction* widthwise to full page size (165 mm) or column size (80 mm). The size of geometrical shapes (used to distinguish different graphs), dots, lines, etc. should be sufficiently *large to permit* the necessary *reduction without loss of detail*. In the case of photographs, *prints must be on glossy paper and contrasty*. If an illustration is taken from another publication, reference to the source should be given and prior permission secured. Illustrations should be referred to in the text by numbers and not by terms like 'above', 'following' etc.

Acknowledgement

Acknowledgements should not be exuberant and must be made only to real assistance rendered in connection with the work reported in the paper.

References

References cited should be limited to the absolute minimum (particularly in the case of short notes) based on their essential relevance. In the text, references to literature should be *numbered consecutively, in the order of their first occurrence*, and should be indicated by superscript Arabic numbers at the relevant places; as far as possible the placement of references on numerals or other symbols should be avoided; in such cases the reference may be given in parenthesis in running text, e.g. "this yielded for n a value of 2.3 (Ref. 5)". Full bibliographic details for all the references mentioned in the text should be listed in serial order at the end of the paper.

In citing references to research papers, names and initials of authors should be followed, in order, by the title of the periodical in the abbreviated form (underlined), the volume number (two lines underneath), the year within circular brackets and the page number [e.g. Chandra B P & Shrivastava K K, *J Phys & Chem Solids (GB)*, 39 (1978) 939]. For names of periodicals, the abbreviations followed by the *Physics Abstracts* should be used. For periodicals not covered by *Physics Abstracts*, the title abbreviations should be according to the *Bibliographic Guide for Editors and Authors*, 1974, published by the American Chemical Society, Washington DC, USA; additionally the country from which the journal is published should be given in parenthesis immediately after the title abbreviation. If a paper has been accepted for publication, the names of the authors and the journal (with volume number and year, if known) should be given followed by the words "in press" [e.g. Wahi P K & Patel N D, *Can J Spectrosc (Canada)*, in press.].

In references containing *up to four authors*, the *names of all* the *authors* with their respective initials should *be given*. The abbreviations *et al.*, idem and ibid should be avoided. When there are more than four authors, *only* the names of the *first three authors* with their respective initials should *be given*, followed by the words '*et al.*'

Reference to a book should include details in the following order: name and initials of authors, the title of the book (underlined), name of publisher and place of publication within circular brackets and year and page (s) [e.g. Clayton G B, *Operational amplifiers* (Newnes-Butterworths, London), 4th Edn, 1977, 26]. If the reference is to the work of an author published in a book by a different person, the fact that it is cited from the source book should be clearly indicated [e.g. Turnhout Van J, 'Thermally stimulated discharge of electrets' in *Topics in applied physics*: Vol. 33—*Electrets*, edited by C M Sessler (Springer Verlag, Berlin), 1980, 130].

Proceedings of conferences and symposia should be treated in the same manner as books. Reference to a paper presented at a conference, the proceedings of which are not published, should include, in the following order, names and initials of authors, title of the paper (underlined), name of the conference, and where and when it was held (e.g. Herczeg P, *Symmetry-violating kaon decays*, paper presented to the International Conference on High Energy Physics and Nuclear Structure, Vancouver, Canada, 13-17 August 1979).

Reference to a thesis should include the name of the author, title of the thesis (underlined), university or institution to which it was submitted and year of submission (e.g. Mehrotra S N, *Many-body techniques and their applications to interacting bosons*, Ph D thesis, Ranchi University, 1976).

Reference to a patent should include names of patentees, country of origin (underlined) and patent number, the organization to which the patent has been assigned (within circular brackets), date of acceptance of the patent and reference to an abstracting periodical where available [e.g. Labes M M, *US Pat.* 4,066,567 (to Temple University), 3 January 1978; *Chem. Abstr.*, **88** (No. 20) (1978), 138350 n].

PROOFS & REPRINTS

Authors will receive galley proofs and a reprint order form. The galley proofs, indicating the essential corrections, should be returned to the Editor without delay, enclosing the reprint order form. Authors are given 25 *free reprints* for each paper. *Extra* reprints can be had *at cost. If the reprint order is not received with the corrected proofs, it will be presumed that the author needs no extra reprints.* Later requests for *more* reprints cannot be complied with. Covers for reprints cannot be provided.

THE WEALTH OF INDIA

An Encyclopaedia of Indian Raw Materials and Industrial Products, published in two series: **(i) Raw Materials**, and **(ii) Industrial Products**.

RAW MATERIALS

The articles deal with Animal Products, Dyes & Tans, Essential Oils, Fats & Oils, Fibres & Pulps, Foods & Fodders, Drugs, Minerals, Spices & Flavourings, and Timbers and other Forest products. Names in Indian languages, and trade names are provided.

For important crops, their origin, distribution, evolution of cultivated types, and methods of cultivation, harvesting and storage are mentioned in detail. Data regarding area and yield and import and export are provided. Regarding minerals, their occurrence and distribution in the country and modes of exploitation and utilization are given. The articles are well illustrated. Adequate literature references are provided.

Eleven volumes of the series covering letters A – Z have been published.

Vol. I(A-B) Rs. 80.00; Vol. II (C) Rs. 95.00; Vol. III (D-E) Rs. 105.00; Vol. IV (F-G) Rs. 65.00; Vol. IV: Suppl. Fish & Fisheries Rs. 40.00; Vol. V (H-K) Rs. 75.00; Vol. VI (L-M) Rs. 90.00; Vol. VI: Suppl. Livestock Rs. 60.00; Vol. VII (N-Pc) Rs. 30.00; Vol. VIII (Ph-Re) Rs. 86.00; Vol. IX (Rh-So) Rs. 104.00; Vol. X (Sp-W) Rs. 152.00; Vol. XI (X-Z) Rs. 102.00.

INDUSTRIAL PRODUCTS

Includes articles giving a comprehensive account of various large, medium and small scale industries. Some of the major industries included are: Acids, Carriages, Diesel Engines, Fertilizers, Insecticides & Pesticides, Iron & Steel, Paints & Varnishes, Petroleum Refining, Pharmaceuticals, Plastics, Ship & Boat-building, Rubber, Silk, etc.

The articles include an account of the raw materials and their availability, manufacturing processes, and uses of products, and industrial potentialities. Specifications of raw materials as well as finished products and statistical data regarding production, demand, exports, imports, prices, etc., are provided. The articles are suitably illustrated. References to the sources of information are provided.

Nine volumes of the series covering letters A – Z have been published.

Part I (A-B) Rs. 54.00; Part II (C) Rs. 64.00; Part III (D-E) Rs. 25.00; Part IV (F-H) Rs. 25.00; Part V (I-L) Rs. 30.00; Part VI (M-Pi) Rs. 28.00; Part VII (Pl-Sh) Rs. 60.00; Part VIII (Si-Ti) Rs. 66.00; Part IX (To-Z) Rs. 80.00.

HINDI EDITION: BHARAT KI SAMPADA—PRAKRITIK PADARTH

Vols. I to VI and two supplements of Wealth of India—Raw Materials series in Hindi already published.

Published Volumes:

Vol. I (अ-औ) Rs. 38; Vol. II (क) Rs. 36; Vol. III (ख-न) Rs. 36; Vol. IV (प) Rs. 83; Vol. V (फ-मेरे) Rs. 60; Vol. VI (मेल-रू) Rs. 80.

Supplements:

Fish & Fisheries (Matsya & Matsyaki) Rs. 49; Liverstock (*Pashudhan aur Kukkut Palan*) Rs. 34.

Vols. VII to XI under publication.

Please contact:

Manager (Sales & Advertisement)

PUBLICATIONS & INFORMATION DIRECTORATE, CSIR

Hillside Road, New Delhi 110012

RN 7092/63

CSIR PUBLICATIONS

WEALTH OF INDIA

An encyclopaedia of the economic products and industrial resources of India issued in two series

RAW MATERIALS SERIES—contains articles on plant, animal and mineral resources

	Rs	$	£
Vol. I (A-B)	80.00	30.00	13.00
Vol. II (C)	95.00	33.00	17.00
Vol. III (D-E)	105.00	32.00	20.00
Vol. IV (F-G)	65.00	27.00	12.00
Supplement (Fish & Fisheries)	40.00	16.00	7.00
Vol. V (H-K)	75.00	28.00	12.50
Vol. VI (L-M)	90.00	34.00	15.00
Supplement (Livestock)	60.00	18.00	6.00
Vol. VII (N-Pe)	30.00	9.00	3.00
Vol. VIII (Ph-Re)	86.00	32.00	14.00
Vol. IX (Rh-So)	104.00	35.00	19.00
Vol. X (Sp-W)	152.00	65.00	23.00
Vol. XI (X-Z)	102.00	42.00	20.00

INDUSTRIAL PRODUCTS SERIES—deals with major, small-scale and cottage industries

Part I (A-B)	54.00	20.00	9.00
Part II (C)	64.00	24.00	11.00
Part III (D-E)	25.00	7.50	2.50
Part IV (F-H)	25.00	7.50	2.50
Part V(I-L)	30.00	9.00	3.00
Part VI (M-Pi)	28.00	8.00	2.80
Part VII (Pl-Sh)	60.00	18.00	6.00
Part VIII (Si-Ti)	66.00	27.00	10.00
Part IX (To-Z)	80.00	34.00	12.00

BHARAT KI SAMPADA (Hindi Edition of Wealth of India, Raw Materials)

Vol. I	(अ-औ)	38.00	16.00	6.50
Vol. II	(क)	36.00	15.00	6.00
Vol. III	(ख-न)	36.00	15.00	6.00
Vol. IV	(प)	83.00	34.00	16.00
Vol. V	(फ-मेरे)	60.00	22.00	10.00
Vol VI	(मेल-ह)	80.00	27.00	13.00
Livestock (Kukkut Palan)		34.00	15.00	6.00
Fish & Fisheries (Matsya aur Matsyaki)		49.00	21.00	8.00
A Dictionary of Generic & Specific Names of Plants and Animals Useful to Man with their English and Latin pronunciation in Devanagari		30.00	11.00	5.00

OTHER PUBLICATIONS

	Rs	$	£
Proceedings:seminar on primary communications in Science & Technology in India by Sh. R.N. Sharma & S. Seetharama	52.00	17.50	9.00
Flora of Delhi by J.K. Maheshwari	28.00	8.00	2.80
Indian Fossil Pteridophytes by K.R. Surange	23.00	8.00	2.30
Indian Thysanoptera by T.N. Ananthakrishnan	26.00	8.00	2.60
The Millipede Thyropygus by G. Krishnan	12.00	3.50	1.20
Drug Addiction with special reference to India by R.N. Chopra & I.C. Chopra	12.00	3.50	1.20
Glossary of Indian Medicinal Plants by R.N. Chopra & I.C. Chopra	35.00	13.00	6.00
Fluidization & Related Processes	12.00	4.00	1.20
Evolution of Life by M.S. Randhawa, A.K. Dey, Jagjit Singh & Vishnu Mitre	22.50	7.00	2.25
Collected Scientific Papers of Meghnad Saha	30.00	9.00	3.00
Proteaceae by C. Venkata Rao	34.00	11.00	3.40
Pinus by P. Maheshwari & R.N. Konar	30.00	11.00	5.00
Cellulose Research I	3.00	0.90	0.30
Cellulose Research II	6.00	1.75	0.60
Chemical Process Design	9.00	2.50	0.90
Low Temperature Carbonization of Non-coking Coals & Lignites & Briquetting Coal Fines:			
Vol. I	17.50	5.50	1.75
Vol. II	17.50	5.50	1.75
Nucleic Acids	10.00	3.00	1.00
IGY Symposium: Vol. I	9.00	2.50	0.90
IGY Symposium: Vol. II	9.00	2.50	0.90
CNS Drugs	16.50	5.00	1.65
Kinetics of Electrode Processes & Null Points of Metals	2.50	0.75	0.25
Indian Sardines by R.V. Nair	22.00	7.00	2.20
Termite Problems in India	9.00	3.00	0.90
Loranthaceae by B.M. Johri & S.P. Bhatnagar	32.00	11.00	3.20
Abies and Picea by K.A. Chowdhury	14.00	6.00	2.10
Gnetum by P. Maheshwari and Vimla Vasil	20.00	6.00	2.00
Aquatic Angiosperms by K. Subramanyam	20.00	6.00	2.00
Supplement to Glossary of Indian Medicinal Plants by R.N. Chopra, I.C. Chopra & B.S. Varma	18.00	7.00	3.00
Herbaceous Flora of Dehra Dun by C.R. Babu	144.00	60.00	22.00
Diosgenin and Other Steroid Drug Precursors by Y.R. Chadha & Miss L.V. Asolkar	36.00	13.00	6.00
Research & Development Management by Inder Dev	25.00	10.00	—
Rural Development and Technology—A Status Report-cum-Bibliography by P.R. Bose & V.N. Vashist	100.00	38.00	17.00

Packing and Postage extra

Please contact:

Manager (Sales & Advertisement)

PUBLICATIONS & INFORMATION DIRECTORATE, CSIR

Hillside Road, New Delhi 110012

Printed & Published by D.S. Sastry, Editor, Publications & Information Directorate (PID), Hillside Road, New Delhi 110012, at PID Photocomposition Unit

D(C)540